

Electronic Thesis and Dissertation Repository

---

8-20-2015 12:00 AM

## Experimental Analysis of Parameters Influencing the Bone Burring Process

Jonathan Kusins  
*The University of Western Ontario*

Supervisor  
Dr. Louis Ferreira  
*The University of Western Ontario* Joint Supervisor  
Dr. Remus Tutunea-Fatan  
*The University of Western Ontario*

Graduate Program in Mechanical and Materials Engineering  
A thesis submitted in partial fulfillment of the requirements for the degree in Master of  
Engineering Science  
© Jonathan Kusins 2015

Follow this and additional works at: <https://ir.lib.uwo.ca/etd>



Part of the [Biomechanical Engineering Commons](#)

---

### Recommended Citation

Kusins, Jonathan, "Experimental Analysis of Parameters Influencing the Bone Burring Process" (2015).  
*Electronic Thesis and Dissertation Repository*. 3089.  
<https://ir.lib.uwo.ca/etd/3089>

This Dissertation/Thesis is brought to you for free and open access by Scholarship@Western. It has been accepted for inclusion in Electronic Thesis and Dissertation Repository by an authorized administrator of Scholarship@Western. For more information, please contact [wlsadmin@uwo.ca](mailto:wlsadmin@uwo.ca).

**EXPERIMENTAL ANALYSIS OF PARAMETERS INFLUENCING THE BONE  
BURRING PROCESS**

(Thesis format: Monograph)

by

Jonathan R. Kusins

Graduate Program in Mechanical and Materials Engineering

A thesis submitted in partial fulfillment  
of the requirements for the degree of  
Master of Engineering Science

The School of Graduate and Postdoctoral Studies  
The University of Western Ontario  
London, Ontario, Canada

© Jonathan R. Kusins 2015

## Abstract

The experimental quantification of the bone removal characteristics associated with bone burring represents a desirable outcome mainly for the selection of optimal parameters. An experimental apparatus was developed that allowed for concurrent measurement of three outputs associated with the bone removal process (cutting force, vibration, and temperature) as a function of various burring-specific parameters. Initial process trends were established on a uniform sawbone analog through use of a fully balanced multivariate statistical analysis. A smaller set of optimal and suboptimal parameters were further validated using a porcine femur. From the parameters tested, an optimal tool configuration, to avoid high temperature and high vibration, was found to be a 6 mm sphere burr at a rotational speed of 15,000 rpm, feed rate of 2 mm/s and a path overlap of 50%. This set of parameters also provided flexibility in tool depth/orientation angle relative to the bone without sacrificing optimal process outcomes.

## Keywords

bone burring, bone resurfacing, bone removal parameters, experimental apparatus, superficial temperature, cutting forces, vibration amplitude

## Co-Authorship Statement

- Chapter 1: Jonathan Kusins - sole author
- Chapter 2: Jonathan Kusins - study design, data collection, wrote manuscript  
Louis Ferreira - study design, reviewed manuscript  
Remus Tutunea-Fatan - study design, reviewed manuscript
- Chapter 3: Jonathan Kusins - study design, data collection, statistical analysis, wrote manuscript  
Louis Ferreira - study design, reviewed manuscript  
Remus Tutunea-Fatan - study design, reviewed manuscript
- Chapter 4: Jonathan Kusins - study design, statistical analysis, wrote manuscript  
Louis Ferreira - study design, reviewed manuscript  
Remus Tutunea-Fatan - study design, reviewed manuscript
- Chapter 5: Jonathan Kusins - study design, data collection, statistical analysis, wrote manuscript  
Louis Ferreira - study design, reviewed manuscript  
Remus Tutunea-Fatan - study design, reviewed manuscript
- Chapter 6: Jonathan Kusins - sole author

## Acknowledgments

First and foremost, I would like to thank both of my supervisors, Dr. Louis Ferreira, and Dr. Remus Tutunea-Fatan. The guidance, encouragement, and support that both of you have provided throughout my graduate studies has been extremely appreciated. Louis, thank you for providing me with an opportunity to study at the HULC; something that I will come to miss. Remus, your willingness to always discuss various issues at hand was appreciated and your drive for weekly meetings definitely kept me on the ball throughout this project. Thank you both for your mentorship throughout.

I would also like to extend my thanks to the entire HULC team. Thank you for providing me with an enjoyable working environment, inside and outside of the lab. I am honored to be part of the TankFM team and grateful for all the listeners/students that made it possible.

Finally, I would like to express my thanks to my family. Thank you Mal and Caleb for helping me along in this process and if not for either of you, I may of never considered graduate studies in the first place. Mom and Dad, thank you for your unwavering support throughout and for providing me with a getaway cottage that was desperately needed at times.

# Table of Contents

Abstract.....	ii
Co-Authorship Statement.....	iii
Acknowledgments.....	iv
List of Tables .....	x
List of Figures.....	xii
List of Equations.....	xv
List of Appendices .....	xvi
<b>Chapter 1 - Introduction .....</b>	<b>1</b>
1.1 Structure and Mechanical Properties of Bone .....	1
1.1.1 Bone Necrosis .....	3
1.2 Bone Resurfacing.....	3
1.2.1 Manual Resurfacing Procedures .....	5
1.2.2 Robotic Methods.....	8
1.2.3 Bone Removal Tools.....	11
1.3 High Speed Bone Burring Characteristics .....	13
1.3.1 Process Parameters.....	13
1.3.2 Outcome Measurements.....	18
1.4 State-of-the-Art in Quantifying the Bone Burring Process.....	21
1.5 Rationale .....	24
1.6 Objectives and Hypotheses .....	26
1.7 Thesis Overview .....	28
<b>Chapter 2 - Development of Experimental Apparatus for Investigation of Bone Burring.....</b>	<b>30</b>
2.1 Process Parameters and Dependent Variables .....	30

2.2	Experimental Apparatus.....	33
2.2.1	Burring Tool Holder .....	33
2.2.2	Workpiece Positioning.....	35
2.3	Measurement of Dependent Variables.....	37
2.3.1	Data Acquisition System.....	37
2.3.2	Cutting Force Measurement.....	38
2.3.3	Vibration Measurement .....	40
2.3.4	Temperature Measurement .....	42
2.4	Sample Experiment.....	44
2.4.1	Signal Post Processing .....	48
2.4.2	Sample Experiment Results .....	56
2.5	Chapter Summary .....	56
<b>Chapter 3 - Experimental Analysis of the Effect of Process Parameters on Selected Outcome Measurements .....</b>		<b>58</b>
3.1	Selection of Process Parameters .....	58
3.1.1	Feed Rate Normalization .....	63
3.2	Statistical Analysis.....	66
3.3	Effects of Process Parameters on Outcome Measurements.....	67
3.3.1	Cutting Force .....	67
3.3.2	Vibration .....	68
3.3.3	Temperature .....	68
3.4	Chapter Summary .....	78
<b>Chapter 4 - Process Parameter Selection for Clinical Implementation.....</b>		<b>80</b>
4.1	Reduction of Parameters.....	80
4.1.1	Criteria for Reduction of Parameters .....	81
4.1.2	Heuristic Filtering Methods .....	82

4.2	Statistical Analysis.....	83
4.3	Local Minimums for Temperature and Vibration.....	86
4.3.1	Heuristic Filtering Results .....	86
4.3.2	Vibration .....	86
4.3.3	Temperature .....	86
4.4	Local Maximums of Temperature and Vibration .....	89
4.4.1	Heuristic Filtering Result.....	89
4.4.2	Vibration .....	89
4.4.3	Temperature .....	89
4.5	Absolute Maximums of Temperature .....	92
4.5.1	Heuristic Filtering Results .....	92
4.5.2	Vibration .....	92
4.5.3	Temperature .....	92
4.6	Absolute Maximums of Vibration .....	94
4.6.1	Heuristic Filtering Results .....	94
4.6.2	Vibration .....	94
4.6.3	Temperature .....	94
4.7	Chapter Summary .....	97
<b>Chapter 5 - Experimental Validation of Process Parameters on Porcine Cadaver Model.....</b>		<b>100</b>
5.1	Parameter Selection .....	100
5.2	Specimen and Data Preparation .....	103
5.2.1	Specimen Selection.....	103
5.2.2	Specimen Preparation .....	104
5.2.3	Bone Removal Burring Testing and Data Preparation .....	104
5.2.4	Feed Rate Normalization .....	108



5.3 Outcome Measurements & Statistical Analysis.....	110
5.4 Effects of Process Parameters on Outcome Measurements - Optimal Set .....	110
5.4.1 Cutting Force .....	110
5.4.2 Vibration .....	111
5.4.3 Temperature .....	111
5.5 Effects of Process Parameters on Outcome Measurements - Suboptimal Set ....	111
5.5.1 Cutting Force .....	116
5.5.2 Vibration .....	116
5.5.3 Temperature .....	116
5.6 Chapter Summary .....	119
<b>Chapter 6 - General Discussion and Conclusions .....</b>	<b>122</b>
6.1 Summary and General Discussion .....	122
6.2 Strengths and Limitations .....	126
6.3 Future Work .....	127
6.4 Conclusion .....	128
<b>References.....</b>	<b>129</b>
<b>Appendix A: Developed Experimental Apparatus Component Drawings.....</b>	<b>135</b>
<b>Appendix B: Supplementary Specification Sheets.....</b>	<b>146</b>
<b>Appendix C: Supplementary Testing Files.....</b>	<b>149</b>
<b>Appendix D: Statistical Analysis Guide.....</b>	<b>160</b>
<b>Appendix E: Burring Trials and Associated Force Results from Results Presented in Chapter 4 .....</b>	<b>163</b>
<b>Appendix F: Burring Trials and Associated Force Results from Results Presented in Chapter 5 .....</b>	<b>169</b>
<b>Appendix G: Characterization and Synthesis of the Acoustics Associated with Bone Burring .....</b>	<b>171</b>

**Curriculum Vitae** ..... 180

## List of Tables

Table 3.1: Selected levels of process parameters.....	62
Table 3.2: Summary of MANOVA results .....	69
Table 3.3: Summary of ANOVA results - Fx .....	69
Table 3.4: Summary of ANOVA results - Fy .....	69
Table 3.5: Summary of ANOVA results - Fz .....	70
Table 3.6: Summary of ANOVA results - vibration.....	70
Table 3.7: Summary of ANOVA results - temperature .....	70
Table 4.1: Summary of statistical analysis for process parameters that resulted in local minimums of temperature and vibration.....	87
Table 4.2: Summary of statistical analysis for process parameters that resulted in local maximums of temperature and vibration .....	90
Table 4.3: Summary of statistical analysis for process parameters that resulted in absolute maximums of temperature .....	93
Table 4.4: Summary of statistical analysis for process parameters that resulted in absolute maximums of vibration.....	95
Table 5.1: Optimal combination of process parameters .....	102
Table 5.2: Suboptimal combination of process parameters .....	103
Table 5.3: Descriptive statistics of outcome measurements - optimal set .....	112
Table 5.4: Descriptive statistics of outcome measurements - suboptimal set.....	112

Table 5.5: Summary of statistical analysis for process parameters that resulted in local minimums of temperature and vibration.....	114
Table 5.6: Summary of statistical analysis for process parameters that resulted in local maximums of temperature and vibration .....	118
Table E.1: Reduced sample set #1: local minimums of temperature and vibration .....	163
Table E.2: Reduced sample set #2: local maximums of temperature and vibration.....	164
Table E.3: Reduced sample set #3: absolute maximum for temperature.....	165
Table E.4: Reduced sample set #4: absolute maximum for vibration .....	167
Table F.1: Optimal combination set of process parameters.....	169
Table F.2: Suboptimal combination set of process parameters .....	170

## List of Figures

Figure 1.1: Structural makeup of bone .....	4
Figure 1.2: Bone removal process .....	6
Figure 1.3: Mastoid process location on the skull .....	7
Figure 1.4: Automated robotic surgery .....	10
Figure 1.5: Orthopaedic reamer .....	11
Figure 1.6: High speed rotary burring tool .....	12
Figure 1.7: Midas Rex Legend rotary burring tool .....	15
Figure 1.8: Design parameters used for bone burring (depth of cut + overlap).....	16
Figure 1.9: Design parameters used for bone burring (inclination angle + tilt angle).....	17
Figure 2.1: Tool holder with adjustable orientation.....	34
Figure 2.2: Workpiece positioning system with adjustable horizontal position.....	36
Figure 2.3: Data acquisition system.....	37
Figure 2.4: ATI 3-axis load cell placement .....	39
Figure 2.5: Uni-axial Endevco accelerometer placement .....	41
Figure 2.6: Infrared pyrometer placement .....	43
Figure 2.7: Simultaneous measurements of dependent variables .....	46
Figure 2.8: Fast Fourier transform of steady state vibration data .....	47
Figure 2.9: Steady state measurement of cutting force (X-direction).....	51

Figure 2.10: Steady state measurement of cutting force (Y-direction).....	52
Figure 2.11: Steady state measurement of cutting force (Z-direction).....	53
Figure 2.12: Steady state measurement of vibration.....	54
Figure 2.13: Temperature measurement obtained from sample cut .....	55
Figure 3.1: Quantifying cooling of the workpiece during a burring trail .....	64
Figure 3.2: Temperature normalized to the center of the burring tool.....	65
Figure 3.3: Main effects of process parameters on cutting force ( $F_x$ , $F_y$ , and $F_z$ ).....	71
Figure 3.4: Main effects of process parameters on temperature and vibration.....	72
Figure 3.5: Maximum and minimum measurements for cutting force - $F_x$ .....	73
Figure 3.6: Maximum and minimum measurements for cutting force - $F_y$ .....	74
Figure 3.7: Maximum and minimum measurements for cutting force - $F_z$ .....	75
Figure 3.8: Maximum and minimum measurements for vibration .....	76
Figure 3.9: Maximum and minimum measurements for temperature .....	77
Figure 4.1: Measurements from experimental matrix.....	84
Figure 4.2: Heuristic filtering process .....	85
Figure 4.3: Temperature measurements of the sphere and cylinder tools at varying inclination and tilt angles .....	88
Figure 4.4: Local minimums and maximums of temperature and vibration measurements .....	91
Figure 4.5: Absolute maximums of temperature and vibration .....	96
Figure 5.1: Preparation of specimen .....	106

Figure 5.2: Simultaneous measurements of outcome variables while burring porcine cancellous bone .....	107
Figure 5.3: Feed rate normalization for porcine bone.....	109
Figure 5.4: Temperature and vibration measurements of sawbone vs. porcine - optimal parameter set .....	113
Figure 5.5: Sensitivity of tool type to changes in inclination angles .....	115
Figure 5.6: Temperature and vibration measurements of sawbone vs. porcine -suboptimal parameter set .....	117
Figure C.1: Noise characterization of accelerometer.....	150
Figure C.2: Noise characterization of pyrometer.....	150
Figure C.3: Noise measurements of 3 DOF load cell .....	151
Figure C.4: Force measurements of original designed workpiece clamp .....	153
Figure C.5: Force measurements with adjustable clamp .....	154
Figure C.6: Sample outputs from load cell verification tests (0, 2N).....	155
Figure C.7: Sample outputs from load cell verification tests (4N, 6 N) .....	156
Figure C.8: Alignment of pyrometer .....	159
Figure G.1: Developed process to synthesize sounds associated with bone burring.....	172
Figure G.2: Authentic and synthesized sound at 45,000 rpm .....	177
Figure G.3: Authentic and synthesized sound at 15,000 rpm .....	178
Figure G.4: Authentic and synthesized sound at 75,000 rpm .....	179

## List of Equations

Equation 2.1: SNR calculation.....	48
Equation G.1: Principle frequency synthesis .....	174
Equation G.2: Second harmonic frequency synthesis.....	174
Equation G.3: Third harmonic frequency synthesis .....	174
Equation G.4: Frequency to time domain translation .....	174
Equation G.5: Noise scaling factor .....	175



## List of Appendices

Appendix A: Developed Experimental Apparatus Component Drawings .....	135
Appendix B: Supplementary Specification Sheets .....	146
Appendix C: Supplementary Testing Files .....	149
Appendix D: Statistical Analysis Guide .....	160
Appendix E: Burring Trials and Associated Force Results from Results Presented in Chapter 4.....	163
Appendix F: Burring Trials and Associated Force Results from Results Presented in Chapter 5.....	169
Appendix G: Characterization and Synthesis of the Acoustics Associated with Bone Burring .....	171

## Chapter 1 - Introduction

***OVERVIEW:** Bone removal is required in multiple surgical resurfacing procedures. A common method to resurface bone involves using a high speed rotary tool for bone removal purposes. This chapter will describe the structure and mechanical properties of bone, and the clinical procedures that require the removal of bone. In addition, both manual and automated processes which have been adapted currently in the clinic are discussed. Current state-of-the-art studies involving optimizing process parameters associated with the burring procedure are summarized. Associated statistical methods related to the current project are explained. The chapter ends with rationale, objectives and hypothesis associated with the current body of work.*

### 1.1 Structure and Mechanical Properties of Bone

Bone is a stiff skeletal material that provides the supportive framework to the body. The major functions of bone include: support of soft tissues, provision of levers for muscles, and protection of internal organs. Bone is a heterogeneous mix of materials and cells that can be further divided into organic and inorganic components. The organic portion of bone consists of the cells that build (primarily osteoblasts) or degrade (primarily osteoclasts) bone, collagen, bone matrix proteins, and blood vessels that supply nutrients. The inorganic component of bone, which is produced by bone cells, consists primarily of calcium phosphate. The amount of mineralized tissue per unit volume is often used to

characterize the mechanical properties of bone and is quantified using a measurement of bone mineral density (BMD) [1, 2]. Unique interactions between the organic and inorganic components of bone, lead in regular bone turnover; an important feature of bone that allows for natural self-repair to injury, or remodeling in response to mechanical stimuli [3, 4]. Therefore, it is important to conceptualize bone as a living substance within the body, one that reacts to external stimuli and contains its own network of blood vessels and cells.

Bone is divided into two fairly distinct structural organizations: cortical (compact) bone and cancellous (spongy) bone. The difference between the structural types is distinguishable to the naked eye due to several distinct differences between structures [5].

Cortical bone is a solid rigid material. A cortical layer makes up the outer shell of the bone and is much denser and stiffer than cancellous bone [1]. Cancellous bone is porous throughout and is less uniform than cortical bone [6, 7]. The mechanical properties of the bone are highly variable and are mainly due to the variation in the apparent density which differ by anatomical location as well as various factors such as age, overuse and pharmaceutical interventions [8-11].

The gross morphology of human bones can be distinguished into four classifications: long bones (femur, tibia, ulna and radius), short bones (wrist and ankle bones), tabular or flat bones (skull and scapula), and irregular shaped bones (located within the skull and parts of the pelvis). Long bones are usually thick walled, hollow tubes (filled with bone marrow), and have expanded ends. The regions of the long bone are classified as the epiphysis (end of the bone or the area of articulation), diaphysis (shaft of the bone), and

metaphysis (between epiphysis and diaphysis) (Figure 1.1). The epiphysis is the elongated ends of the long bone and have a thin cortical shell that encloses the cancellous bone. The diaphysis of the bone is primarily composed of a thick cortical shell (cortex) that surrounds the medullar canal filled with bone marrow.

### 1.1.1 Bone Necrosis

As bone is a living organism, exposure to high temperature, even for a short period of time, could result in permanent thermal damage (osteonecrosis). Previous studies have attempted to quantify the severity of osteonecrosis dependent on the temperature that the bone is exposed to and the duration of time that may cause damage to the bone [12-15]. Previous studies give indication that there is a distribution of temperature levels for specified time durations that can possibly lead to osteonecrosis. Lundskog *et al.* found histochemical evidence of thermal damage when the bone was heated to 50 °C for 30 seconds [12]. Eriksson *et al.* indicated that bone tissue is sensitive to temperatures in the range of 47-53 °C for the duration of 1 minute [13, 14]. Specific to an orthopaedic cutting process, Krause *et al.* used a threshold of 50 °C to determine osteonecrosis [15]. Collectively, these studies indicate the importance of avoiding exposing bone tissue to elevated temperatures as it may result in hindered bone remodeling post operation.

## 1.2 Bone Resurfacing

Bone removal or resurfacing is required in various surgical treatments. The surgical procedures and tools involved vary by surgical intervention. In context with the overall theme of this work, procedures that involve or have the potential to involve high speed rotary bone burring tools are discussed.

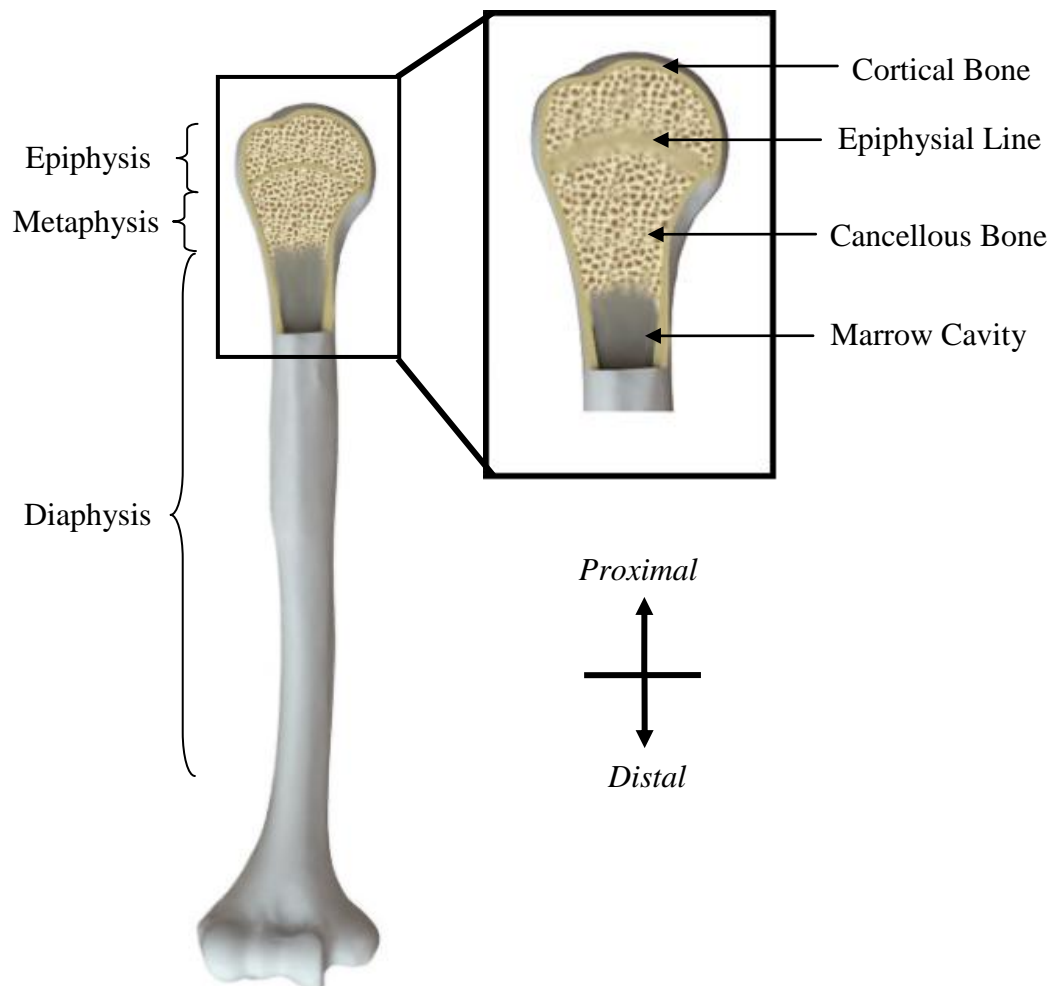


**Figure 1.1: Structural makeup of bone**

*The structural components of a long bone, humerus shown above, are illustrated in the diagram above. The long bone is divided into three sections including the: epiphysis, metaphysis, and diaphysis. The bone itself is composed of two main distinct structural organizations: cortical and cancellous bone.*

## 1.2.1 Manual Resurfacing Procedures

### 1.2.1.1 Orthopaedics

Joint replacement/resurfacing is a surgical procedure used with the goal of alleviating pain and restoring function to a damaged joint (hip, knee, shoulder). Although there exists many clinical conditions that may require joint replacements for treatment, the majority of these conditions can be grouped into the broad categories of arthritic conditions and fractures [16-18]. In the majority of arthritic conditions, the joint surface becomes damaged as a result of chronic inflammation (as in the case of rheumatoid arthritis) or chronic wear and tear (as in the case of osteoarthritis). If left untreated, progressive joint immobilization and loss of function will ensue. Currently, several types of joint replacements are used clinically which include: total joint (whole joint is replaced), hemiarthroplasty (one side of the joint is replaced) and joint resurfacing (only the articular surface is replaced).

The surgical procedure for a joint replacement calls for a synthetic material to replace the damaged articular cartilage and/or joint. To insert the joint replacement into a patient, a volume of the bone must first be removed to provide a cavity for insertion. The machining and removal of the bone can be performed by multiple means and may individually or collectively involve: drilling, reaming, or milling to prepare the cavity. These surgical procedures are traditionally performed manually by a surgeon. After the cavity is prepared, the joint replacement is inserted and fixed in place. Fixation of the joint replacement can be performed by several methods which include: screw, cement, or press-fit. Regardless of the fixation technique, a cavity must be formed for the bone to allow for insertion of the joint replacement.

Joint resurfacing arthroplasty offers an appropriate application for use of a high speed rotary tool as it may require the bone cavity to be precisely shaped. The procedure is considered to be a bone-conserving alternative to total joint replacement as the joint resurfacing replacements are closely shaped to the patients anatomy with shorter stems used for fixation [19, 20] (Figure 1.2). The resurfacing procedure may require a complex bone cavity with high geometrical accuracy to attain secure fixation and may only be achievable using a small diameter (approximately 4 mm) rotary burring tool.

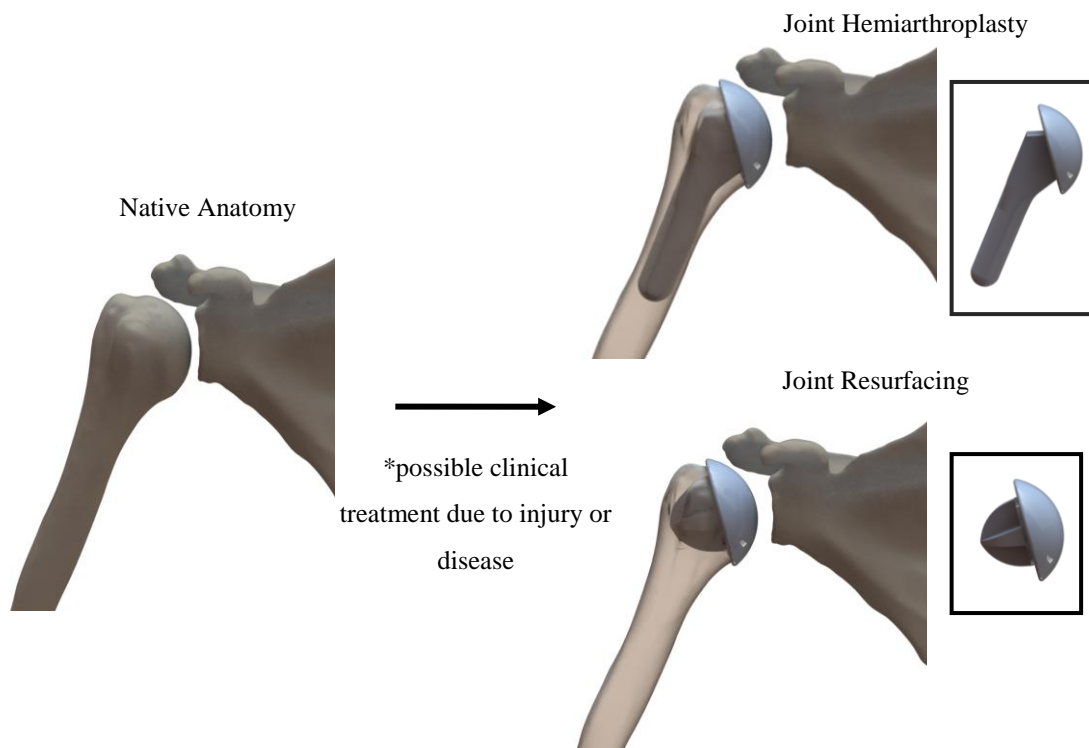


**Figure 1.2: Bone removal process**

*Various types of implants are used in orthopaedics as shown above. To fixate the implant into a patient; bone must first be removed to form a cavity to allow for insertion. A possible implementation for a high speed rotary tool would be the process of bone removal to form a cavity which may require intricate geometries that can be achievable using only a small diameter burring bit.*

### 1.2.1.2 Neurotology

Neurotology is a branch of medicine that deals with treating disorders of the ear. Otologic surgeries are performed on the temporal bone which is located on the sides of the skull and house the structures vital to hearing (Figure 1.3). The temporal bone is divisible into four parts: the squamous, mastoid, petrous, and tympanic portions. Relevant to the present project is a specific surgery known as a mastoidectomy.

A mastoidectomy is surgical procedure that requires the removal of temporal bone within the mastoid region, using a high speed rotary tool. A mastoidectomy is performed to expose the cells within the mastoid structure, which may be required due to cholesteatoma (cyst), or mastoiditis (infection) [21]. The procedure is especially relevant as the surgical practice currently involves the use of a high speed rotary tool for bone removal within the temporal bone region.

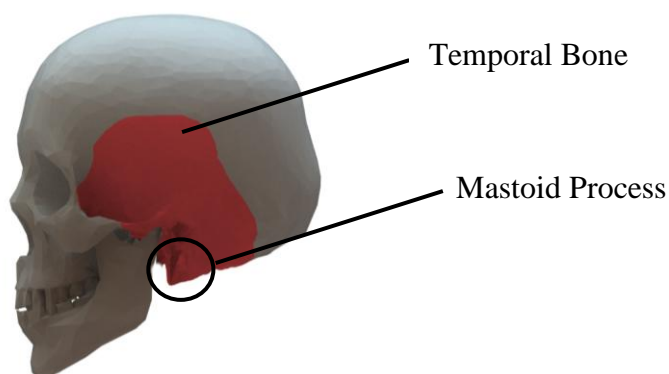


**Figure 1.3: Mastoid process location on the skull**

*A mastoidectomy is a surgical procedure that involves removing the outer surface of temporal bone on the skull. A high speed rotary tool is currently used clinically to remove the bone.*



### 1.2.2 Robotic Methods

Automated robotic bone burring first appeared with commercial success in surgical procedures which involved joint replacement and resurfacing. Automated robotic burring takes advantage of the rigidity of the bone and high accuracy of the registration techniques developed. The registration techniques allow for pre-operative planning of the automated tool path trajectory comparable to that of computer numerical control (CNC) machining. There are many advantages of employing robotic systems including: increased accuracy and precision that lead to improvements in surgical outcomes compared to the manual procedure [22-24]. Within the orthopaedic field, three developed systems are the Robodoc, MAKO™ platform, and Acrobot.

The Robodoc (Integrated Surgical Supplied Ltd., Sacramento, CA) surgical system was the first orthopaedic surgical robot approved by the Food and Drug Association (FDA) [25]. Clinical use of the automated burring robot, Robodoc, was implemented in 1992 for femoral canal preparation in total hip arthroplasty [26]. Results showed, through patient and cadaveric studies, that the Robodoc was able to match results compared to the manual technique as well as provide better stability and fit in placement of the femoral component in total hip arthroplasty [23, 24, 27]. Additionally, the Robodoc removed less bone within the same procedure compared to the manual techniques [28].

The MAKO® surgical robot (MAKO Surgical Corp., Fort Lauderdale, FL) is a passive robot which assists the surgeon in partial knee and total hip replacement by providing haptic feedback (Figure 1.4). The MAKO® surgical robot limits machining errors during the surgical procedure by ensuring the cutting tool is within predefined boundaries while

removing bone [29]. The MAKO<sup>®</sup> platform has been found to significantly increase the accuracy and precision involved in total hip arthroplasty in cadaveric studies [30].

The Acrobot is an active constraint control robot that has had clinical success in knee and hip replacement surgery. The Acrobot features a control system; which implements tool tracking to aid the surgeon in live surgery [31]. The Acrobot has also shown to be effective in *in-vitro* and *in-vivo* studies to aid the surgeon in providing feedback of the tool for total knee replacement surgeries [32].

Additionally, several robotic systems have been developed in an *in-vitro* setting to prove the feasibility of implementing robotic system for mastoidectomy [33, 34]. Danilchenko *et al.* successively burred a cavity in the mastoid on three separate specimens using a industrial robot equipped with a high speed rotary tool as an end effector [33]. Federspil *et al.* also had success with experimental burring of two human skulls using an industrial robot and a high speed rotary tool [34].

The emergence of robotic systems provides an opportunity to implement feedback loops which monitor burring data and adjust control parameters accordingly. A full understanding of the characteristics associated with bone burring would prove beneficial in the design of robotic systems.



**Figure 1.4: Automated robotic surgery<sup>1</sup>**

*The MAKOplasty® surgical robot is a passive robotic system that assists the surgeon by providing haptic feedback to the surgeon during partial knee resurfacing. Additional information, such as location of the tool, is provided by the MAKO® system that would otherwise would not be available in a traditional manual surgical operation.*

<sup>1</sup>Modified from MAKOplasty® Surgical Robot [Internet]. MAKO® Surgical Corp., Fort Lauderdale, FL; cited [June 26, 2015]. Available from: <http://www.makoplasty.com/>.

## 1.2.3 Bone Removal Tools

### 1.2.3.1 Reaming (Low Speed)

Low speed rotational cutting tools, also known as reamers, are used in a variety of orthopaedic surgeries which involve nail insertion into long bones (primarily the tibia) and resurfacing of the bone for joint replacement. An orthopaedic reamer, used for joint replacement, has an end bit of approximately 30 mm in diameter and is used to produce axisymmetric cavities for joint replacement. The reamer design depends primarily on the manufacturing company. Typical reamer design for joint replacement is often comprised of reamer blades, varying blade orientations, and altering the gap between the blades. The rotary speed of the reamer is typically between 250 to 500 revolutions per minute (rpm). Current research studies exploring bone removal using the reamer show high temperatures involved during the surgical procedure that could potentially lead to necrosis [35, 36]. Additionally, previous *in-vitro* studies have found that the design of the reamer (number of blades, spindle speed) can result in varying the temperatures involved [37, 38].

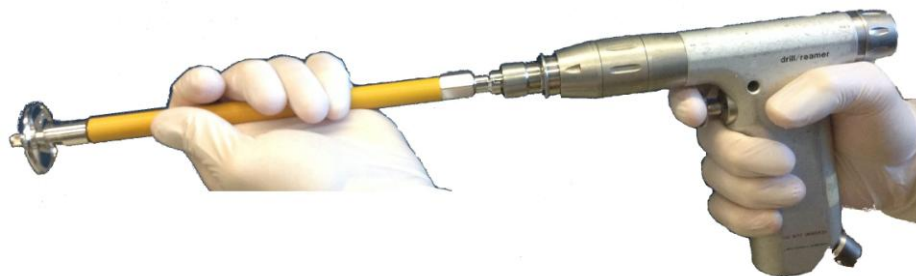


**Figure 1.5: Orthopaedic reamer**

*An orthopaedic reamer/drill with reamer attachment is pictured above. The reamer bit shown is 30 mm in diameter and spins at rotary speed of 250 rpm.*

### 1.2.3.2 Burring (High Speed)

High speed rotary tools, used primarily for burring of the bone, are used in various surgical settings; including orthopaedic and neurotologic applications. The burring tool is designed to be a hand held tool which spins at high rotational speeds during the bone removal process (10,000 to 80,000 rpm). The burring end bit is typically in the range of 2 to 10 mm which allows for more intricate operations to be performed by the burring tool compared to the larger reaming tool. The common high speed burring tool is composed of a motor (handpiece), burring bit, as well as an 'attachment' to cover the shaft of the burr. The design of the tool and bits available depend on the manufacturer. Popular manufactures include Medtronic (Medtronic Inc, Minneapolis, MN) and Anspach (The Anspach Effort, Inc., Palm Beach Gardens, FL). The Medtronic's Midas Rex Legend Stylus system rotates at spindle speeds between 200 to 75,000 rpm and is controlled via an integrated closed loop controller. The Anspach Emax 2 Plus is an alternative burring tool which spins at speeds between 10,000 to 80,000 rpm. Previous *in-vitro* studies have attempted to quantify the temperatures and cutting forces involved within the burring process [39-42].



**Figure 1.6: High speed rotary burring tool**

*The Midas Rex Legend rotary burring tool is pictured above. The burring bit is typically small in diameter (2 to 10 mm) and can spin at speeds of up to 75,000 rpm.*

## 1.3 High Speed Bone Burring Characteristics

To maximize the efficiency of the bone burring process, care must be taken into the choice of process parameters (rotary speed, type of cutter, depth of cut) to reduce the dynamic effects and temperature rises associated with high speed burring. The selection of process parameters has been shown to have an effect on the outcome measurements, such as temperature generation and cutting force [39-42].

### 1.3.1 Process Parameters

The main process parameters used in previous studies that involve a high speed rotary tool for bone burring include [34, 39-41, 43-46]:

- Shape of burring bit
- Diameter of burring bit (mm)
- Rotational speed of the tool (rpm)
- Depth of cut (mm)
- Feed rate (mm/s)
- Cutting track overlap (%)
- Inclination angle (°)
- Tilt angle (°)

The shape of the burring bit varies on the manufacturer. There are two main types of burring bits; fluted and diamond coated. Fluted bits are used to remove larger volume of bone as they have cutting flutes running up the bit. Different shapes of fluted burring bits exist and include: sphere, cylinder, acorn, match and oval (Figure 1.7). Diamond coated bits are commonly spherical in shape and rely on the coating of diamonds on the surface

to abrade the bone. The diameter of the bits range from 1 to 10 mm. The rotational speed of the tool is the speed of the burr measured in revolutions per minute (rpm). Typical speeds of a high speed rotary tool are in the ranges of 10,000 to 80,000 rpm.

The depth of cut (mm) is defined as the thickness of material that is removed with one pass of the burring tool (Figure 1.8). The feed rate (mm/s) of the tool is the linear advancement rate of the tool itself. The burring process of bone, commonly employs very shallow depths of cut (<1 mm) with feed rates in the range of 1 to 10 mm/s [44]. Additionally, cutting track overlap (%) is defined as the overlap of burring paths between successive paths of the burring tool (Figure 1.8).

Inclination and tilt angles ( $^{\circ}$ ) make up the orientation of the tool with respect to the workpiece. The inclination and tilt angle are defined in Figure 1.9. The angle of the tool is of particular importance in the context of surgical procedures due to the limited milling cavities that may be unavoidable. The direction of the cut with respect to the previous burring path (conventional and climb milling) is also of importance when designing a tool path trajectory. Down milling is typically desired as the tool leaves the workpiece with zero force compared to up milling which leaves the workpiece with force on the bit.

The process parameters mentioned above collectively represent those that can be varied in the design of a tool path trajectory. The most effective combinations of parameters, that minimize temperature, forces and vibrations, as well as providing a realistic procedure time would be desirable for implementation in a clinical setting.

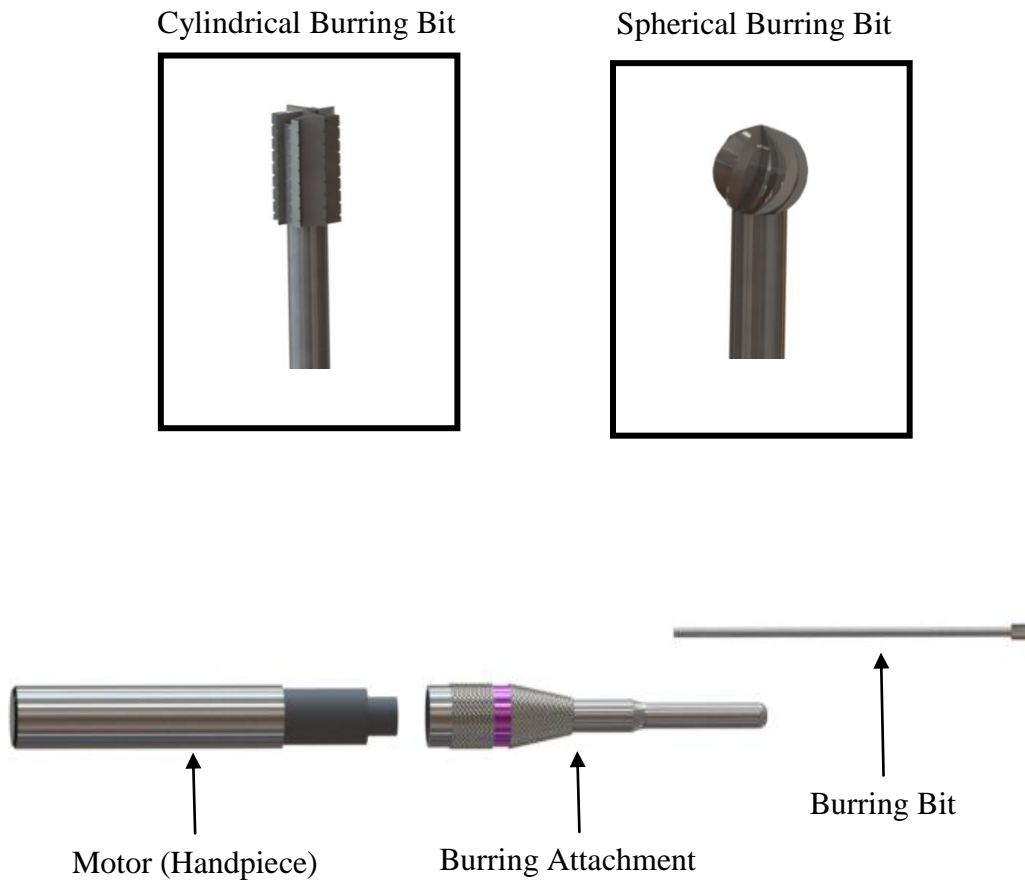


**Figure 1.7: Midas Rex Legend rotary burring tool**

*A CAD rendering of the Midas Rex Legend rotary burring tool is shown above. The burring tool consists of three main components: motor, attachment, and a burring bit. The bits are long and slender (2.35 mm shank diameter) and come in various sizes dependent on the manufacturer. Two common bits are the cylindrical and spherical burring bit, depicted in the insets above.*



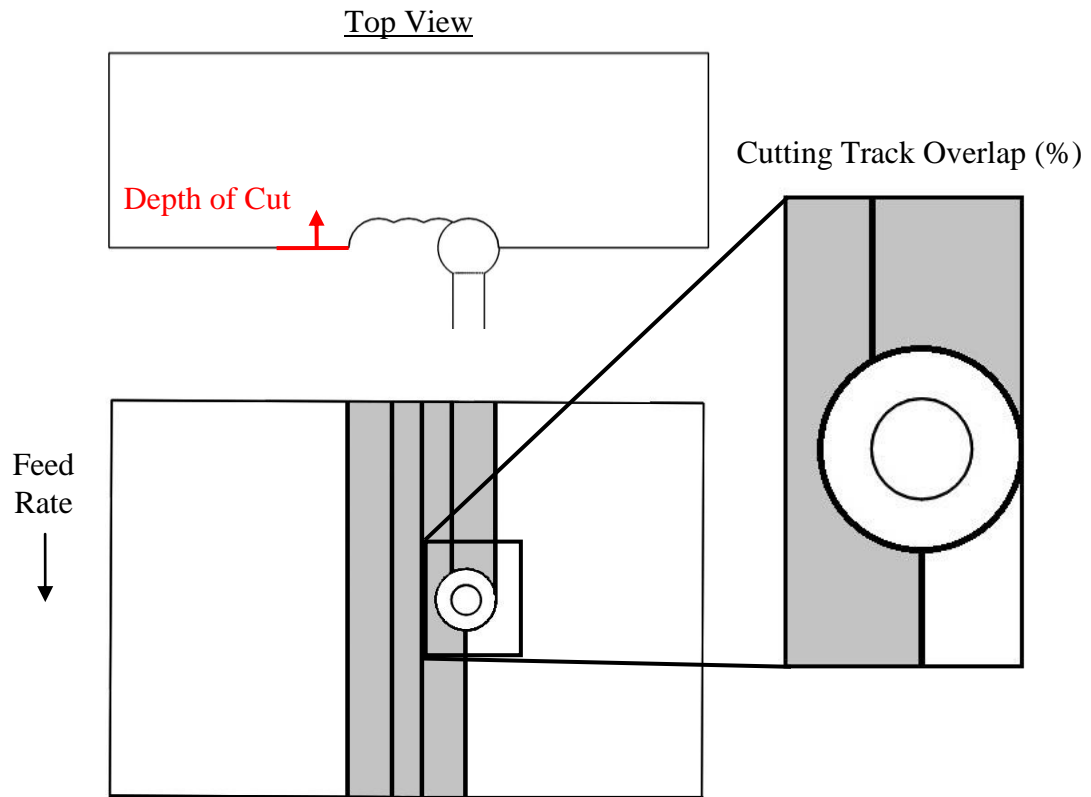


**Figure 1.8: Design parameters used for bone burring (depth of cut + overlap)**

*Characteristic parameters (overlap and depth of cut) associated with the bone burring process are illustrated above. Depth of cut (mm) is defined as the thickness of the material that is removed during a burring run. Overlap is the % of overlap between successive cutting tracks (shown in the inset is 50% overlap).*

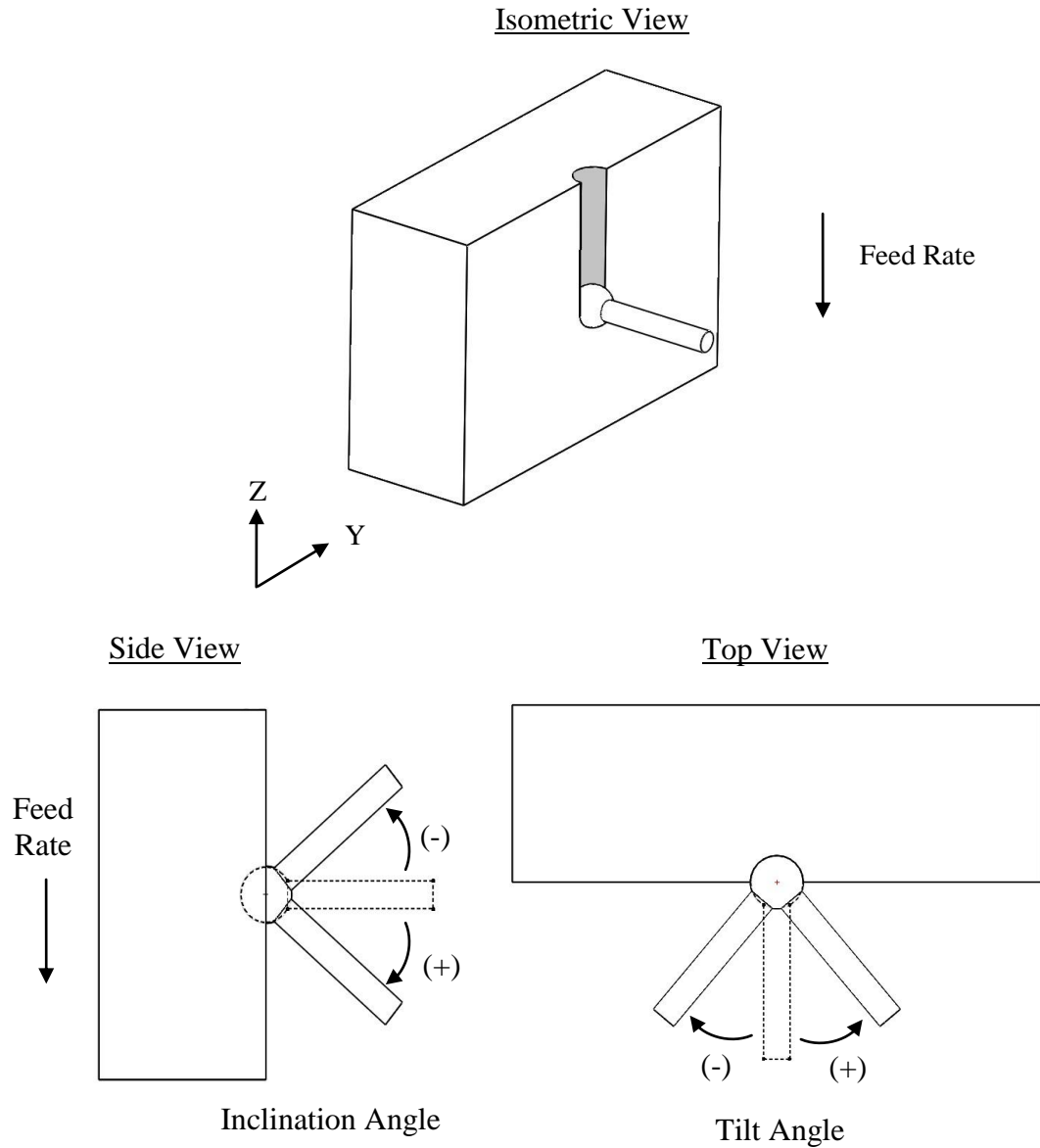


**Figure 1.9: Design parameters used for bone burring (inclination angle + tilt angle)**

*Characteristic parameters (inclination and tilt angle) associated with the bone burring process are illustrated above. Shown in the isometric view is the tool oriented at a normal to the workpiece face. Inclination angle is the rotation of the tool about the Y axis. Tilt angle refers to rotation of the tool about the Z axis.*

### 1.3.2 Outcome Measurements

Various outcome measurements are used to evaluate the process parameters in terms of safety and accuracy of the burring process. To quantify the process outcomes, various transducers are instrumented to monitor the burring process. Relevant methods to instrument and quantify the associated outcome measurements are discussed in the following subsections.

#### 1.3.2.1 Cutting Force

Cutting force is the total force exerted in three planes by the burring tool in order to remove material from the workpiece. Cutting force is important in the context of the burring process as it can be used in the design of robotic systems to optimize accuracy and safety of the procedure [41, 46]. Experimental methods, involving bone burring, have been performed using strain measurements to quantify the cutting force between the workpiece and tool [41, 43, 46].

Dillon *et al.* selected a force sensing device (ATI Six-Axis Sensor System) which was mounted between the robotic arm and burring tool [41]. Federspil *et al.* selected a force and torque sensor (JR-3 Inc., Woodland, CA) which had a range of 63 N and was placed between the robot arm and burr [43]. Sugita *et al.* also selected a 6 DOF force sensor installed in the spindle with rated values of 400N, 800N, and 40 Nm [46]. An additional method to measure the cutting force during a burring procedure was performed by Plaskos *et al.* which used a piezoelectric dynamometer. The dynamometer was placed underneath the clamp that held specimen in place [45].

To quantify cutting force and allow for comparison between process parameters, Dillon *et al.* and Plaskos *et al.* averaged the cutting forces from the entry to exit points of the burring trial [41, 45]. Federspil *et al.* and Sugita *et al.* did not compute an average cutting force, as the authors reported only a single run to validate their developed automated systems [43, 46].

### 1.3.2.2 Vibration

The vibration generated due to the burring procedure has a direct influence on the accuracy and surface finish of the cut. Additionally, vibration generated may introduce noise into the system that may be undesirable for other transducers monitoring the burring process.

To knowledge, no previous experimental study has directly measured the vibration of the tool during a bone burring process. Indirect attempts have been made by Denis *et al.* by measuring the surface flatness, which is a product of the dynamic effects of the tool [39]. Federspil *et al.* also measured the vibrations of a skull during robotic burring using a piezoelectric crystal that was mounted to the workpiece [34]. Vibrations of a dental handpiece have been previously studied, primarily in the context of hand-arm vibration exposure to dentists using high speed rotary dental tools [47, 48]. Rytönen *et al.* mounted a piezoelectric charge accelerometer (B&K 4393) to the handpiece using a fabricated adapter and subsequently glued the adapter to the handpiece [48]. Additional research has also been devoted to quantifying harmful effects resulting from hand-arm vibration from a biomechanics perspective [49-51]. The authors typically mount

piezoelectric accelerometers to the tool to report the total vibration over a certain bandwidth of frequencies for a duration of time [49-51].

To quantify the vibration of a single burring trial, Federspil *et al.* reported the measurements quantified by an accelerometer mounted on the workpiece over the entire trial (magnitudes less than 1.5 g) [34]. As only one trial was performed within the mentioned experimental trial, no protocol to allow for comparison of the accelerometer measurements was taken. In other applications for quantifying the dynamic effects of hand held tools, and allow for comparisons to be quantified, a weighted vibration is generally calculated dependent on a bandwidth of frequencies that is important to the author [48-51].

### 1.3.2.3 Temperature

In a conventional machining process, a bulk of the energy consumed is converted into heat [52]. If high temperatures were to occur during a bone resurfacing procedure, specifically bone burring, thermal damage (osteonecrosis) could occur. If osteonecrosis occurs, the bone would lose its ability to remodel and repair itself post surgery. This loss of remodeling has been linked to loosening in joint replacements which in turn may require a subsequent revision surgery [53]. Therefore, it is vital to quantify process parameters that may lead to osteonecrosis in order to avoid them.

Experimental methods have been developed to measure temperature generation during the bone removal process. Temperature systems can be broken into two distinct methods: contact and non-contact. The contact method commonly involves a thermocouple or resistance temperature detector (RTD) that is inserted into the bone or workpiece. The

contact method of quantifying temperature of the workpiece has been implemented primarily in quantifying the temperature of the bone during a drilling process [54-56]. More relevant to bone burring, common measurement systems used to quantify temperature has been a non-contact method of an infrared pyrometer [39, 40]. Shin *et al.* selected an IKS-T14-06 model from Infrapoint<sup>®</sup> with accuracy of 1 °C and trailed the burring process by 10 and 20 mm; whereas, Denis *et al.* selected a Raytek ThermalertTX pyrometer with accuracy of 1.5 °C. Infrared cameras have also been adapted to measure temperature in *in-vivo* joint resurfacing procedures [35, 36].

To quantify temperature and allow for comparison between multiple burring trials, the average temperature of a burring trail was calculated from the start to exit points of the process [39, 40].

#### 1.4 State-of-the-Art in Quantifying the Bone Burring Process

Previous studies have aimed to characterize the process parameters involved in the bone burring process [34, 39-41, 43-46]. These studies have investigated the effects of varying the process parameters on temperature generation and cutting force applied in both manual and robotic bone removal procedures. The clinical relevance of the studies vary dependent on the field but are primarily performed in the orthopaedic and neurotological fields with a main goal of finding an optimal combination of parameters to minimize or maximize the outcome measurement [34, 39-41, 43-46].

Shin *et al.* and Denis *et al.* examined the effects of varying the process parameters and used temperature as an outcome measurement [39, 40]. Both studies used an infrared pyrometer to measure the temperature of the workpiece of a freshly burred specimen.

Denis *et al.* investigated the influence of feed per tooth and milling speed using a high speed milling machine [39]. It was found that increasing the feed per tooth and decreasing the milling speed altered the temperature experienced by the bone. The burring parameters were varied between various feed rates and rotational speeds of the tool between 10,000 to 40,000 rpm. Denis *et al.* recommended that in order to limit rises in temperature, the feed rate per tooth should be increased and the milling speed should be decreased [39].

A similar study was performed by Shin *et al.* which investigated temperature rise using a spherical burr [40]. Feed rates were adjusted at levels of 2, 3.2, 5.5, and 9.8 mm/s. The depth of cut was adjusted from 0.3, 0.5, and 1 mm and the burring was performed in a range of 30,000 to 50,000 rpm. Shin *et al.* concluded that increasing feed rate and decreasing the depth of cut was desirable to reduce thermal damage during bone burring [40].

Previous studies have also varied the process parameters and examined the effects they have on the applied cutting force. Plaskos *et al.* aimed to quantify the cutting forces involved in a high speed burring process with very shallow depths of cut [45]. The authors demonstrated that the cutting forces are significantly different in high speed machining processes compared to a traditional means of machining using lower speeds [45].

Dillon *et al.* investigated the effects of choosing certain combinations of parameters for use in a robotic mastoidectomy [41]. The authors' combination of parameters included measuring the cutting force for several surgical burr types, drill angles, depths of cut,

cutting velocities, and bone types (temporal bone and the mastoid). The burring process was conducted using an autonomous robot and used human temporal bone specimens. The authors concluded that certain combination of parameters were more efficient than others and high linear cutting velocities should be combined with shallow depths of cut for optimal performance. The authors also suggested the possibility of using different parameters within different regions of bone [41].

Arbabtafti *et al.* performed experimental measurements in order to validate a haptic feedback system they developed. The effects of feed rate, spindle speed, and drill angle were examined with respect to their effects on resulting burring forces. Feed rates in the range of 1.4 to 3 mm/s, spindle speeds between 15,000 to 31,000 rpm and drill angles of 22 to 63° were chosen as the process parameters. Arbabtafti *et al.* reported that increasing feed rate and decreasing rotational speed resulted in an increase of burring force.

In addition to the studies that varied certain process parameters to view the effects, other authors have attempted to quantify the burring process dependent on their application, primarily for feedback controllers for automated burring. Sugita *et al.* developed a force-feedback control loop to monitor forces during burring and to select an optimal feed rate to reduce temperature generation and surgical procedure time [46]. Federspil *et al.* demonstrated the feasibility of automating the burring process on temporal bone. The authors through separate studies, detail a burring path strategy and evaluated it using various feedback controllers [34, 43]. The study reports the first development of an *in-vitro* automated burring robot for use in creating cavities in the temporal bone.



## 1.5 Rationale

Experimental quantification of the bone removal characteristics associated with bone burring represents a desirable outcome for an array of surgical applications, manual or automated, and also in the design of the burring tools themselves. Optimizing the burring process, via the selection of process parameters offers the potential to improve the success rate of clinical procedures by limiting osteonecrosis, which may occur with selection of suboptimal parameters [39, 40, 46]. Subsequently, as robotic technology continues to emerge, the ability to control process parameters becomes less challenging.

Previous authors have identified the importance of experimentally quantifying the bone removal characteristics associated with bone removal [34, 39-41, 43-46]. However, as the burring process itself offers a large array of process parameters (depth of cut, cutting overlap, rotational speed, feed rate, angle of tool, type and diameter of tool) and a vast amount of levels within each process parameter, a full factorial analysis involving a bulk of the process parameters has not been undertaken. Previous authors were required to fix certain process parameters to levels within the machining process, which in turn limits the amount of combinations that were tested. For example, Shin *et al.* fixed the burring process parameters by selecting a 9.1 mm sphere burr oriented at a normal to the workpiece face and a fully immersed burring path [40]. The experimental analysis conducted by Shin *et al.* included various feed rates and depths of cut and the authors recommended a suitable combination of parameters to avoid thermal damage to the bone [40]. However, the combinations of parameters suggested are exclusive to the fixed parameters.

An additional method to reduce the sample size of the experimental protocol is to perform a fractional factorial experimental design. A fractional factorial design reduces the amount of observations or machining trials typically required by selecting certain process parameters and evaluating the effects within the selected subsections [41]. Although the fractional factorial design proves effective at providing trends within the main effects, no indications into the interactions are provided. A full factorial experimental design is advantageous as all testing conditions or combinations of process parameters are analyzed and does not alias any effects which may be found in the fractional factorial analysis. Therefore, by performing a full factorial statistical analysis, no combination of parameters are missed which may lead to optimal or suboptimal bone burring outcomes.

Not only is the selection of process parameters important, it is equally significant to quantify their efficiency in the form of an appropriate outcome measurement. Although previous authors have contributed to quantifying the temperature generation and cutting force associated with the bone burring process; an experimental study to quantify the dynamic effects of the tool has yet to be undertaken. The selection of the outcome measurement (*i.e.*, temperature generation, forces experienced, and dynamic effects) is essential as it provides the rationale in selection of process parameters that are to be optimal or suboptimal. With selection of only one outcome measurement, a thorough understanding from multiple aspects of the outcome measurements and the tradeoffs that ensue may not be fully understood. Previous studies commonly select only one outcome measurement, typically force or temperature, and proceeded to deem certain process parameters optimal in regards to the single measurement [39, 41, 42, 46]. However, the

use of only one outcome measurement for rationale in selection of process parameters may prove consequential as the selection may be optimal for one outcome measurement but not another.

Although previous authors have contributed to experimentally quantifying the characteristics of bone burring, a gap still remains with respect to understanding how the process parameters interact with one another. Specifically, the tradeoffs in selection of process parameters and their efficiency quantified using multiple outcome measurements. Furthermore, previous studies have not quantified the dynamic effects of the tool during a bone burring procedure.

Advancements made by a full factorial experimental protocol that involves varying the process parameters and evaluating the outcome measurements of force, temperature and vibration, can lead to a fuller understanding of the burring process. The understanding of these tradeoffs can subsequently be applied to multiple applications of interest including: knowledge for clinical implementation, tool path trajectory planning, controllers for automated bone burring systems, design of surgical simulators, and design of the tools involved.

## 1.6 Objectives and Hypotheses

The overall goal of this research was to quantify the characteristics of bone burring (*i.e.*, temperature generation, forces experienced, and dynamic effects) for clinical implementation. In pursuit of a thorough understanding of the effects of the process parameters in the bone burring operation, three specific objectives were explored as part of this research project. The corresponding hypothesis follows each objective.

**Objective 1:** To develop and design an experimental apparatus with capability to simultaneously quantify cutting force, temperature, and vibration. As well, the experimental apparatus must offer a means to precisely control the various process parameters associated with the burring process. The experimental apparatus must also produce burring trials with high repeatability coupled with a high signal-to-noise ratio, comparable to that of previously published experimental studies.

**Hypothesis 1:** It was hypothesized that an experimental apparatus can be designed to control and manipulate the process parameters involved in a bone burring procedure, and measure the subsequent cutting force, temperature, and vibration of the system. The experimental apparatus must provide a repeatability ( $\pm 1$  standard deviation) of:  $F_x$ ,  $F_y$ , and  $F_z < 0.3$  N, temperature  $< 2.5$  °C, vibration  $< 0.5$  g-rms, and signal-to-noise  $> 5$  dB.

**Objective 2:** To perform a full factorial analysis to quantify the main effects and interdependencies of the process parameters involved in bone burring. The developed experimental apparatus designed in objective 1 will be used to vary the process parameters and quantify the outcome measurements using a sawbone analog as a workpiece. An appropriate statistical analysis will be performed on the outcome measurements and the results of the statistical analysis should give indication to a small set of combination parameters that are deemed to be optimal and suboptimal.

**Hypothesis 2:** It was hypothesized that varying certain process parameters would result in statistically significant differences in the outcome measurements of cutting force, temperature, and vibration. Based on previous findings, it was expected that process parameters that lead to high material removal rates would increase cutting force,

temperature and vibration [40, 41]. It was also believed that certain combinations of process parameters would result in optimal or suboptimal means of performing the burring process.

**Objective 3:** To validate optimal and suboptimal combinations of process parameters on cancellous bone. A cadaveric specimen will be selected that provides a realistic representation of human bone for bone burring. The developed apparatus will be used to quantify the outcome measurements for a statistical analysis to be performed and evaluate the optimal and suboptimal process parameters.

**Hypothesis 3:** It was hypothesized that the optimal and suboptimal combinations of parameters would produce similar results in cancellous bone. It was also expected that the trends established in objective 2 would be transferrable to burring in a cadaveric specimen.

## 1.7 Thesis Overview

Chapter 2 describes the design and development of an experimental apparatus that has the capability to precisely control specific process parameters, and to perform concurrent measurements of three outputs associated with the bone burring process (*i.e.*, cutting force, vibration, and temperature). Chapter 3 presents a full factorial analysis with the various process parameters and an evaluation of their effects on the outcome measurements in a sawbone analog. Chapter 4 expands on the analysis in Chapter 3 by identifying and selecting certain combinations of process parameters that are hypothesized to produce optimal or suboptimal process outputs. Chapter 5 presents a validation of the experimental apparatus from Chapter 2, and the method of quantifying

process parameter's effects from Chapter 3, by using the subsets of parameters determined in Chapter 4 on cadaveric porcine specimens. A general discussion and summary of the research is found within Chapter 6, as well as concluding statements and suggested future work.

## Chapter 2 - Development of Experimental Apparatus for Investigation of Bone Burring

*OVERVIEW: Experimental quantification of the characteristics associated with bone burring represents a desirable outcome from the perspective of design of bone burring tools as well as control feedback loops involved in orthopaedic robotic systems. The scope of the current chapter is focused on the development of an experimental apparatus capable to assess the parameters associated with light bone removal operations. The developed system allows for concurrent measurement of the three outputs associated with the bone removal process (cutting force, vibration, and temperature) as a function of various machining-specific parameters such as cutting tool's size and type, rotary speed, feed rate, depth of cut as well as the orientation of the tool with respect to the workpiece. A representative sample of the outcome measurements is presented in this chapter as a demonstration of the capabilities of the developed device.*

### 2.1 Process Parameters and Dependent Variables

An experimental apparatus was designed to quantify essential characteristic parameters associated with the bone burring process. For the purpose of this study, the following variables were regarded as the controlled inputs of bone burring:

- Shape of burring bit
- Diameter of burring bit (mm)

- Rotational speed of the tool (rpm)
- Depth of cut (mm)
- Feed rate (mm/s)
- Cutting track overlap (%)
- Inclination angle (°)
- Tilt angle (°)

The above process parameters encompass all of the machining-specific parameters associated with the bone burring process used in previous studies [34, 39-46]. A more in depth explanation of each of the process parameters can be found in section 1.3.1.

Measurands were chosen to quantify and evaluate the effects of the burring parameters.

The measurands selected to evaluate the performance of the bone removal process were:

- Three-axial cutting force components (N)
- Vibro-accelerations ( $\text{m/s}^2$ )
- Superficial temperature of specimen (°C)

Cutting force between the burring tool and the workpiece is an essential component in the design of robotic systems to optimize accuracy of the cut and safety of the patient. Process parameters that lead to low cutting forces or below a certain threshold would be viewed as ideal parameters in which to carry out the burring process. Previous studies have investigated the cutting forces involved in joint resurfacing procedures, predominately for implementation into control feedback loops for robotic systems [34, 39, 41, 43, 45]. The quantification of cutting forces has also been used for validation of haptic feed back systems [42].



The vibrations generated due to the burring procedure have a direct influence on accuracy of the cut. Additionally, in the context of control feedback loops for robotic systems, the vibrations generated may introduce noise into the system that may influence other transducers monitoring the cutting process. No study has yet to quantify the dynamic effects of the burring tool during the burring process.

Bone resurfacing procedures (*i.e.* bone burring) may cause thermal damage (osteonecrosis) to the bone due to the high temperature generations that are associated with the procedures. Therefore, to avoid causing bone damage, it is vital to quantify process parameters which may lead to osteonecrosis. These parameters should be avoided to minimize the risk for a revision surgery. Attempts to quantify the effects of changing certain process parameters have been investigated using experimental measurements [39, 40, 44, 46].

The structure of the developed experimental apparatus consists of the following: burring tool mount, workpiece clamp, and a servo-hydraulic actuator. Additional details regarding each of the components are provided in the following sections.

## 2.2 Experimental Apparatus

### 2.2.1 Burring Tool Holder

The Midas Rex Legend<sup>®</sup> rotary burring tool (Medtronic Inc, Minneapolis, Minnesota) was selected as the orthopaedic bone burring system. The Midas Rex Legend model is a clinically relevant burring tool used by surgeons predominately in neurotology resurfacing procedures. The rotational speed of the tool ranges from 200 to 75,000 rpm and is controlled by an integrated closed-loop controller. The rationale behind selection of the Midas Rex Legend rotary burring tool for the current study was based primarily on the clinical relevance of the tool.

The translational motion required between the cutting tool and the workpiece was supplied by means of an Instron<sup>®</sup> actuator to which the bone removal system was securely attached. The orientation of the burring tool, with respect to the workpiece, was determined by two different angles: inclination and tilt, respectively. While the tilt of the cutting tool with respect of the workpiece normal at the cutter contact point (*e.g.* the theoretical contact point between the tool and workpiece) was performed in a horizontal plane by means of the Instron kinematics, its inclination in the vertical plane enclosing the workpiece normal passing through the cutter contact point was ensured by means of the circular pattern of holes depicted in Figure 2.1. These holes allow for an incremental change in the inclination of the tool between  $-45^{\circ}$  and  $45^{\circ}$  ( $5^{\circ}$  increments). The diameter of the circular pattern of holes align with the length of the burring tool; such that, at any angle, the center of the end tooling bit remains stationary (Figure 2.1). Detailed drawings of the fabricated components associated with the burring tool holder can be found in Appendix A.

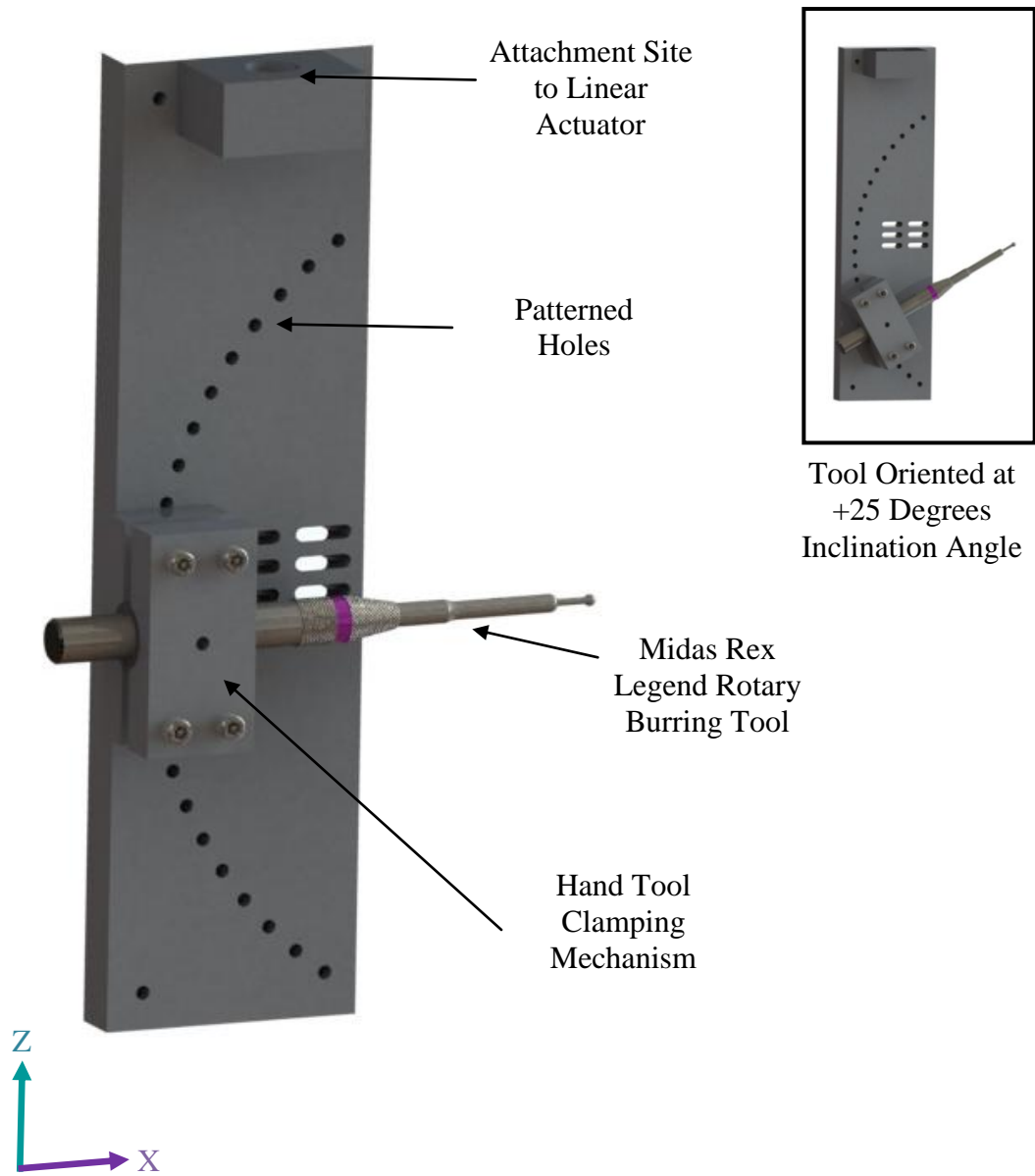


**Figure 2.1: Tool holder with adjustable orientation**

*The Midas Rex Legend<sup>®</sup> rotary burring tool (Medtronic Inc, Minneapolis, Minnesota) oriented at 0 degrees inclination and fastened in place on the tool holder apparatus. An inset of the tool positioned at +25 degrees inclination is also shown to illustrate the apparatus' ability to vary the inclination angle.*

### 2.2.2 Workpiece Positioning

The workpiece positioning system was designed to maintain the workpiece in a fixed spatial position with respect to the Instron frame (Figure 2.2). The primary component ensuring the location, support as well as clamping of the prismatic samples was a conventional tool shop vise. This allowed for the interchangeability of samples that could be gripped in place using the vise.

To ensure that the workpiece was perpendicular to the feed rate of the tool; a series of nuts were fastened between the vise and the aluminum back plate. The addition of nuts between the vise and back plate allowed for the plane parallel to the workpiece face to be dependent on the location of the nuts. Four lock nuts were then used to fasten the vise in plane, locking any relative movement between the vise and tool.

The workpiece fixture was mounted on a two-axis stage which allowed for the depth of cut and overlap of cut to be adjusted. Detailed drawings of the fabricated components associated with the workpiece positioning system can be found in Appendix A.

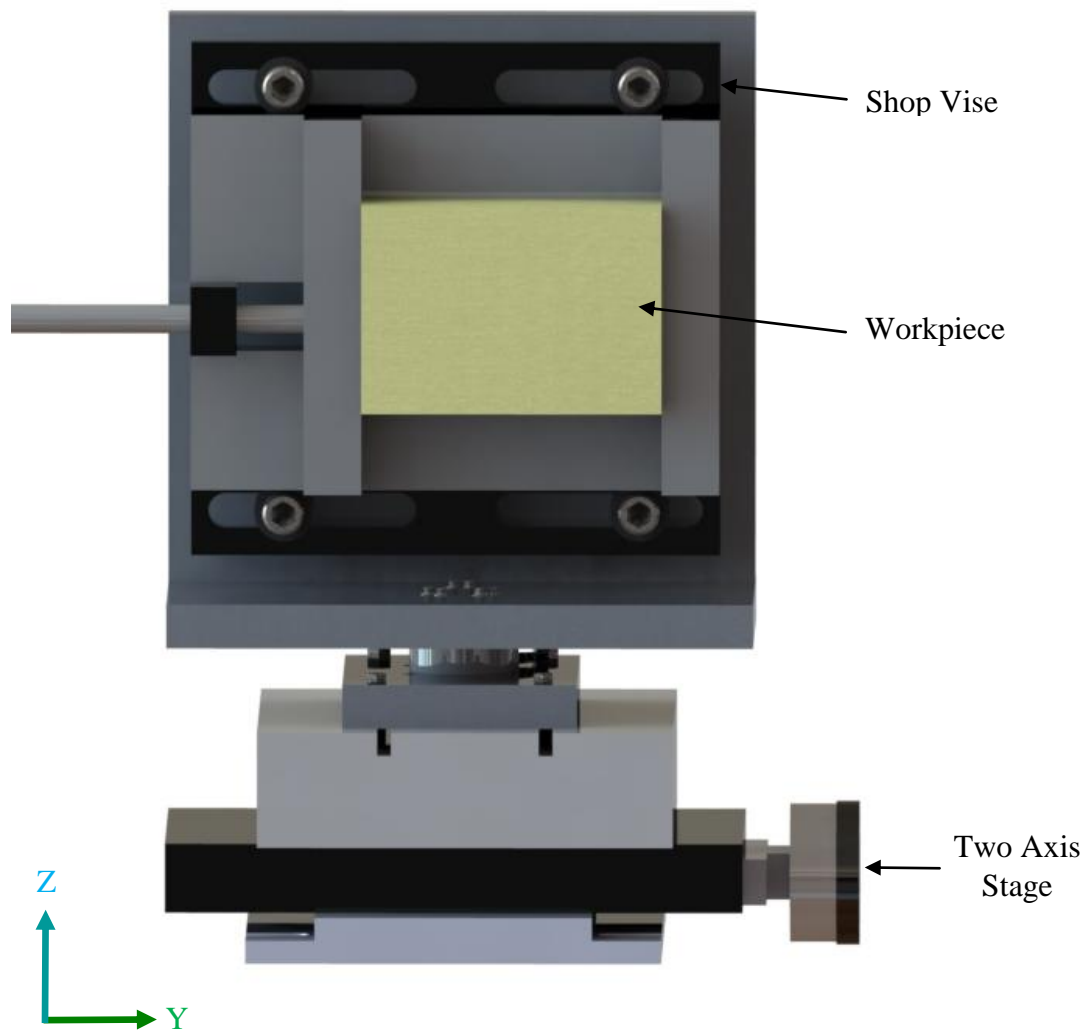


**Figure 2.2: Workpiece positioning system with adjustable horizontal position**  
*The workpiece positioning system used a shop vise to clamp the workpiece in place. A two axis stage was used to control the depth of cut and overlap of the burring process.*

## 2.3 Measurement of Dependent Variables

### 2.3.1 Data Acquisition System

To ensure the correct time synchronization of all three measurands, all data collected by the sensors was supplied to an USB-6210 data acquisition unit (National Instruments Corporation, Austin, Texas) (Figure 2.3). The measurands were time stamped to allow for simultaneous comparison of the signals. NI LabVIEW software was used for collection and post-processing of the data that was sampled at 25 kHz for all transducers. Specification sheets of the transducers can be found in Appendix B.

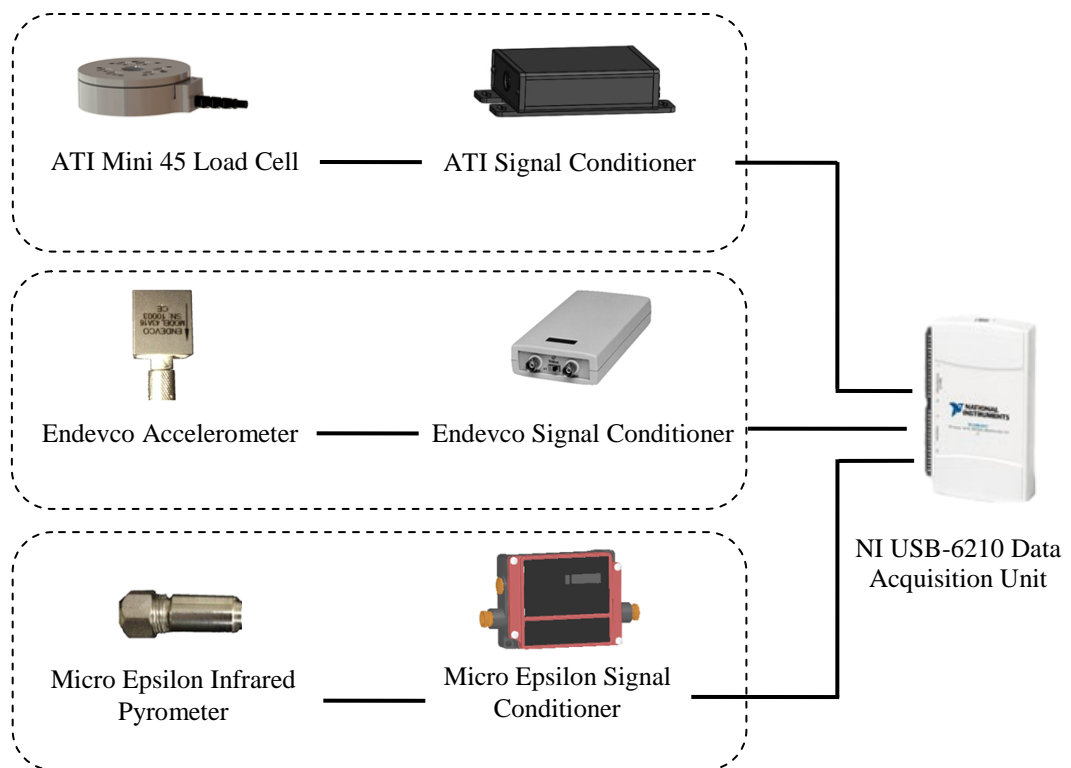


**Figure 2.3: Data acquisition system**

*Three transducers (load cell, accelerometer, and infrared pyrometer) were used to quantify the dependent variables. The transducers were integrated onto the tool holder and workpiece apparatus and sampled via a NI-USB data acquisition unit.*

### 2.3.2 Cutting Force Measurement

A three-axis load cell (Mini45, ATI Technologies, Markham, Ontario) with a resolution of 1/16 N was used to acquire the triaxial components of the cutting force. The Mini 45 load cell was selected due to its suitable range ( $\pm 145$  N) associated with the burring procedure as measured by previous studies and its ability to measure force in three planes [41, 42, 46]. The load cell was instrumented between the workholding device and the two-axis stage (Figure 2.4). A double Butterworth low pass filter of 10 Hz was applied on the cutting force signal that was decimated at 1 kHz for post-processing purposes.

Six voltages supplied by the strain gauges instrumented within the load cell were sampled by the data acquisition unit. A transformation matrix, supplied by the manufacturer, was applied to the voltages to transform the voltages into forces. Forces in the X, Y, and Z direction were recorded. The axis of the load cell are described by the following axis:

Z- direction: Parallel to feed direction of burring tool

X-direction: Normal to workpiece face

Y-direction: Orthogonal to both Z and X (parallel to workpiece face)

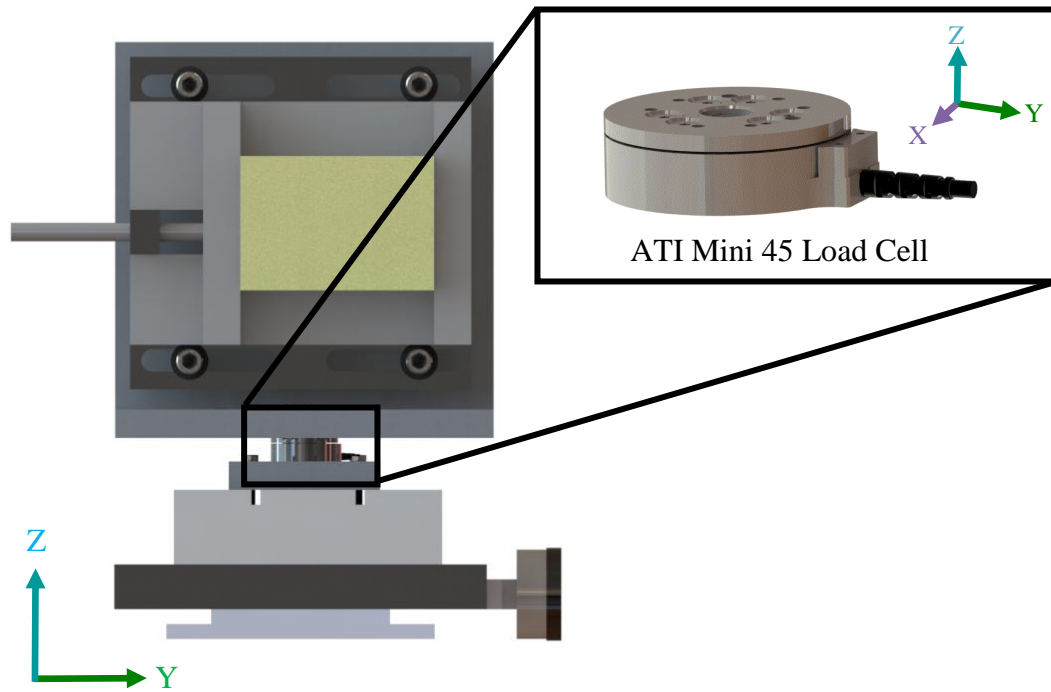


**Figure 2.4: ATI 3-axis load cell placement**

*A three-axis load cell (shown in the inset) was instrumented between the shop vise and two axis stage. The load cell was used to capture the cutting force of the burring process.*



### 2.3.3 Vibration Measurement

A single-axis piezoelectric accelerometer (Endevco<sup>®</sup> model 42A16, Meggitt Sensing Systems, Fribourg, Switzerland) was used in dynamic data acquisition (Figure 2.5). To monitor the dynamic effects of the system via an accelerometer, the accelerometer must be mounted to the object. As indicated by ISO 5349, the addition of mass caused by the accelerometer, can affect how the object vibrates [57]. A piezoelectric accelerometer was selected due to its light weight properties (8 grams). The accelerometer was stud mounted to a custom fabricated shaft collar which was in turn mounted to the burring tool (Figure 2.5). The relevant technical specifications of the accelerometer are:  $\pm 50$  g range, 100 mV/g sensitivity, and an amplitude response ( $\pm 5\%$ ) of 1 to 10 kHz. The accelerometer was coupled with a power supply and signal conditioner (Model 4416B Endevco<sup>®</sup>). A double Butterworth low pass filter of 10 kHz was applied to the accelerometer.

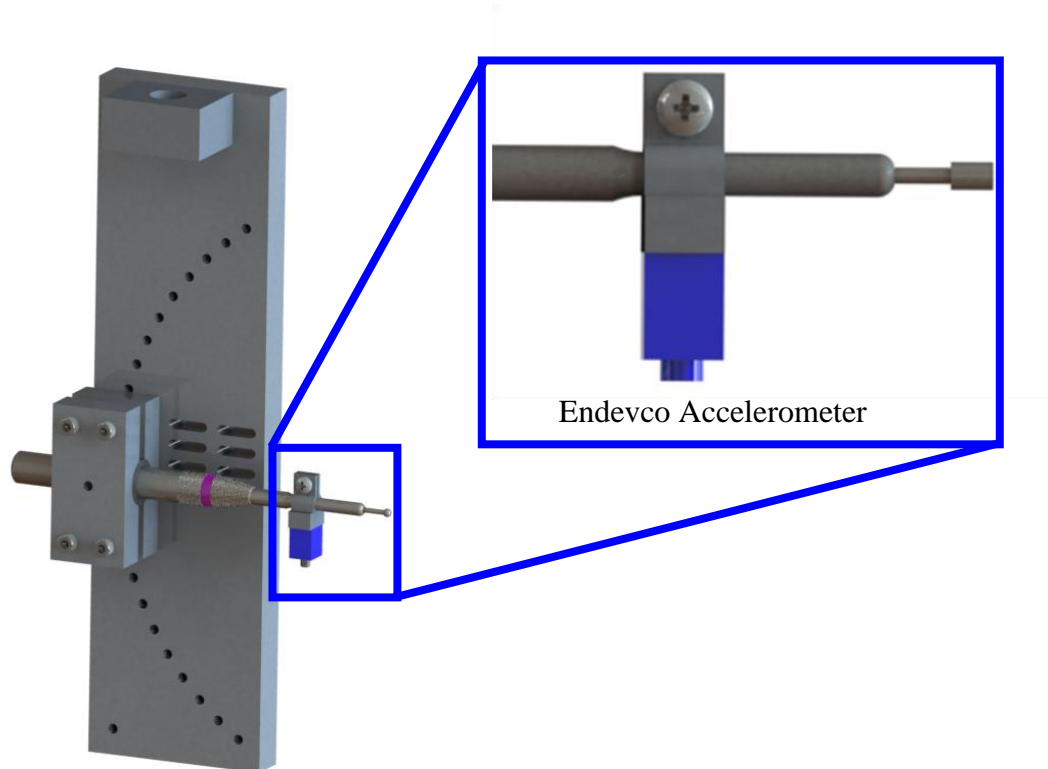


**Figure 2.5: Uni-axial Endevco accelerometer placement**

*The single DOF accelerometer (shown above in blue) was stud mounted to a custom fabricated shaft collar, to capture the vertical (e.g. parallel to tool feed) vibrations of the tool holding system.*

### 2.3.4 Temperature Measurement

An infrared pyrometer (Micro-Epsilon, Model CT-SF02, Raleigh, North Carolina), was used for temperature measurement. An infrared pyrometer was selected as it provides a non-contact means of temperature measurement. A non-contact method has advantages over traditional contact methods (*i.e.* thermocouple) as the workpiece/bone does not need to be altered by placement of the transducer. Additionally, the non-contact method provides a less strenuous means of measuring successive burring paths, as the pyrometer does not need to be recalibrated based on the position of the measurement with respect to the sensor. The infrared pyrometer selected provides an accuracy of 1°C and resolution of 0.1°C. As the width of cutting channels associated with "light resurfacing" procedures can be very small (approximately 2 to 6 mm), a CF02 lens was added to the pyrometer to reduce the spot size to 2.4 mm at a standoff distance of 30 mm. The main rationale in selection of the Micro-Epsilon infrared pyrometer and lens was due to the capability to produce such a small measurement spot size.

The infrared pyrometer was instrumented to measure the cutting track of the workpiece immediately after the resurfacing. Although the ideal measurement of temperature should happen at the cutter contact point, this optimal position is permanently occluded by the cutting tool itself. Therefore, the pyrometer was focused on an area located immediately behind the cutting tool (Figure 2.6).

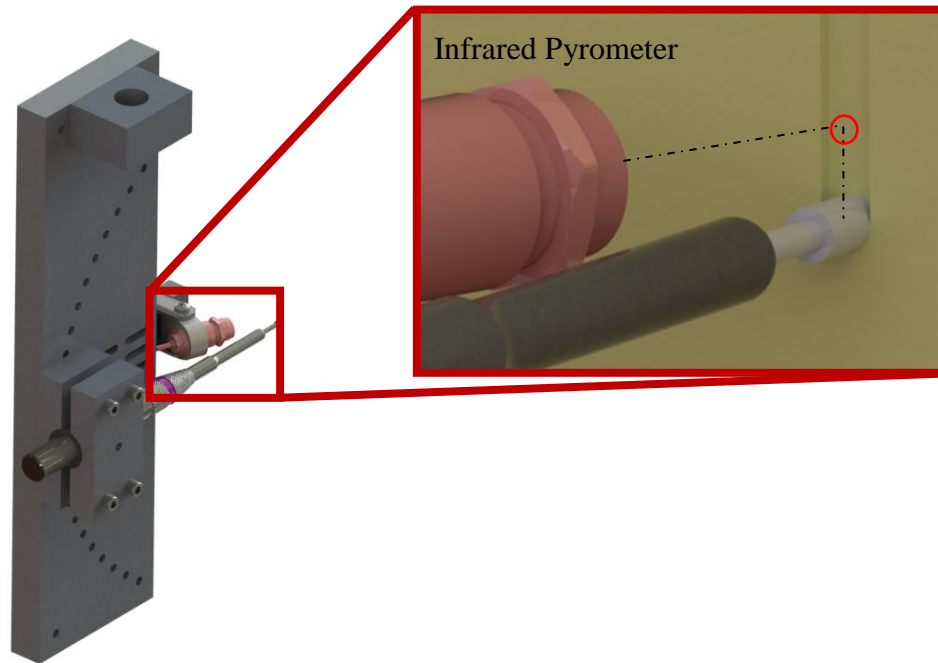


**Figure 2.6: Infrared pyrometer placement**

*The pyrometer (shown above in red) was instrumented to capture the post-cutting surface temperature and was mounted in a position to ensure a direct line of sight to the machined track located immediately behind the cutting tool. A sample cutting track is shown in the inset for visual purposes to illustrate the lagging measuring spot of the pyrometer during a burring trail.*

## 2.4 Sample Experiment

Pre-testing verification of the experimental apparatus was performed to ensure the accuracy of the developed apparatus. The procedure and results of these studies can be found in Appendix C. A list of the trails performed in the pre-testing verification include:

- Noise testing of all transducers
- Depth of cut calibration
- Load cell measurement verification
- Effect of time between successive burring trials on temperature measurements
- Alignment of pyrometer

Following the pre-testing verification of the experimental apparatus, the following parameters were used for a sample cut with the developed apparatus:

- Rotational speed of the tool: 45,000 rpm
- Tool type: spherical burring tool of 6 mm diameter
- Depth of cut: 1.0 mm
- Feed rate: 6 mm/s
- Cutting track overlap: 50%
- Inclination angle: 0°
- Tilt angle: 45°

For the testing and validation purposes of the present study, cancellous-grade sawbone was chosen as the workpiece material since it ensures a uniform and consistent biomechanical structure [58]. In agreement with the overall context of the present study,

the selected sawbone has a density of  $0.32 \text{ g/cm}^3$  which is comparable to that of a healthy joint bone [27].

Under these cutting conditions, a representative sample of the pyrometer, load cell and accelerometer measurements is presented in Figure 2.7. Depending on the status of the cutting tool as well as its relative position with respect to the workpiece, the plots indicate that the cutter could be either off, disengaged/idling or engaged in a cut. As such, all subsequent results will only be discussed in the context of the engaged state of the tool. Furthermore, during the bone removal phase associated with tool/workpiece engagement, it can be noticed that a stable cutting regime is attained when the tool has become fully engaged with the material and this should preclude the start and end portions of the cut when the tool is less than the diameter of the tool away from the material boundaries. A fast Fourier transform (FFT) was performed on the stable regime of the vibration data and is presented in Figure 2.8.

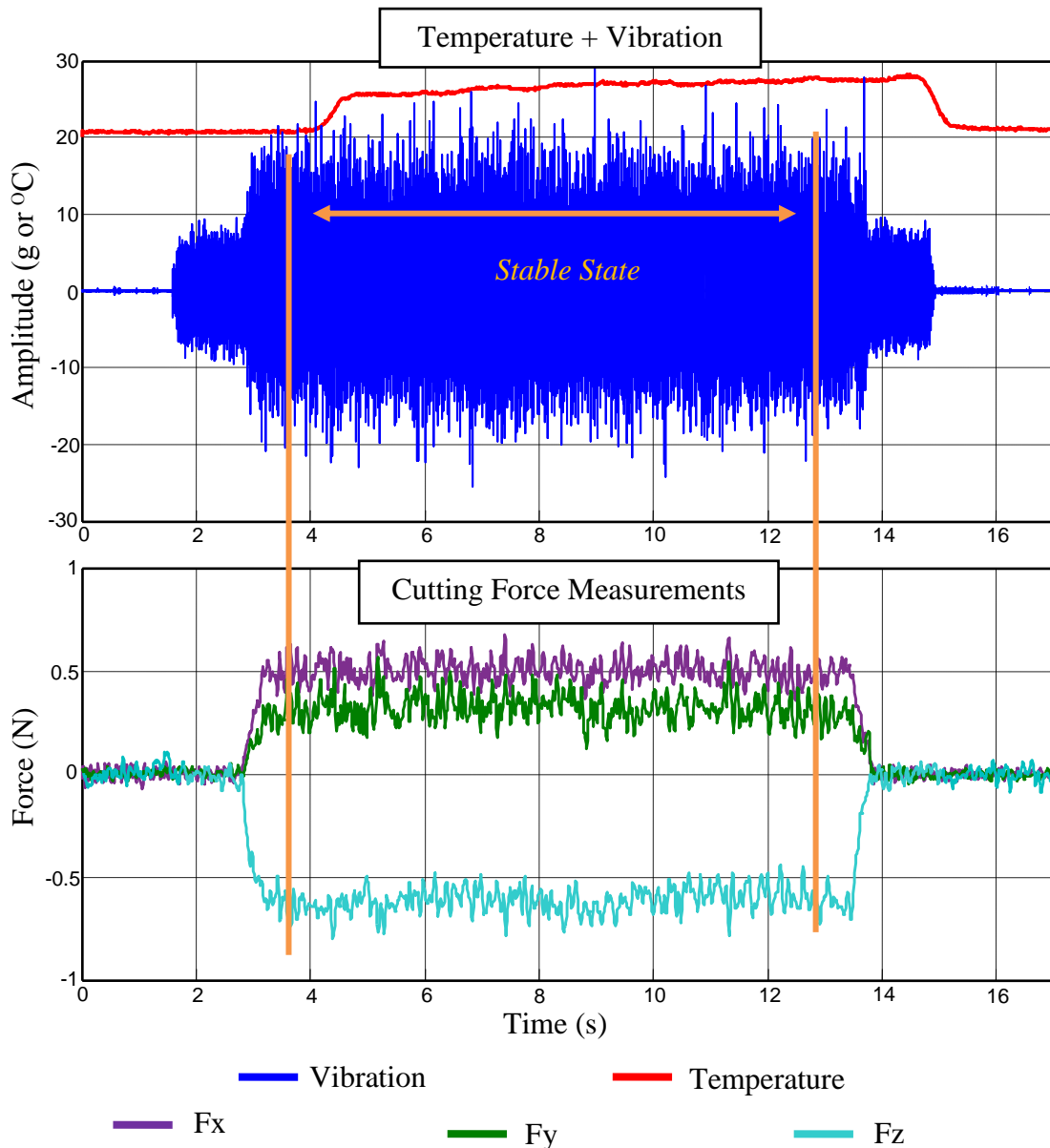


**Figure 2.7: Simultaneous measurements of dependent variables**

A sample output of the outcome measurements (temperature, vibration, and cutting force) is shown above. The stable state of the cut, defined as one tool diameter away from the entry and exit points, is indicated by orange lines on the graph above. The stable state of the cut was used for statistical analysis of the burring trials.

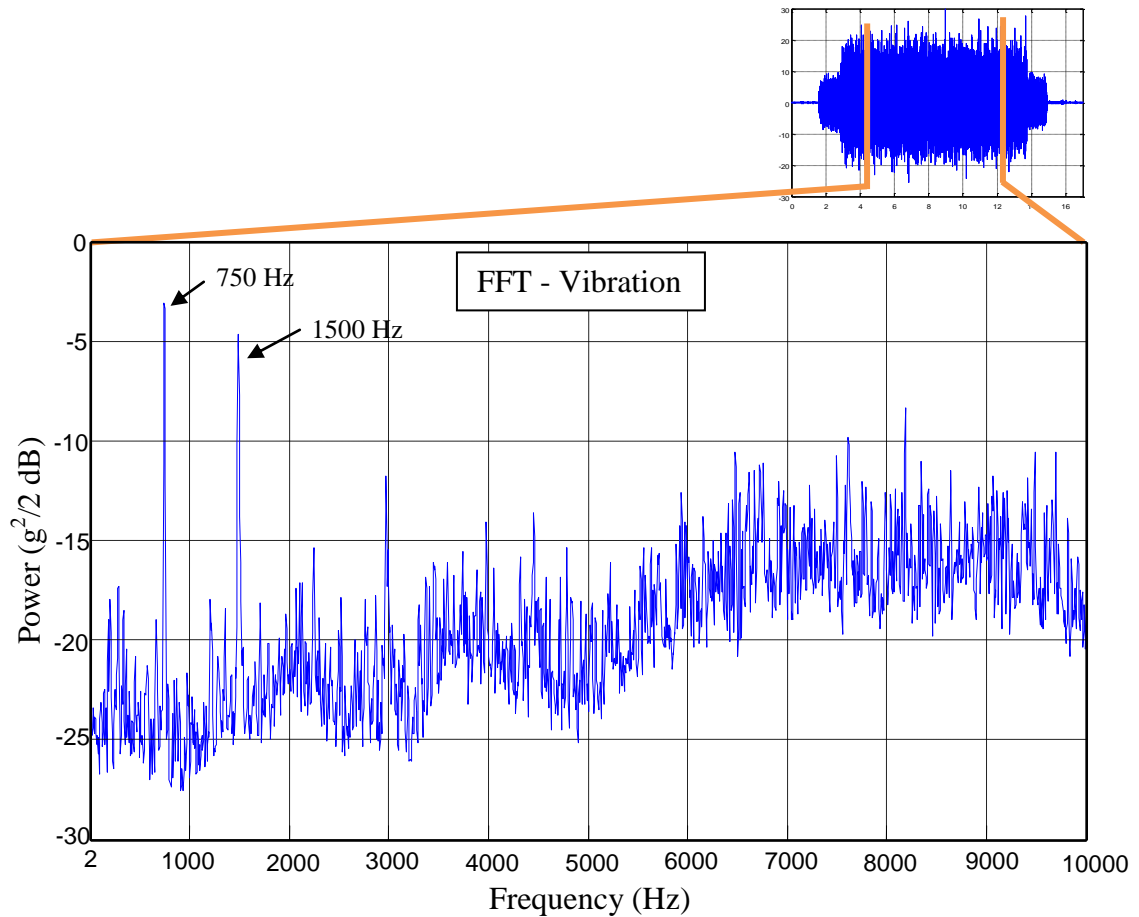


**Figure 2.8: Fast Fourier transform of steady state vibration data**

A fast Fourier transform (FFT) was applied to the stable regime of vibration measurements to translate data from the time domain into the frequency domain. Vibration frequencies peaked at 750 and 1500 Hz, corresponding to the tool's rotational speed (45,000 rpm) and the second harmonic of the base frequency, respectively.



## 2.4.1 Signal Post Processing

To prepare the data for a statistical analysis, post processing was performed on the stable region of the outcome variables.

### 2.4.1.1 Cutting Force

To provide a repeatable measurement for comparison of cutting forces; the mean of all samples within the stable region was used. The clipped data of the sample experiment along with a histogram of the results are shown in Figure 2.9-Figure 2.11. To ensure an accurate means of measurement, signal to noise ratio (SNR) was used to characterize the performance of the load sensing device. To calculate the SNR, the average of the quantified signal ( $P_{\text{signal}}$ ) was divided by the noise of the system ( $P_{\text{noise}}$ ) and converted into decibels (Eq. 2.1).

$$SNR_{dB} = 10\log_{10}\left(\frac{P_{\text{signal}}}{P_{\text{noise}}}\right) \quad (2.1)$$

The higher the SNR of the signal, the easier it is to extract an accurate measurement. A SNR of greater than 5 dB was deemed appropriate to be in line with previous experimental force measurements acquired in a bone burring process [41].

### 2.4.1.2 Vibration

To evaluate the dynamic effects of the tool between various process parameters and allow for a statistical analysis to be performed, a means to quantify the vibration was needed. A previous relevant study performed by Federspil *et al.* quantified the vibration of the workpiece during the burring process; however, only a single trial was performed during the experimental protocol [34]. Therefore, no means of evaluating the dynamic effects

between experimental trails was needed within the author's methods [34]. To allow for a statistical analysis to be performed on the dynamic effects of the tool holder; a metric adapted from the standard involving measuring hand-arm vibrations was used [57]. The typical standard employs a frequency-weighting (range 8-1,000 Hz) bandwidth to quantify the harmful effects resulting from hand tool vibration. Previous studies have used the root-mean-square vibration and quantified it through use of frequency-weighting technique for biomechanical applications [48-51]. However, as the main goal of the current work is to quantify the whole bandwidth of dynamic effects rather than certain harmful frequencies (8-1,000 Hz), the entire frequency bandwidth quantified by the accelerometer (1-10,000 Hz) was used to calculate the root-mean-square vibration (g-rms). The clipped data of the sample experiment along with a histogram of the results are shown in Figure 2.12.

#### 2.4.1.3 Temperature

A sample output of the temperature of the workpiece throughout the burring process is provided in Figure 2.13. A limitation in the context of providing a mean steady state value for temperature data was exposed when analyzing the stable region of the cutting process. The limitation is such that the temperature increases throughout the burring process, thus never entering a steady state condition. To allow for a consistent comparison of temperature generation, a constant length (65 mm) was used for each sawbone specimen. The maximum 100 samples of temperature measurements were then extracted and post processed to determine the mean temperature of the burring trial. The temperature data along with a box plot of the sample experiment are shown in Figure 2.13.

#### 2.4.1.4 Normality Testing

Normality testing was performed on the steady state outcome variables of cutting force and vibration. As the sample sizes were very large for cutting force ( $n=9000$ ) and vibration ( $n=225,000$ ), skewness and kurtosis were used to evaluate normality of the data. An absolute skewness or kurtosis  $> 2$  was used as a reference for departure from normality [59].

#### 2.4.1.5 Repeatability Testing

Repeatability of the experimental apparatus was quantified based on three separate burring trials. The outcomes of the dependent variables, as outlined above, were compared and the repeatability of the system was reported as  $\pm 1$  standard deviation. Benchmarks ( $\pm 1$  standard deviation) for the experimental apparatus was based upon previously developed experimental studies which were: forces in all three planes  $< 0.3$  N, temperature  $< 2.5$  °C, and vibration  $< 3$  g-rms. The mentioned numbers were obtained from previous experimental apparatuses designed to quantify the characteristics of bone burring [40, 41]. Although the process parameters and workpiece do not exactly align, the context of burring bone with a light resurfacing procedure is similar. Therefore, it is reasonable to postulate that the developed experimental apparatus will have similar repeatability traits to that of the mentioned studies. To determine an appropriate benchmark for vibration measurements, a pilot study was performed to view the effects at various ranges of process parameters. It was determined that 0.5 g-rms would serve as an appropriate benchmark to draw out significant effects in a statistical analysis.

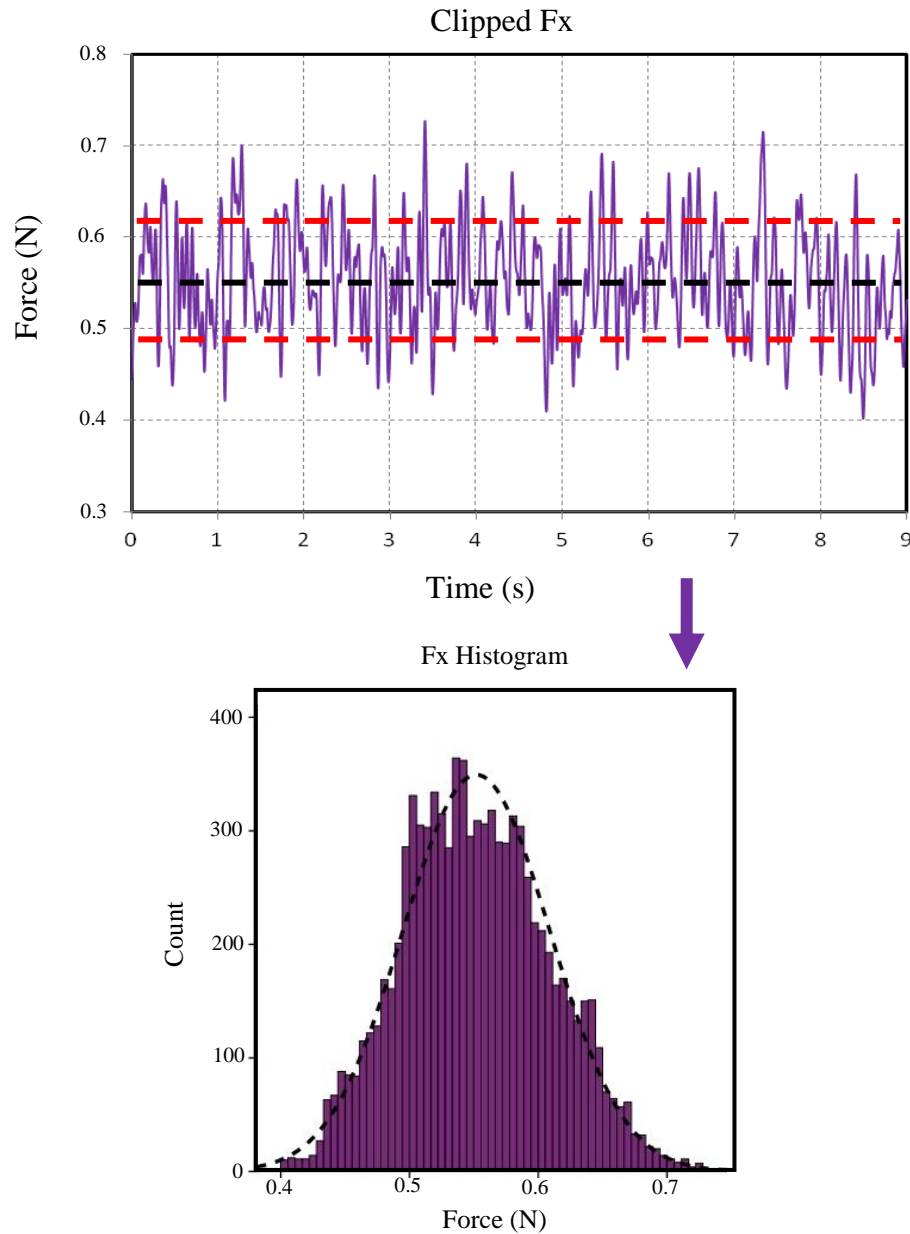


**Figure 2.9: Steady state measurement of cutting force (X-direction)**

*The measurements of  $F_x$  in stable state ( $n=9000$ ) and histogram of measurements are shown above. The mean force (black dashed line)  $\pm$  one standard deviation (red dashed line) is overlaid on the force measurements. The mean force ( $0.55 \pm 0.06$  N) of the samples within the stable state was used for statistical analysis. The SNR was found to be 8.8 dB. A histogram, along with an overlaid normally distributed curve (black dashed line) is also plotted. The skewness of the  $F_x$  histogram was 0.161; the kurtosis was -0.334.*

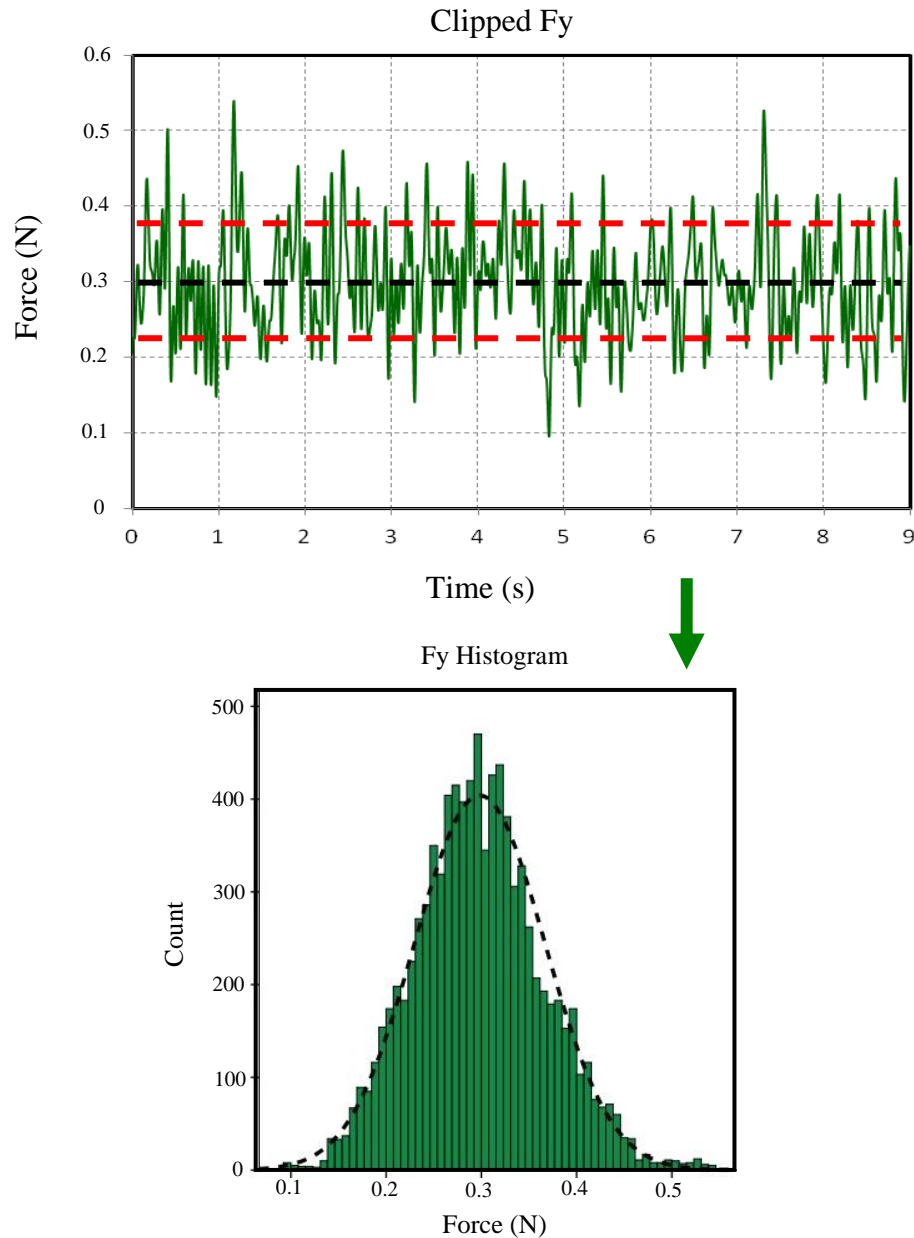


**Figure 2.10: Steady state measurement of cutting force (Y-direction)**

The measurements of  $F_y$  in stable state ( $n=9000$ ) and histogram of measurements are shown above. The mean force (black dashed line)  $\pm$  one standard deviation (red dashed line) is overlaid on the force measurements. The mean force ( $0.30 \pm 0.07$  N) of the samples within the stable state was used for statistical analysis. The SNR was found to be 6.8 dB. A histogram, along with an overlaid normally distributed curve (black dashed line) is also plotted. The skewness of the  $F_y$  histogram was 0.25; the kurtosis was 0.15.

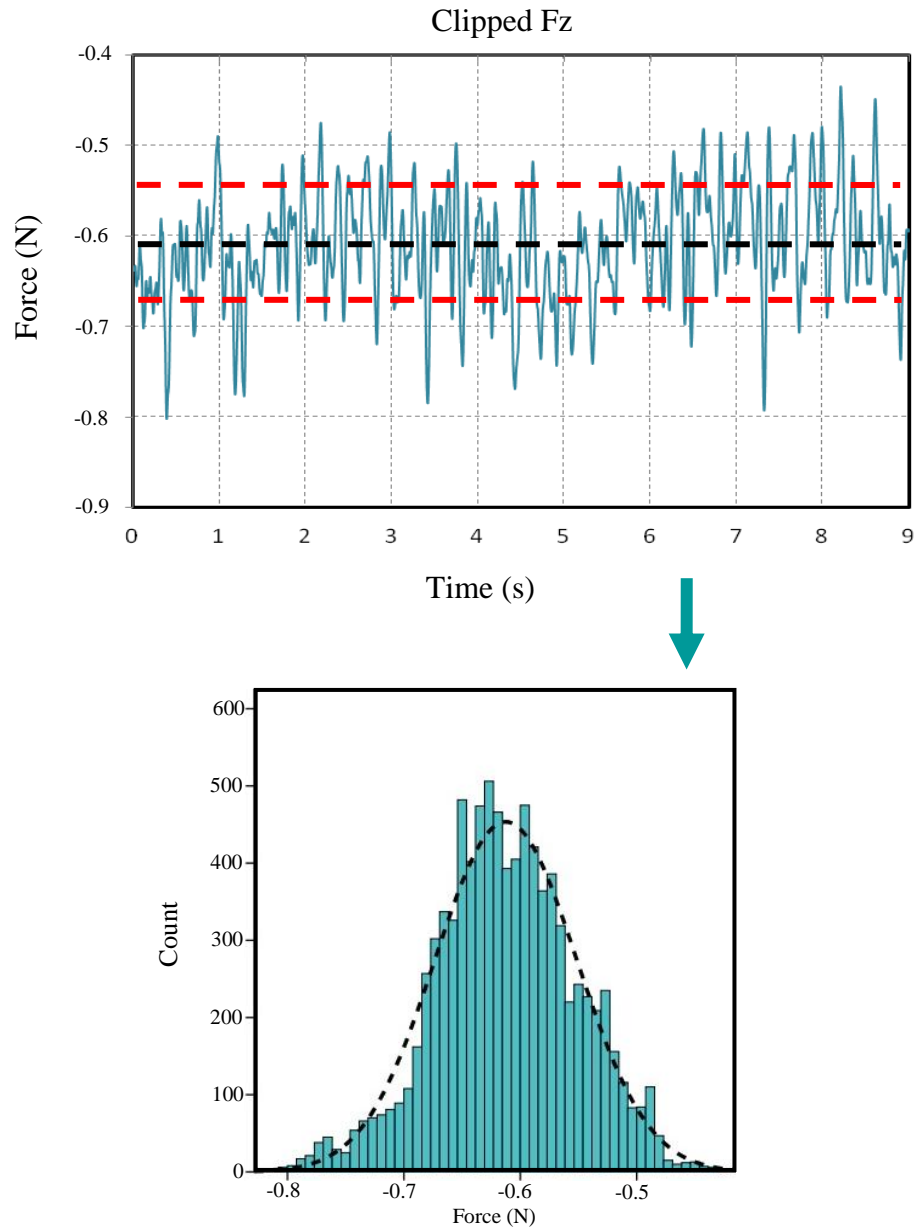


**Figure 2.11: Steady state measurement of cutting force (Z-direction)**

The measurements of  $F_z$  in stable state ( $n=9000$ ) and histogram of measurements are shown above. The mean force (black dashed line)  $\pm$  one standard deviation (red dashed line) is overlaid on the force measurements. The mean force ( $-0.61 \pm 0.06$  N) of the samples within the stable state was used for statistical analysis. The SNR was found to be 10.1 dB. A histogram, along with an overlaid normally distributed curve (black dashed line) is also plotted. The skewness of the  $F_z$  histogram was  $-0.10$ ; the kurtosis was  $0.04$ .

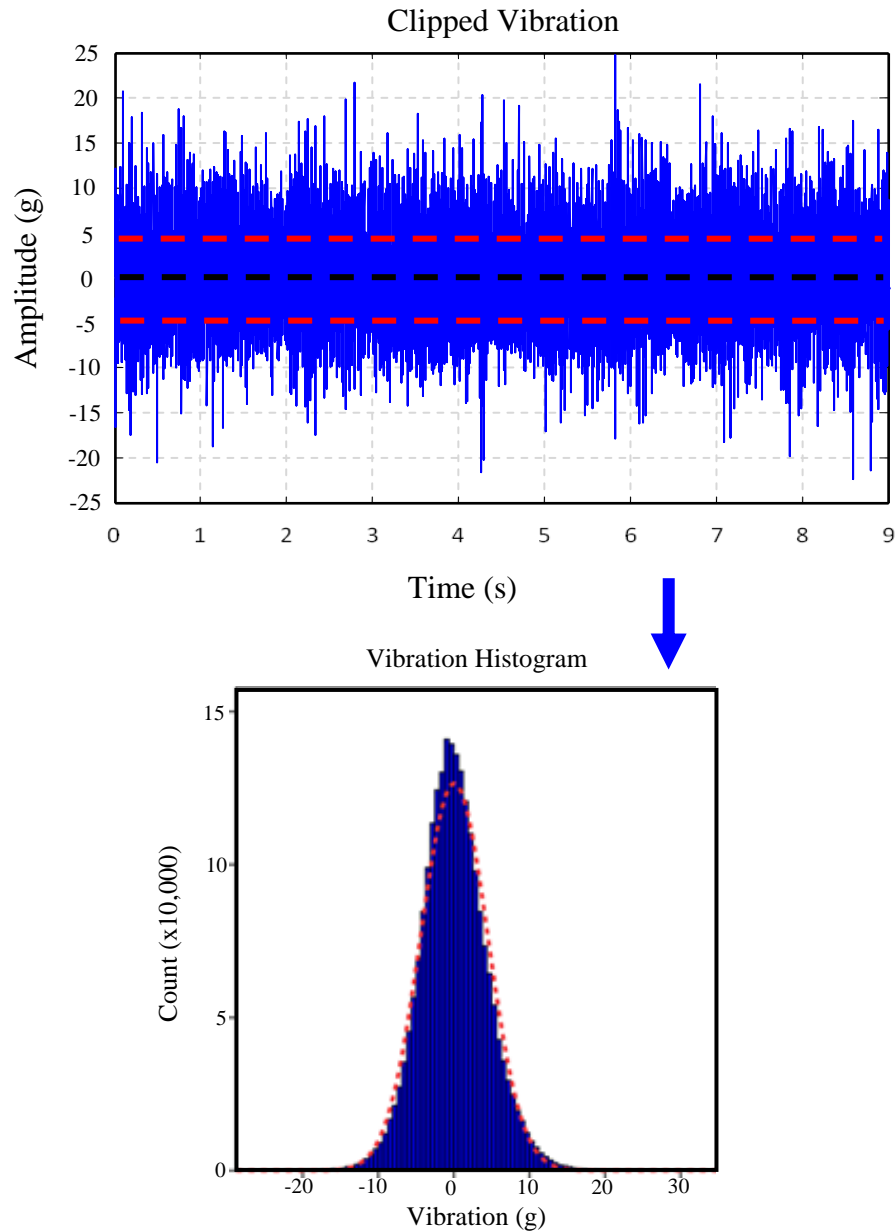


**Figure 2.12: Steady state measurement of vibration**

*The measurements of vibration in stable state ( $n=225,000$ ) and histogram of measurements are shown above. The mean vibration (black dashed line)  $\pm$  one standard deviation (red dashed line) is overlaid on the vibration measurements. The mean vibration ( $0.04 \pm 4.43$  g) of the samples within the stable state was found and a root mean square of 4.4g was used for statistical analysis. A histogram, along with an overlaid normally distributed curve (red dashed line) is also plotted. The skewness of the vibration histogram was 0.19; the kurtosis was 0.84.*

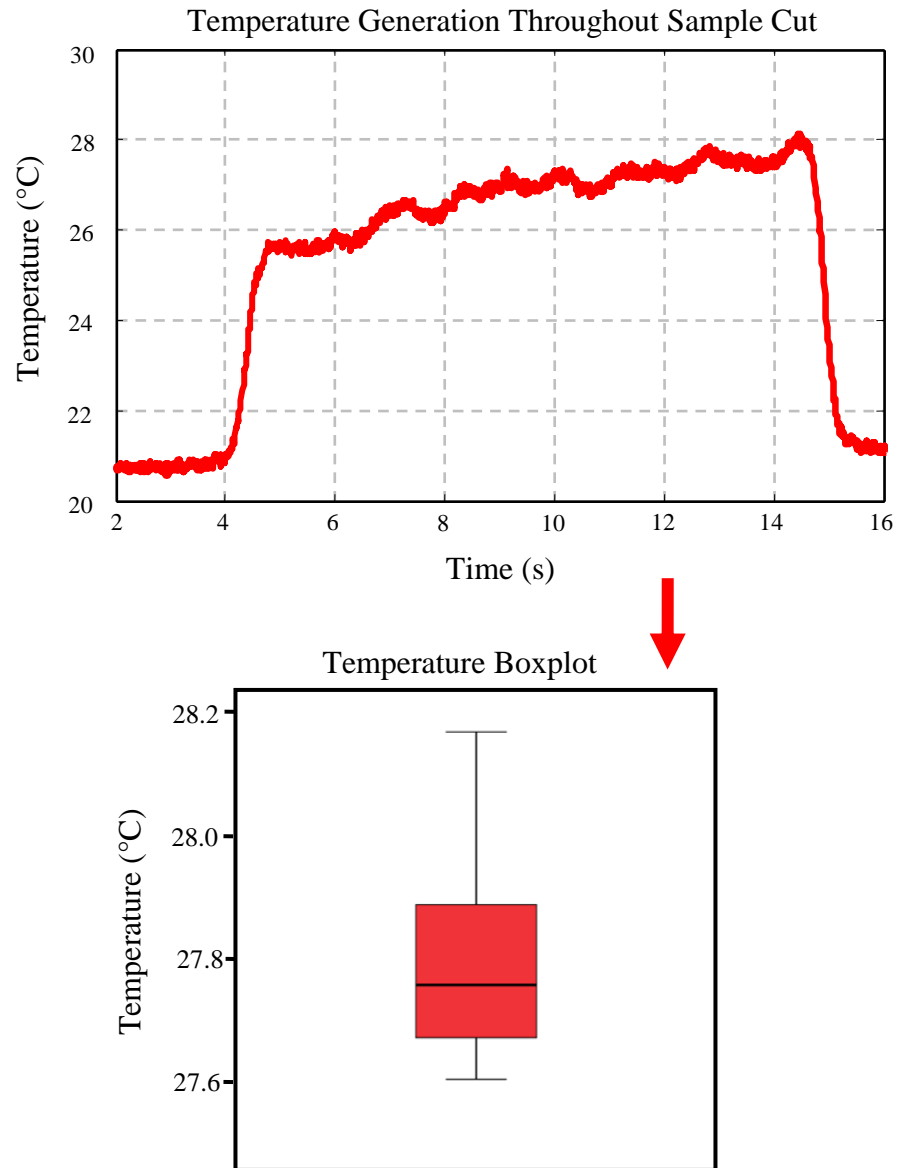


**Figure 2.13: Temperature measurement obtained from sample cut**

*The results produced by the infrared pyrometer throughout the sample experiment are shown above. A limitation encountered during the sample experiment, is that the temperature measurements do not reach a steady state. To allow for consistent comparisons to be made, an array ( $n=100$ ) of maximums was averaged. A boxplot of these 100 values is shown to check for outliers. An average temperature of 27.8 °C was calculated as shown by the boxplot.*



## 2.4.2 Sample Experiment Results

The analysis of the acquired sample data indicates that – under the tested cutting conditions – the superficial temperature of the workpiece increased from  $20.7 \pm 0.1$  °C to  $27.8 \pm 0.1$  °C, while the cutting forces generated in the process were all less than 1 N ( $F_x = 0.55 \pm 0.06$  N,  $F_y = 0.30 \pm 0.07$  N,  $F_z = -0.61 \pm 0.06$  N). The vibrations generated during the process varied between +25 and -22 g (peak to peak values) with a root-mean-square value of 4.4 g. In the frequency domain (FFT transform), peaks were recorded at 750 and 1500 Hz corresponding to the tool's rotational speed (45,000 rpm) and the second harmonic of the base frequency, respectively. In the disengaged state of the tool, vibration and cutting forces were identical before and after the cut, while the temperature dropped gradually after the cut before reaching room temperature value. The repeatability of the system ( $\pm 1$  standard deviation) was found to be:  $F_x = 0.08$  N,  $F_y = 0.01$  N,  $F_z = 0.09$  N, vibration = 0.36 g-rms, and temperature = 1.4 °C. The SNR of the load cell in each direction was found to be:  $F_x = 8.8$  dB,  $F_y = 6.8$  dB, and  $F_z = 10.1$  dB.

## 2.5 Chapter Summary

The experimental apparatus was able to monitor the cutting force and temperature data simultaneously with the dynamic measurements. Dominant frequencies, as found in the FFT, corresponded to the base and harmonic frequencies of the rotational speed of the tool. These measurements of the system were found to be highly repeatable showing small differences ( $\pm 1$  standard deviation) of: cutting force  $< 0.1$  N, temperature  $< 2$  °C, and vibration  $< 0.4$  g-rms. The repeatability of the developed apparatus is in line with previously developed experimental studies that quantified force and temperature,

performed by Dillon *et al.* and Shin *et al.*, respectively [40, 41]. The SNR of the load cell was also comparable to that of previous experiments, greater than 5 dB in all directions; thus satisfying our first hypothesis [41]. The measurements during a burring trial are also normally distributed for cutting force and vibration, confirming that the burring process has entered a steady state for these measurements and that the transducers are capturing this accurately. Although the temperature of the workpiece did not appear to enter a steady state, a consistent comparison can still be made by ensuring a constant length of the workpiece.

To fully quantify the effects of the process parameters associated with bone burring, a larger experimental study, which involves varying the levels of the process parameters, is needed. The developed apparatus offers the ability to evaluate and prescreen specific machining parameters in an *in-vitro* bench top setting before implementation into an *in-vivo* surgical setting.

## **Chapter 3 - Experimental Analysis of the Effect of Process Parameters on Selected Outcome Measurements**

*OVERVIEW: The aim of the current chapter is to quantify the main effects and interdependencies of eight independent variables on five outcome measurements associated with a bone burring procedure in a cancellous sawbone analog. Rationale for selection of the independent variables as well as the associated levels are discussed. As well, a method to normalize the infrared pyrometer temperature measurements to specified feed rates is presented. A full factorial analysis with repeated trials was performed. A statistical analysis (multivariate analysis of variance) was conducted to quantify the main-effects and interactions between the parameters. Descriptive statistics were also used to identify process parameters that led to maximums and minimums for each of the outcome measurements (cutting force in three planes, vibration and temperature).*

### **3.1 Selection of Process Parameters**

An investigational study to characterize the burring process associated with bone removal was conducted using the experimental apparatus developed in Chapter 2. The rationale behind selection of levels regarding the burring process was based upon relevant previous published studies, and practical relevance.

In selection of the tool shape and diameter it is important to consider the bone removal rate (cross-sectional area of the engaged burr times the feed rate) which is in part dictated by the selection of the burring tool. A larger diameter of tool offers the ability to increase the bone removal rate; however, the size of the tool may be limited by the geometrical constraints of the burring cavity. Additionally, if the process was to be automated, a tool path would be required before conducting the burring procedure. Medtronic fluted burrs, sphere and cylinder shaped, were selected as possibilities to be implemented in the burring process. Although the cylinder tool offers the possibility of shorter procedure times due to the larger cross-sectional area, the cylinder tool complicates the design of a tool path due to its inherent complex burring channels that ensue upon rotation of the tool. The effect of changing burr types (fluted vs. diamond coated) has been evaluated in the context of cutting force [41]. However, in other relevant studies, a sphere burr was selected exclusively within the burring process [39, 40]. A direct comparison, using a sphere and cylinder fluted burr has yet to be quantified with outcome measurements of temperature, vibration, and cutting force. The diameter of the tool was also varied between 4 and 6 mm. In total, four fluted burrs were chosen within this experimental matrix (4 mm sphere, 6 mm sphere, 4 mm cylinder, 6 mm cylinder).

Arbabtafti *et al.* examined the effects of rotational speed of the tool on cutting force using experimental measurements [42]. Arbabtafti *et al.* selected spindle speeds between 17,000 to 28,000 rpm and found that increasing the rotational speed resulted in a decrease of cutting force in all directions. Other relevant studies fixed rotational speeds at or in the ranges of: 30,000 to 50,000 rpm [40], 10,000 to 40,000 rpm [39], and 120,000 rpm [45].

Therefore, within this experimental study, tool rotational speeds of 15,000, 45,000, and 75,000 rpm were selected to represent a range of the previous studies.

Quantifying the effects of varying feed rate and depths of cut has been investigated using cutting force and temperature generation as the outcome measurements. Shin *et al.* selected feed rates in the range of 2.0 to 9.8 mm/s and depths of cut between 0.3 to 1.0 mm [40]. Additionally, Dillon *et al.* selected depths of cut in the range of 0.6 to 1.6 mm and feed rates in the range of 1 to 8 mm/s [41]. It was found that increasing depth of cut increased cutting force and temperature, and increasing feed rate increased cutting force but decreased temperature. For this experimental study, feed rates of 2 and 6 mm/s and depths of cut of 0.5 and 1.0 mm were selected. A 0% overlap or "fully immersed" burring path is typically used in previous experimental studies to quantify process parameters [40, 41]. However, a 0% percent overlap is rarely encountered practically in a burring procedure, as it only occurs on the first path of the tool. Therefore, the effects of varying overlap between successive burring paths was investigated by choosing levels of 0%, 10%, and 50%.

Due to the nature of minimally invasive surgeries and the limited burring cavity, the workspace of the tool may be limited to certain orientations. Therefore, the effects of varying the angle of the tool with respect to the workpiece was evaluated. The inclination angle and tilt angle were varied with associated increments within this study. Dillon *et al.* investigated the effects of tilt angle on cutting force, by selecting angles of 0,30,50, and 70 degrees [41]. Tilt angles of 0 and 45 degrees were selected within the current experimental protocol. Inclination angles of 0, +40, and -40 degrees were also chosen. Although, a -40 degrees inclination angle may not be ideal due to the cutting edge and

design of the tool, the orientation of the tool may be unavoidable in a minimally invasive surgery.

With the large amount of burring trials to be performed within the full factorial analysis (864 unique conditions) the use of cadaveric specimens was disregarded due to the quantity of specimens that would be needed to carry out the experiment. As cadaveric specimens are expensive and not-readily available; coupled with the fact that the bone can only be burred once and would subsequently limit the amount of burring trials that could be performed on a single specimen (primarily restricted by the amount of cancellous bone within the epiphysis of the bone), a sawbone analog was selected as a substitute. A sawbone analog provided a uniform workpiece to allow for comparison of the process parameters and ensured a consistent biomechanical structure [58]. The main benefit of using a sawbone analog is that the differences evoked from the statistical analysis would be due to the process parameters rather than differences between the workpiece that might be exhibited in cadaveric specimens. Although the differences between magnitudes will surely be different in sawbone and a cadaveric specimen, the trends drawn out from using a sawbone will be relevant moving forward. In agreement with the overall context of the present study, the selected sawbone that was used was comparable to that of a health joint bone (density =  $0.32 \text{ g/cm}^3$ ) [27].

Although previous conducted studies have investigated a bulk of the parameters outlined, tool type and overlap are the only process parameters novel to this experiment, no study has yet to quantify the process parameters with the five outcome measurements discussed in Chapter 2 (cutting force in three planes, temperature, and vibration). Therefore,

tradeoffs in how the outcome measurements are affected by the process parameters have not been fully quantified and thoroughly understood.

Additionally, no previous study has incorporated a full factorial analysis with eight of the process parameters varied. Previous studies relied on fixing parameters to certain levels within the burring process, which in turn limits the amount of conditions that were tested. The full factorial design is advantageous as all combinations of process parameters are analyzed and does not alias any effects which may be found in a fractional factorial analysis. Therefore, by performing a full factorial statistical analysis, no combination of parameters are missed which may lead to desirable or undesirable burring outcomes.

Table 3.1: Selected levels of process parameters

	<i>Tool Type</i>	<i>Diameter (mm)</i>	<i>Rotational Speed (rpm)</i>	<i>Tilt Angle (°)</i>	<i>Inclination Angle (°)</i>	<i>Feed Rate (mm/s)</i>	<i>Depth of Cut (mm)</i>	<i>Overlap (%)</i>
<u>Level-1</u>	Sphere	6	15,000	0	0	2	0.5	0
<u>Level-2</u>	Cylinder	4	45,000	45	+40	6	1.0	10
<u>Level-3</u>	-	-	75,000	-	-40	-	-	50

*The above table outlines the parameters chosen in the experimental design. The levels of process parameters are specified underneath their respective column.*

*Note: tool type, diameter, tilt angle, feed rate, and depth of cut have only 2 levels.*

### 3.1.1 Feed Rate Normalization

A limitation of the experimental apparatus designed in Chapter 2 was that the infrared pyrometer was positioned such that it was focused on an area located immediately behind the cutting tool. A consequence of introducing a lag between the pyrometer and the cutting tool, was that a cooling time was introduced into the system. Therefore, without a way to account for the cooling, the measured temperature would underestimate the actual temperature at the tool-workpiece interface.

The amount of time the workpiece was allowed to cool before a measurement was made was dependent on the feed rate that was chosen. For the two feed rates selected, 2 and 6 mm/s, a cooling time of 2.5 and 0.8 seconds occurred respectively. To account for the cooling introduced into the system and allow for comparisons of different feed rates, Newton's law of cooling model was applied to the experimental machining process.

Newton's law of cooling was applied by fitting an exponential curve to experimental measurements at different time points. To apply Newton's law of cooling model to the experimental burring process, the burring parameters were fixed to produce repeatable temperature measurements. The infrared pyrometer was then adjusted to different lagging distances, which corresponded to different cooling times. Three lagging distances (with 5 repeated measurements) were used to quantify the cooling of the system which are:

X1 - 5 mm trailing

X2 - 10 mm trailing

X3 - 15 mm trailing



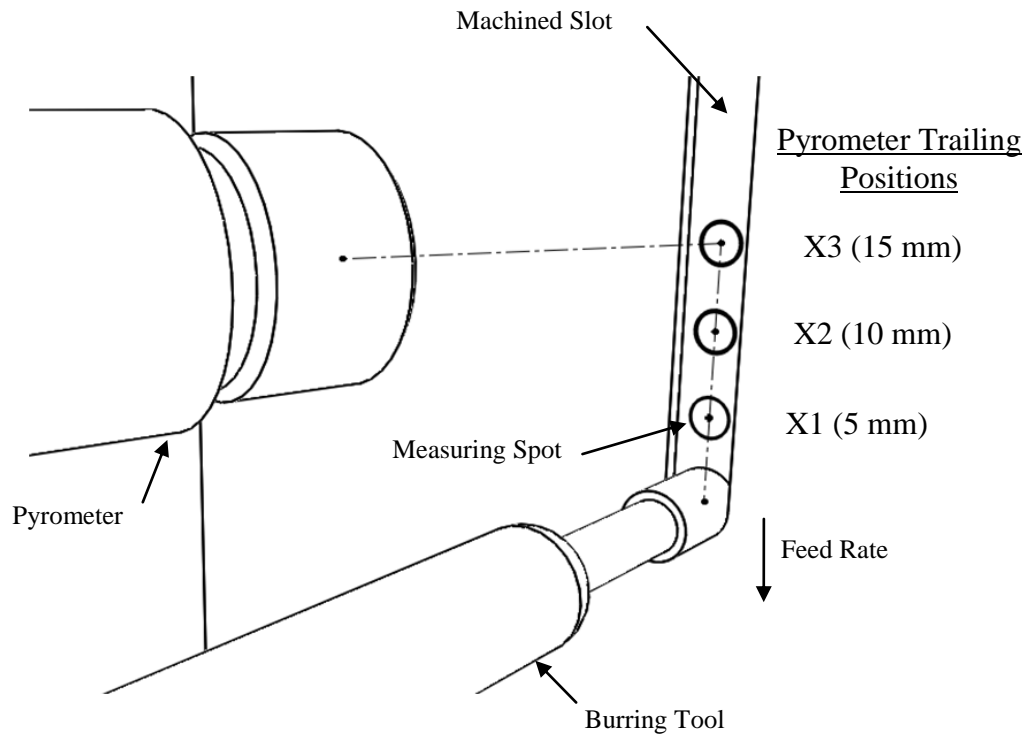


**Figure 3.1: Quantifying cooling of the workpiece during a burring trail**

*An illustration of the infrared pyrometer at different lagging distances is shown above. Three lagging distances were used: X1 (5 mm trailing), X2 (10 mm trailing), and X3 (15 mm trailing). The measurements were repeated five times at each lagging distance, and for both feed rates; 2 and 6 mm/s.*

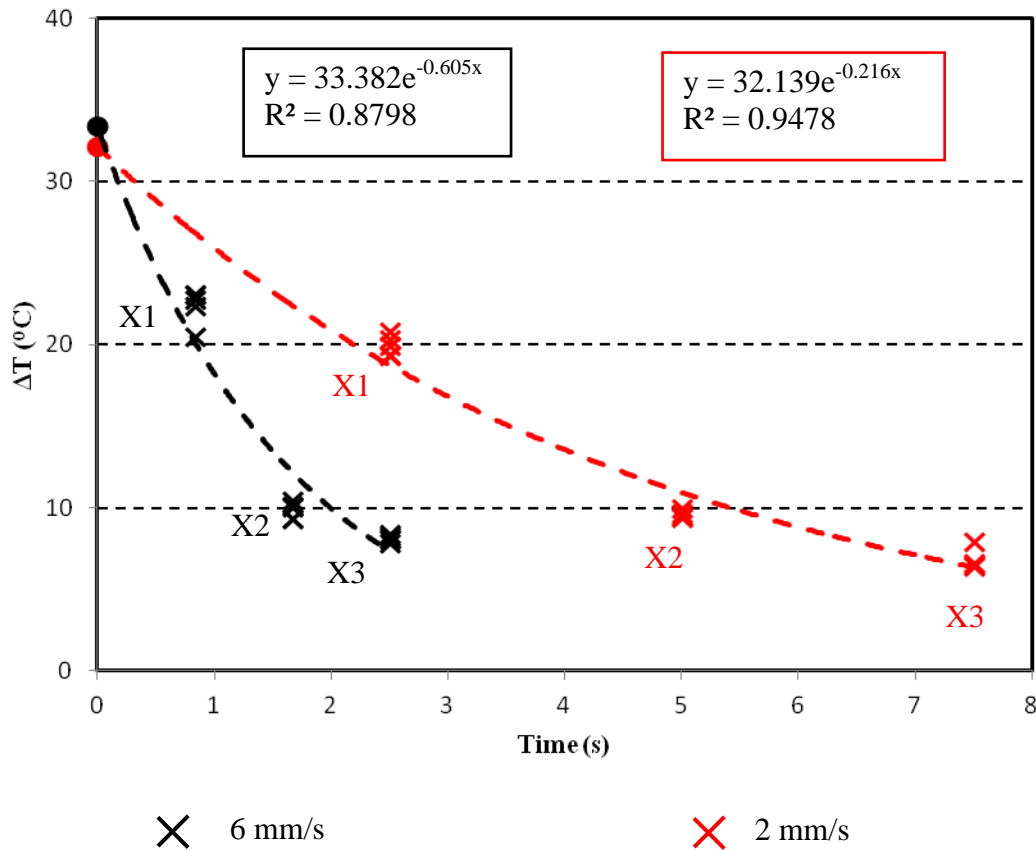


**Figure 3.2: Temperature normalized to the center of the burring tool**

Results from the feed rate normalization experiment are shown above. X1, X2, and X3 are plotted along with their respective feed rates, 2 mm/s (red) and 6 mm/s (black). An exponential line of best fit was applied to both feed rates; the equation and  $R^2$  values can be found within the outlined boxes above. The lines of best fit were used to extrapolate the temperature at the theoretical contact point between the tool and workpiece.

An exponential curve was fitted to the experimental temperature measurements at both feed rates. The curves of best fit showed strong correlation ( $R^2 > 0.87$ ). Extrapolating these curves to the center of the tool, the points intersect at approximately the same point ( $\Delta T \approx 33$  °C).

Moving forward, the cooling curves quantified in this developmental test were applied to the temperature measurements. The temperature at the center of the tool was then extrapolated based on the cooling time with the associated feed rate. By normalizing the temperature to the center of the tool, separate feed rates could be compared.

## 3.2 Statistical Analysis

A full factorial analysis was conducted to determine the effects of the burring process parameters had on the selected outcome measurements. Outcome measurements that were chosen include: temperature generation, vibration, and cutting forces in the X, Y, and Z direction. An experimental matrix was constructed based on the levels of each process parameter  $2 \times 2 \times 2 \times 3 \times 3 \times 2 \times 2 \times 3$  with three replications, thus resulting in a total of 2592 observations.

A multivariate analysis of variance (MANOVA) was conducted to determine whether a parameter was statistically significant on producing an effect on the overall statistical model. The results were further analyzed by conducting a univariate analysis of variance (ANOVA) on each of the dependent variables. To determine which criteria to use for significance testing, the homogeneity of variances-covariance was analyzed. If the assumption of homogeneity of variances-covariance as indicated by Box's M test was met, Wilk's Lambda test was used; if the assumption was violated, Pillai's Trace was

used. If statistical significance was found at the univariate level, a pairwise comparison test was also conducted using the bonferroni correction factor. An overall alpha of 0.05 ( $p < 0.05$ ) was used to determine statistical significance. All results are reported as the population mean  $\pm$  95% confidence interval. A more in-depth discussion of the statistical tools employed within the current work can be found in Appendix D.

To examine the combinations of process parameters that led to maximum and minimum conditions, descriptive statistics were used. Five of the process parameters were fixed, and the average of the resulting three parameters were used to examine sensitivity of the outcome measurements to the process parameters. These conditions are important as they demonstrate the variability that the selection of certain process parameters (fixing five process parameters and altering three throughout the machining process) could have on the outcome measurements.

### 3.3 Effects of Process Parameters on Outcome Measurements

Each process parameter was found to be statistically significant at the multivariate level ( $p < 0.001$ ). A summary of the MANOVA, and ANOVA results can be found in Table 3.2-Table 3.7. The main effects of the pairwise comparison are illustrated in Figure 3.3 and Figure 3.4.

#### 3.3.1 Cutting Force

A rotational speed of 75,000 rpm produced the lowest average forces ( $F_x = 0.22 \pm 0.04$  N,  $F_y = 0.06 \pm 0.04$  N,  $F_z = -0.14 \pm 0.04$  N), compared to 15,000 rpm ( $F_x = 0.56 \pm 0.04$  N,  $F_y = 0.15 \pm 0.04$  N,  $F_z = -0.34 \pm 0.04$  N) ( $p < 0.001$ ) and 45,000 rpm ( $F_x = 0.31 \pm 0.04$  N,

$F_y=0.09\pm 0.04$  N,  $F_z=-0.21\pm 0.04$  N) ( $p<0.001$ ) (Figure 3.3). Increasing the feed rate from 2 to 6 mm/s resulted in an increase of forces of  $F_x=0.13\pm 0.04$  N,  $F_y=0.03\pm 0.04$  N, and  $F_z=-0.14\pm 0.04$  N ( $p<0.001$ ). As well, increasing the depth of cut from 0.5 to 1.0 mm resulted in an increase of forces of  $F_x=0.14\pm 0.04$  N,  $F_y=0.06 \pm 0.04$  N, and  $F_z=-0.16 \pm 0.02$  N ( $p<0.001$ ). It was found that based on the selection of process parameters, the variability of the cutting force (maximum-minimum) was:  $F_x=2.0$  N,  $F_y=0.8$  N, and  $F_z=-0.9$  N (Figure 3.5 - Figure 3.7).

### 3.3.2 Vibration

A rotational speed of 75,000 rpm produced the highest average vibration of  $5.80\pm 0.04$  g-rms compared to the 15,000 and 45,000 rpm which produced  $2.46\pm 0.04$  g-rms ( $p<0.001$ ) and  $4.02\pm 0.04$  g-rms respectively ( $p<0.001$ ) (Figure 3.4). Increasing the feed rate from 2 to 6 mm/s on average increased the vibration by  $0.69\pm 0.04$  g-rms ( $p<0.001$ ). Also, increasing the depth of cut from 0.5 to 1.0 mm resulted in an increase in vibration by  $0.54\pm 0.04$  g-rms ( $p<0.001$ ). The selection of process parameters was found to alter the vibration quantified up to 5.6 g-rms depending on which parameters were fixed and at the specified level (Figure 3.8).

### 3.3.3 Temperature

A sphere tool ( $34.8\pm 0.2$  °C) produced lower average temperatures than the cylinder tool ( $38.4\pm 0.2$  °C) ( $p<0.001$ ) (Figure 3.4). An inclination angle of +40 degrees resulted in the lowest average temperature ( $30.5\pm 0.2$  °C) compared to 0 degrees ( $40.1\pm 0.2$  °C) and -40 degrees ( $39.1\pm 0.2$  °C) inclination angle ( $p<0.001$ ). A rotational speed of 75,000 rpm produced the lowest average temperature ( $35.0\pm 0.2$  °C) compared to 15,000 rpm

(37.2±0.2 °C) and 45,000 rpm (37.6±0.2 °C) ( $p < 0.001$ ). The selection of process parameters was found to alter the temperature measured of up to 33.5 °C depending on which parameters were fixed and at the specified level (Figure 3.9).

Table 3.2: Summary of MANOVA results

<b>MANOVA</b>					
<i>Process Parameter</i>	<i>Criterion</i>	<i>F Value</i>	<i>p-value</i>	<i>Partial Eta Squared</i>	<i>Conclusion</i>
Tool Type	Pillai's Trace	1144.8	<0.001	0.769	Significant
Diameter	Pillai's Trace	557.8	<0.001	0.618	Significant
Tilt Angle	Pillai's Trace	12138.7	<0.001	0.972	Significant
Inclination Angle	Pillai's Trace	12422.1	<0.001	0.973	Significant
Rotational Speed	Pillai's Trace	895.1	<0.001	0.722	Significant
Feed Rate	Pillai's Trace	2053.8	<0.001	0.856	Significant
Depth of Cut	Pillai's Trace	2510.3	<0.001	0.879	Significant
Overlap	Pillai's Trace	233.3	<0.001	0.403	Significant

Table 3.3: Summary of ANOVA results - Fx

<b>ANOVA - Fx</b>				
<i>Process Parameter</i>	<i>F Value</i>	<i>p-value</i>	<i>Partial Eta Squared</i>	<i>Conclusion</i>
Tool Type	20.6	<0.001	0.012	Significant
Diameter	925.8	<0.001	0.349	Significant
Tilt Angle	19235.7	<0.001	0.918	Significant
Inclination Angle	16945.8	<0.001	0.951	Significant
Rotational Speed	16266.0	<0.001	0.950	Significant
Feed Rate	6896.3	<0.001	0.800	Significant
Depth of Cut	7303.4	<0.001	0.809	Significant
Overlap	612.6	<0.001	0.415	Significant

Table 3.4: Summary of ANOVA results - Fy

<b>ANOVA - Fy</b>				
<i>Process Parameter</i>	<i>F Value</i>	<i>p-value</i>	<i>Partial Eta Squared</i>	<i>Conclusion</i>
Tool Type	69.0	<0.001	0.038	Significant
Diameter	245.1	<0.001	0.124	Significant
Tilt Angle	321.3	<0.001	0.157	Significant
Inclination Angle	35551.8	<0.001	0.976	Significant
Rotational Speed	2300.2	<0.001	0.727	Significant
Feed Rate	564.4	<0.001	0.246	Significant
Depth of Cut	2978.7	<0.001	0.633	Significant
Overlap	405.9	<0.001	0.320	Significant

Table 3.5: Summary of ANOVA results - Fz

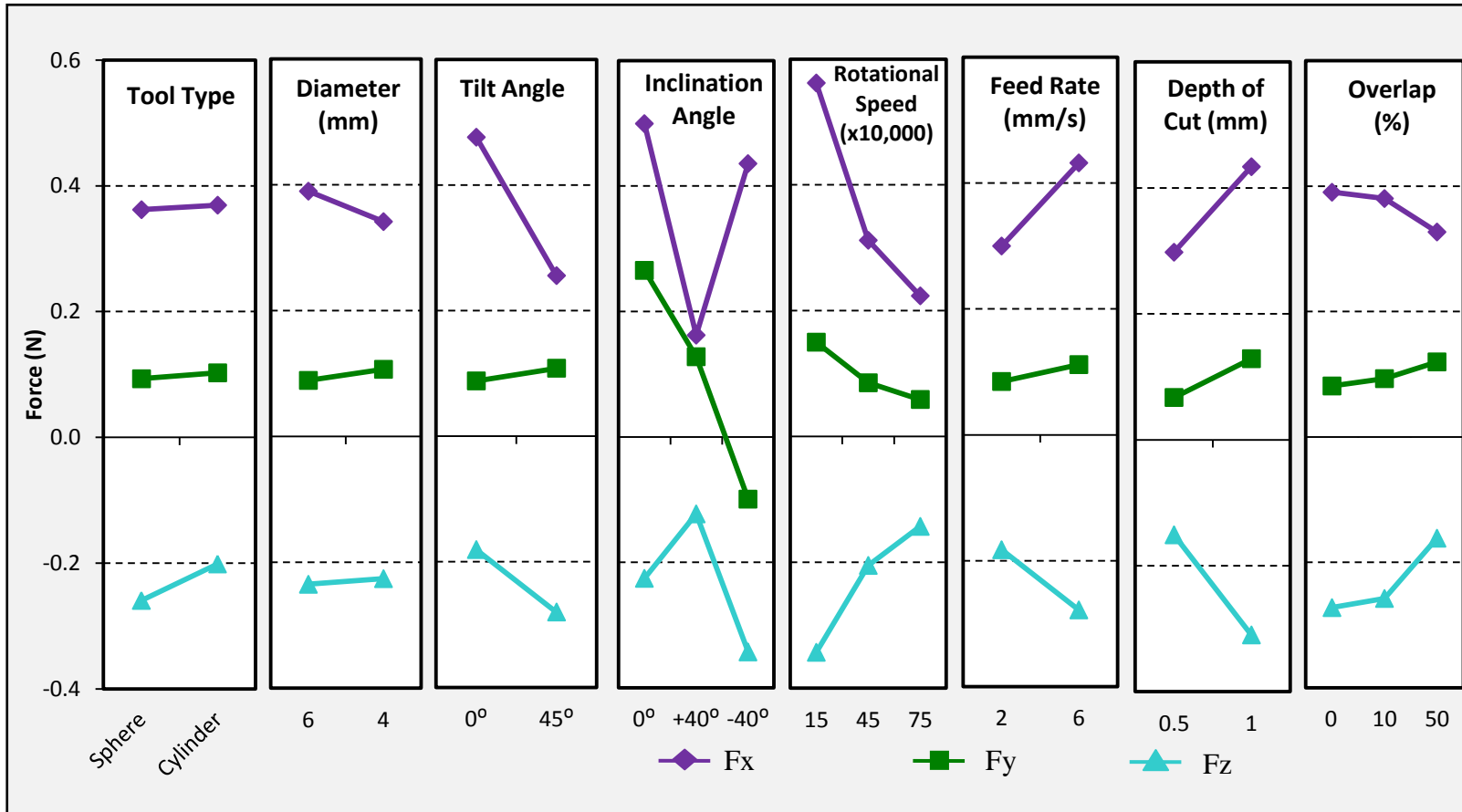
<b>ANOVA - Fz</b>				
<i>Factor</i>	<i>F Value</i>	<i>p-value</i>	<i>Partial Eta Squared</i>	<i>Conclusion</i>
Tool Type	1033.1	<0.001	0.374	Significant
Diameter	24.6	<0.001	0.014	Significant
Tilt Angle	3033.7	<0.001	0.637	Significant
Inclination Angle	4962.9	<0.001	0.852	Significant
Rotational Speed	4297.8	<0.001	0.833	Significant
Feed Rate	2804.7	<0.001	0.619	Significant
Depth of Cut	7755.8	<0.001	0.818	Significant
Overlap	1480.2	<0.001	0.631	Significant

Table 3.6: Summary of ANOVA results - vibration

<b>ANOVA - Vibration</b>				
<i>Factor</i>	<i>F Value</i>	<i>p-value</i>	<i>Partial Eta Squared</i>	<i>Conclusion</i>
Tool Type	49.4	<0.001	0.367	Significant
Diameter	19.0	<0.001	0.501	Significant
Tilt Angle	81.0	<0.001	0.478	Significant
Inclination Angle	165.8	<0.001	0.818	Significant
Rotational Speed	5532.6	<0.001	0.365	Significant
Feed Rate	714.5	<0.001	0.027	Significant
Depth of Cut	433.8	<0.001	0.736	Significant
Overlap	121.9	<0.001	0.464	Significant

Table 3.7: Summary of ANOVA results - temperature

<b>ANOVA - Temperature</b>				
<i>Factor</i>	<i>F Value</i>	<i>p-value</i>	<i>Partial Eta Squared</i>	<i>Conclusion</i>
Tool Type	2537.3	<0.001	0.595	Significant
Diameter	2782.1	<0.001	0.329	Significant
Tilt Angle	9796.6	<0.001	0.633	Significant
Inclination Angle	7165.0	<0.001	0.892	Significant
Rotational Speed	500.9	<0.001	0.367	Significant
Feed Rate	1119.8	<0.001	0.393	Significant
Depth of Cut	5244.5	<0.001	0.752	Significant
Overlap	777.6	<0.001	0.474	Significant



**Figure 3.3: Main effects of process parameters on cutting force ( $F_x$ ,  $F_y$ , and  $F_z$ )**

The pairwise comparison results,  $F_x$  (purple),  $F_y$  (green), and  $F_z$  (teal), are presented in the figure above. Only the main effect plots are shown.



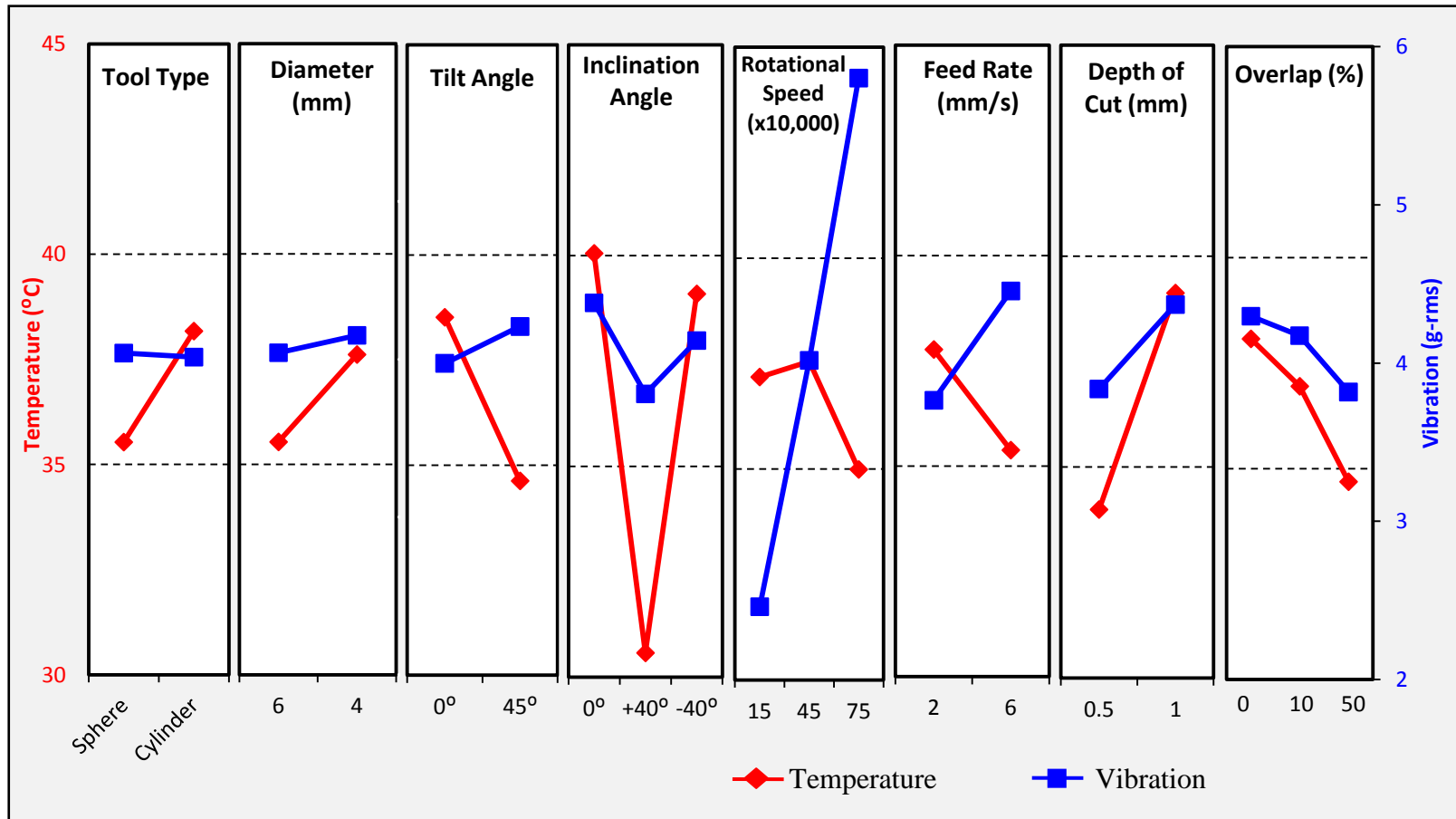


**Figure 3.4: Main effects of process parameters on temperature and vibration**

*The pairwise comparison results, vibration (blue) and temperature (red), are presented in the figure above. Only the main effect plots are shown.*

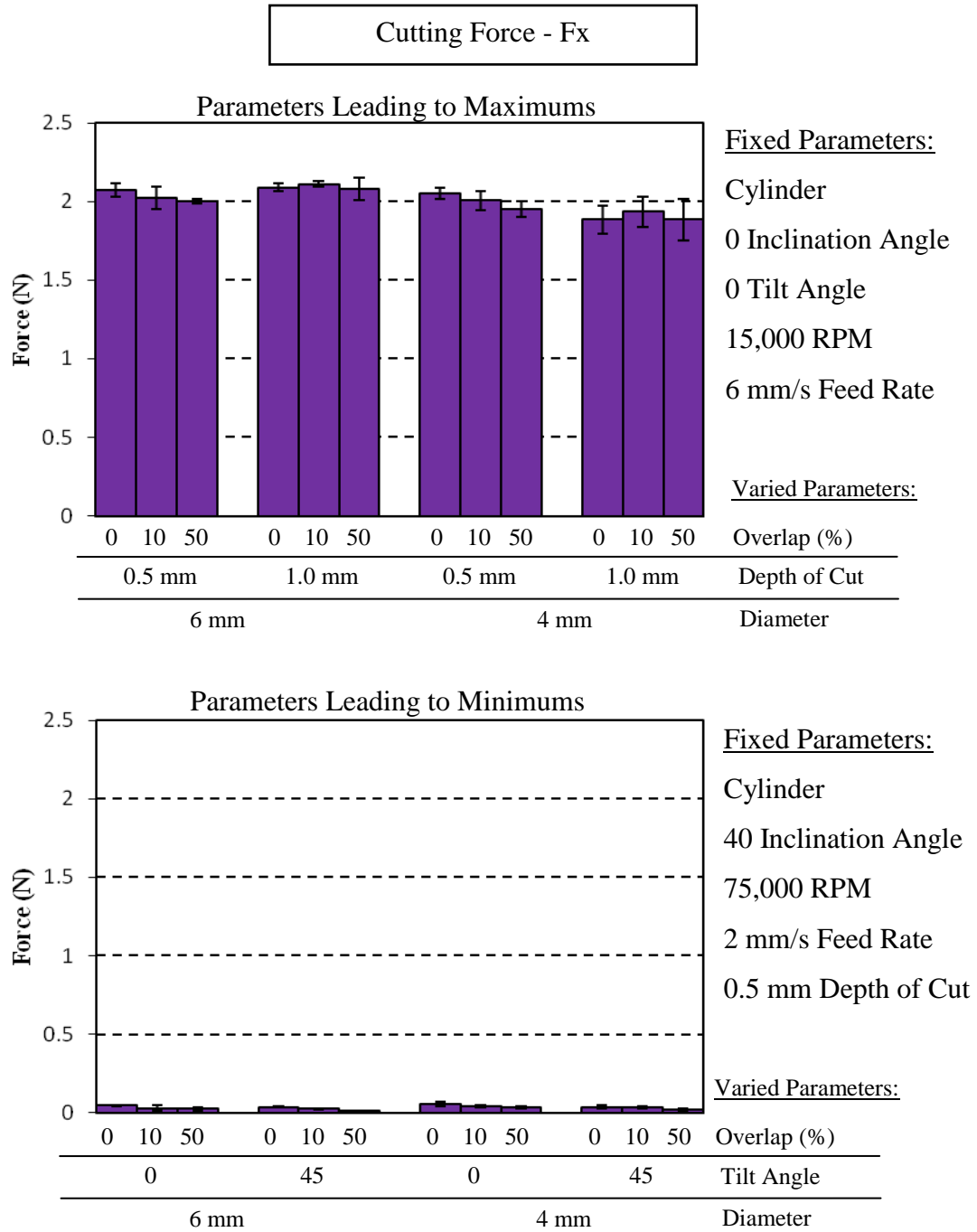


**Figure 3.5: Maximum and minimum measurements for cutting force - F<sub>x</sub>**

Parameters that lead to maximum and minimum measurements for cutting force in the X direction are presented above. A fixed combination of parameters (listed above) that led to maximum outcomes resulted in an average cutting force of  $2.01 \pm 0.08$  N. A combination of parameters that led to minimum outcomes resulted in forces of  $0.03 \pm 0.01$  N.

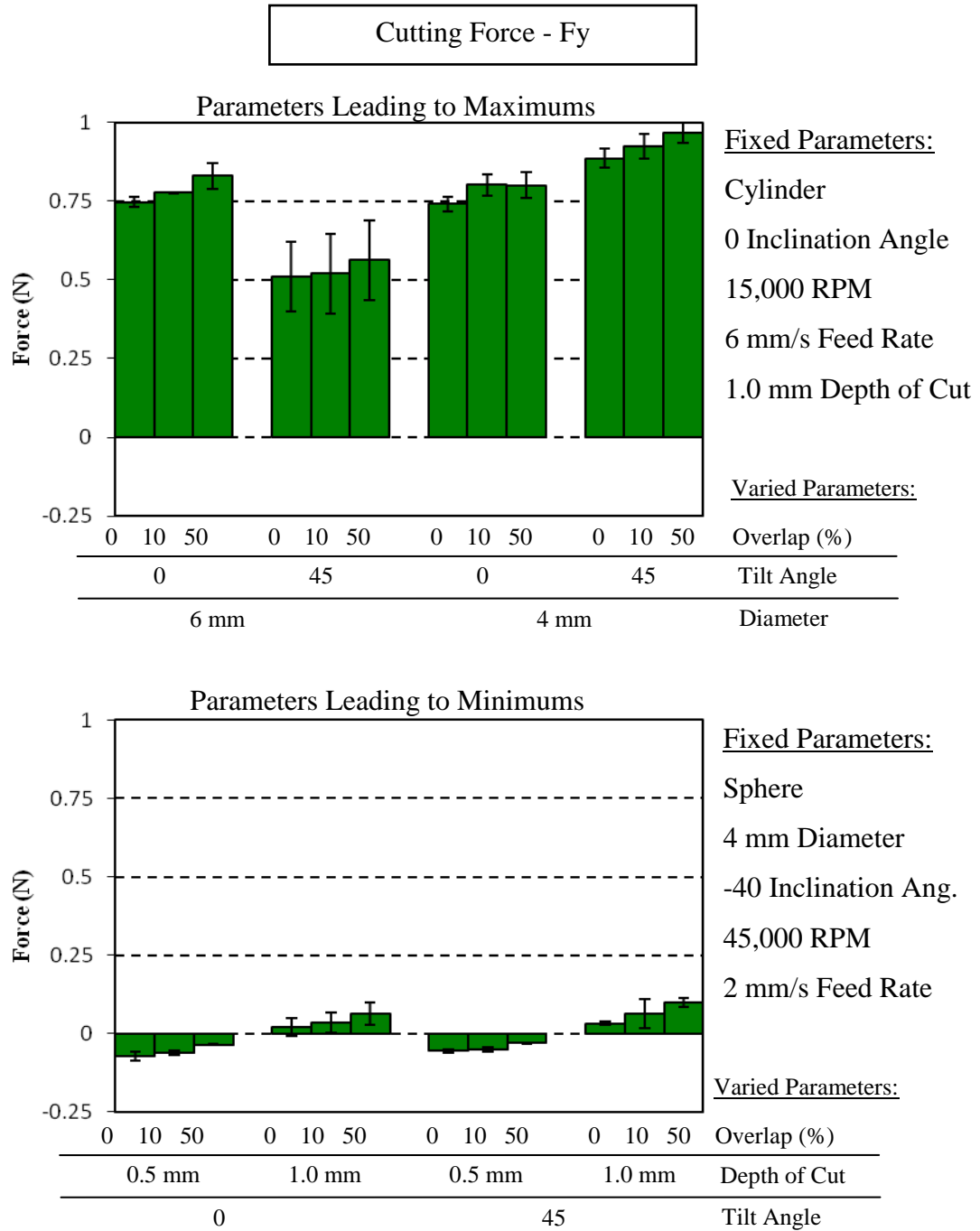


**Figure 3.6: Maximum and minimum measurements for cutting force - F<sub>y</sub>**

Parameters that lead to maximum and minimum measurements for cutting force in the Y direction are presented above. A fixed combination of parameters (listed above) that led to maximum outcomes resulted in an average cutting force of  $0.76 \pm 0.15$  N. A combination of parameters that led to minimum outcomes resulted in forces of  $0.00 \pm 0.06$  N.

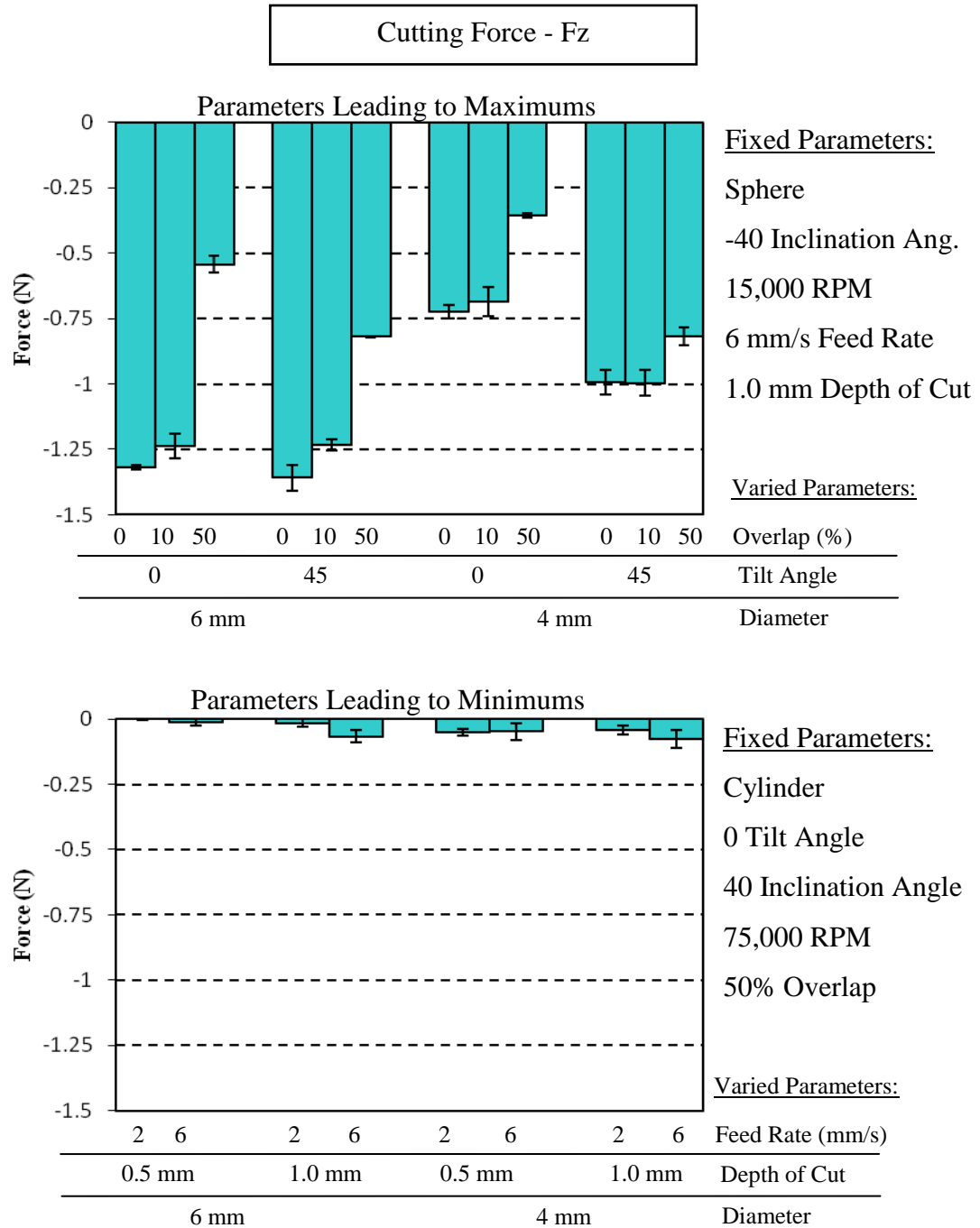


**Figure 3.7: Maximum and minimum measurements for cutting force - Fz**

Parameters that lead to maximum and minimum measurements for cutting force in the Z direction are presented above. A fixed combination of parameters (listed above) that led to maximum outcomes resulted in an average cutting force of  $-0.92 \pm 0.32$  N. A combination of parameters that led to minimum outcomes resulted in forces of  $-0.04 \pm 0.03$  N.

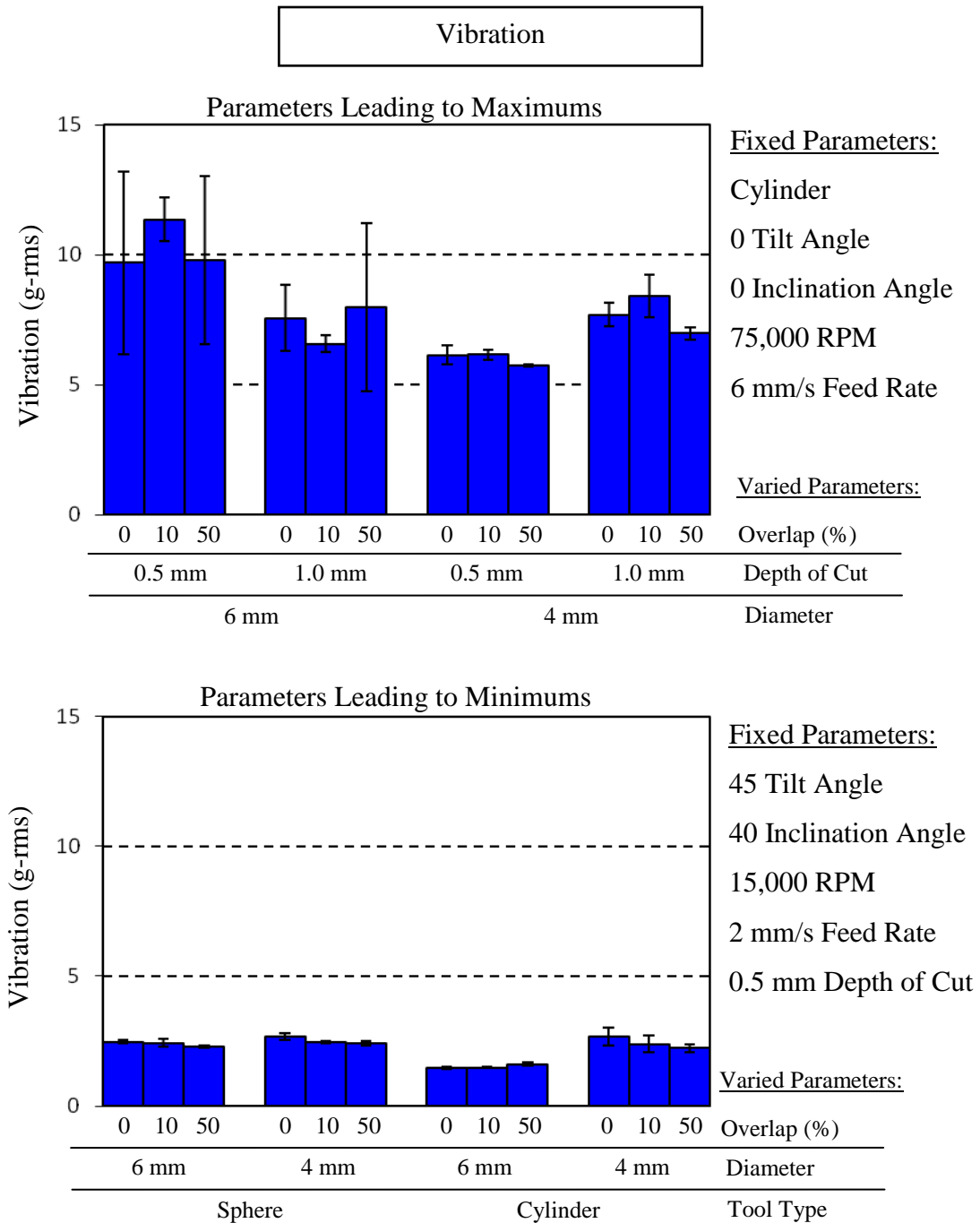


**Figure 3.8: Maximum and minimum measurements for vibration**

Parameters that lead to maximum and minimum measurements for vibration are presented above. A fixed combination of parameters (listed above) that led to maximum outcomes resulted in an average vibration of  $7.8 \pm 1.7$  g-rms. A combination of parameters that led to minimum outcomes resulted in vibrations of  $2.2 \pm 0.4$  g-rms.

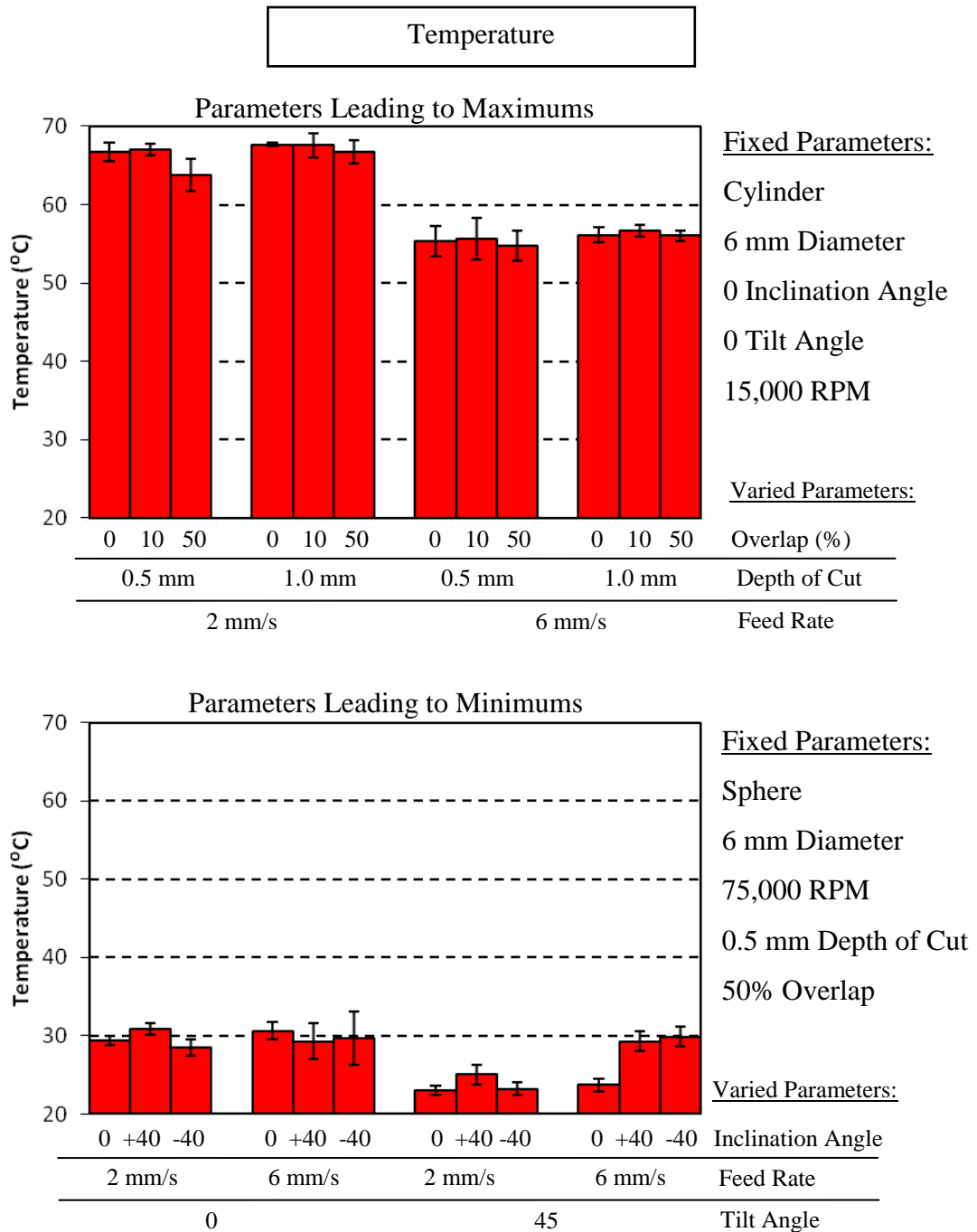


**Figure 3.9: Maximum and minimum measurements for temperature**

Parameters that lead to maximum and minimum measurements for temperature are presented above. A fixed combination of parameters (listed above) that led to maximum outcomes resulted in an average temperature of  $61.2 \pm 5.8$  °C. A combination of parameters that led to minimum outcomes resulted in an average temperature of  $27.7 \pm 3.0$  °C.

### 3.4 Chapter Summary

A full factorial analysis of eight process parameters with various levels was conducted. Statistical significance was found at the multivariate level for each of the process parameters. Statistical significance was also found at the univariate level for each of the outcome measurements and process parameters. This was likely due to the very high performance levels of repeatability and measurement precision that the apparatus was able to produce in Chapter 2. High signal-to-noise, coupled with high repeatability and high precisions, improve the statistical power of finding significance in even small effect sizes. As such, even small changes in any process parameter produced statistically significant effects in the outcomes measurements. While strong performance metrics are positive for the apparatus design in Chapter 2, this posed difficult in identifying specific influential parameters.

The variability in outcome measurements was also examined, through use of process parameters the led to maximum and minimums for each of the outcome measurements. The variability in selection of process parameters is important, as it quantifies to what amount the selection of process parameters can affect the outcome measurements independently. The selection of process parameters can bring the cutting force values all below a threshold of 0.25 N. The dynamics of the system can also be minimized from an average of  $7.8 \pm 1.7$  g-rms to an average of  $2.2 \pm 0.4$  g-rms. Additionally, temperatures can be altered to the extent of 34 °C based solely on the selection of process parameters within the experimental matrix. The ability to constrain certain process parameters proves advantageous from these findings, as the outcome measurements can be optimized based

on fixing certain process parameters which may be possible in an automated burring procedure.

The parameters that led to maximum and minimums are useful in the selection of process parameters for optimizing outcome measurements independently. However, the descriptive statistics do not take into account the tradeoffs between the outcome measurements. Although a handful of parameters may be efficient for one outcome measurement, they may in turn not be optimal for a separate outcome measurement. Further analysis should be taken in evaluating the tradeoffs and clinical relevance in selection of the process parameters for all five outcome measurements collectively.

It was originally anticipated that the statistical model would aid in the selection of the process parameters; however, as statistical significance was seen virtually everywhere, it becomes increasingly difficult to distinguish between importance and non-importance in selection of the parameters. Although, the high statistical significance did support the second hypothesis, the ability to form a rationale in selection of optimal or suboptimal parameters with these findings alone is difficult. The trends in the data could help to form a rationale as seen in the main effects plots; however, these plots encompass pooled results of all other parameters, minimizing the differences that could ensue due to selecting synergistic factors that lead to desirable or undesirable results. Higher order interactions (up to eight-factors which corresponds with the current experimental matrix) can be viewed, but they become increasingly difficult to comprehend and interpret.

Therefore, moving forward, methods to narrow the statistical model on certain areas of the experimental matrix which would allow for smaller, and more concise statistical analyses, should be pursued.



## Chapter 4 - Process Parameter Selection for Clinical Implementation

***OVERVIEW:** The aim of the current chapter is to reduce the experimental matrix presented in chapter 3 to fewer combinations of parameters to allow for more concise statistical analyses to be performed. The main goal of selecting smaller subsections of parameters was to select parameters which would result in maximizing or minimizing a specified objective function. The combinations of parameters and their associated outcome measurements will help form a rationale in the selection of process parameters in which to carry out or avoid in a bone burring procedure.*

### 4.1 Reduction of Parameters

An eight-way MANOVA with five outcome measurements was conducted in Chapter 3 to aid in the selection of process parameters. However, as statistical significance was seen practically everywhere, it was difficult to form a rationale behind selection of certain parameters. Therefore, the experimental matrix was broken up into smaller subsections to allow for smaller and more concise statistical analyses to be performed.

A heuristic filtering method, described in section 4.1.2, was conducted to restrict the parameters to certain levels which resulted in maximizing or minimizing the associated objective functions. Forces were removed from the filtering process as the forces were

not clinically relevant based on the magnitudes reported by the descriptive statistics ( $F_x$ ,  $F_y$ ,  $F_z < 3$  N).

#### 4.1.1 Criteria for Reduction of Parameters

Four separate areas were regarded as key areas of the experimental matrix and reduced sample sets were generated. The criteria which led to the reduced sample sets are:

- Reduced sample set 1 - local minimums of temperature and vibration measurements
- Reduced sample set 2 - local maximums of temperature and vibration measurements
- Reduced sample set 3 - absolute maximums of temperature measurements
- Reduced sample set 4 - absolute maximums of vibration measurements

Parameters that led to local minimums of temperature and vibration were viewed as optimal parameters to perform the burring procedure at to avoid thermal damage to the bone and to ensure a dynamically safe burring process. The knowledge of how to minimize temperature and dynamic effects via selection of process parameters would be invaluable in the design of a burring pathway to the tool; as it provides rationale for tool selection and machining parameters associated with bone burring.

Parameters that lead to local maximums of temperature and vibration are parameters that should be avoided as they may lead to unsafe implementation. The parameters that result in high temperatures and high vibrations may be synergistic with one another. This in turn may result in temperatures that lead to necrosis or a dynamically unsafe burring process, based solely on the choice of a select few parameters.

The rationale in selection of viewing parameters that led to maximums in temperature and vibration separately, was that the parameters that lead to maximums of both measurements may not necessarily result in absolute maximums independently. For example, based on the pairwise comparison of the main effect results of Chapter 3, the rotational speed of the tool had opposite effects on the measurements of vibration and temperature. Increasing the rotational speed from 15,000 to 75,000 rpm increased the dynamic effects of the system, but decreased the temperature experienced by the workpiece. Therefore, parameters that result in maximums of temperature and vibration were additionally investigated independently of one another.

#### 4.1.2 Heuristic Filtering Methods

To narrow down the combinations of process parameters; a heuristic filtering process was applied. The main goal of the filtering process was to select a handful of process parameters that led to the criteria outlined in section 4.1.1. To aid in this process, forces were ignored. The rationale behind excluding forces was that they were not clinically significant due to their low magnitudes ( $F_x, F_y, F_z < 3\text{N}$ ). Therefore, regardless of which parameters are settled upon in the filtering process, the burring process will not result in high cutting forces ( $> 3\text{ N}$ ).

The temperature and vibration measurements were plotted against one another for every combination of process parameters within the experimental matrix (Figure 4.1). Key areas, which corresponded to the criteria were highlighted. Three of the process parameters were fixed to reduce the matrix size and filter out process parameters that led to the specified criteria (Figure 4.2). The remaining combinations were then plotted (with

temperature and vibration measurements), and were visually confirmed to meet the overlying criteria. This was repeated for each criteria which was associated with the reduced sample set.

## 4.2 Statistical Analysis

After the filtering process was complete, forces which corresponded to the associated burring trial, were reintroduced into the reduced sample set for statistical analysis. A five-way MANOVA was performed on each of the reduced sample sets. If significance was found at the multivariate level; an ANOVA was conducted. Pairwise comparison tests were then performed on any factors that led to statistical significance at the univariate level. An overall alpha of 0.05 ( $p < 0.05$ ) was used to determine statistical significance. All results are reported as the population mean  $\pm$  95% confidence interval.

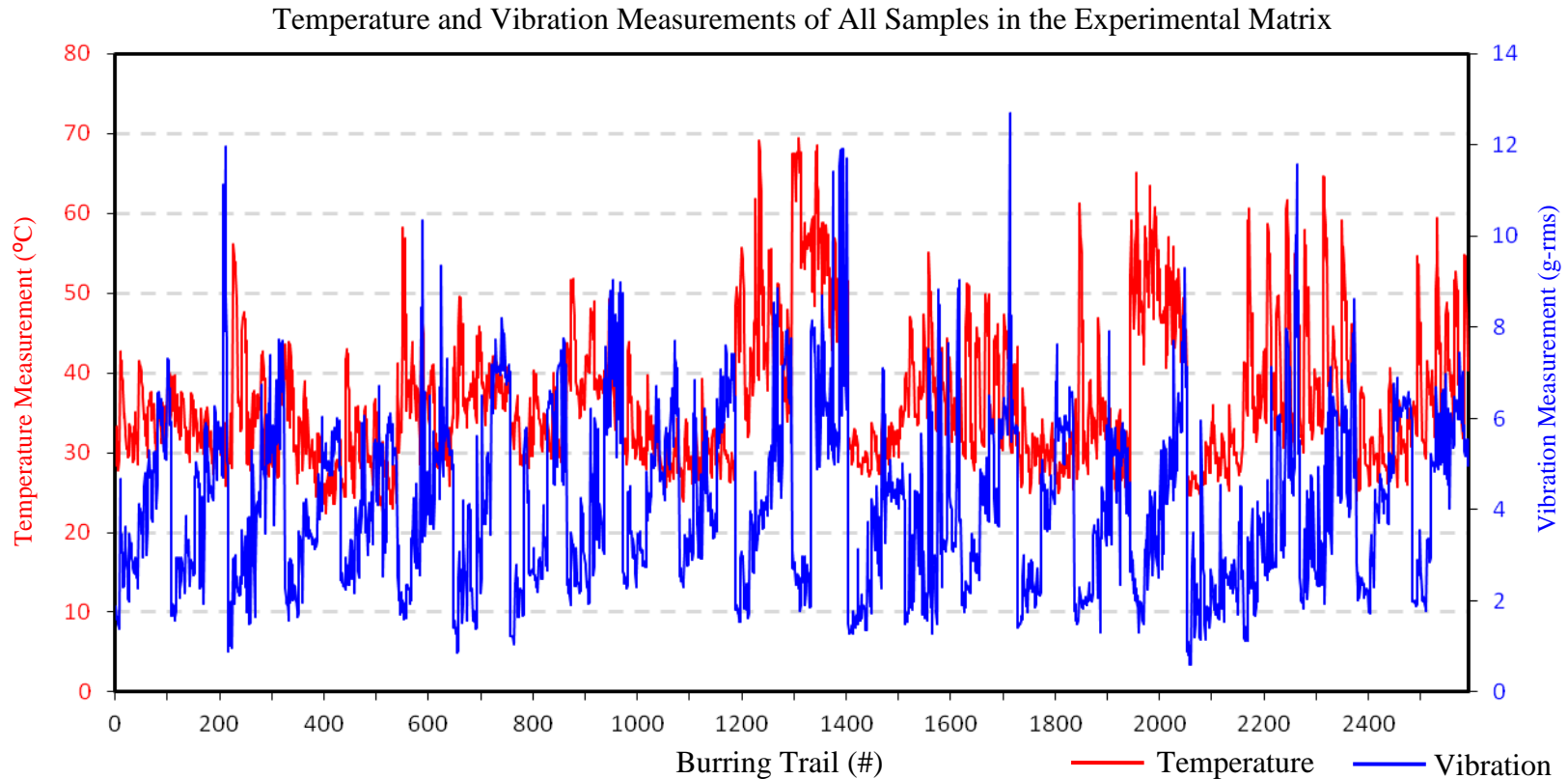


**Figure 4.1: Measurements from experimental matrix**

*All samples in the experimental matrix with outcome measurements for temperature (red) and vibration (blue) is presented above. Force results were excluded as they were not clinically relevant due to their low absolute forces ( $< 3\text{ N}$  in all directions). The graph shown was used in attempt to reduce the experimental matrix to smaller sample sizes which would aid in the selection of process parameters for the burring process.*



## 4.3 Local Minimums for Temperature and Vibration

### 4.3.1 Heuristic Filtering Results

The heuristic filtering method led to fixing the parameters of rotational speed, feed rate and overlap at levels 15,000 rpm, 2 mm/s, and 50% which produced local minimums of temperature and vibration. The remaining process parameters (tool type, diameter, tilt angle, inclination angle, and depth of cut) were not fixed and comprised of the reduced sample set. Each of the process parameters produced statistically significant differences at the multivariate level ( $p \leq 0.002$ ) (Table 4.1).

### 4.3.2 Vibration

An inclination angle of +40 degrees resulted in an average vibration of  $1.80 \pm 0.07$  g-rms, whereas 0 and -40 degrees inclination resulted in  $2.10 \pm 0.07$  g-rms ( $p < 0.001$ ) and  $2.00 \pm 0.07$  g-rms ( $p < 0.001$ ). A depth of cut of 0.5 mm produced a mean vibration of  $0.47 \pm 0.08$  g-rms less than a 1 mm depth of cut ( $p < 0.001$ ). Tool type and diameter of the tool did not produce statistically significant differences in vibration.

### 4.3.3 Temperature

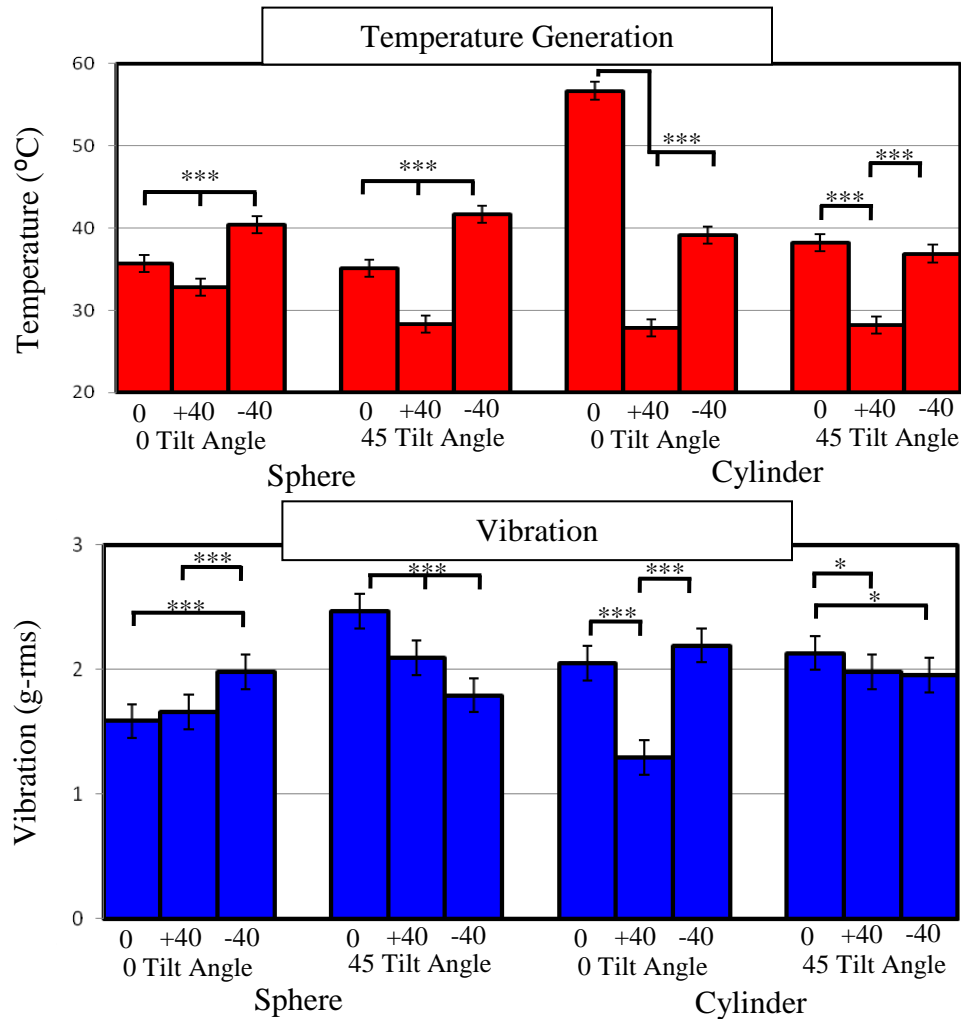
An inclination angle of +40 degrees ( $29.3 \pm 0.5$  °C) produced the lowest average temperature compared to the 0 ( $41.5 \pm 0.5$  °C) ( $p < 0.001$ ) and -40 degrees ( $39.5 \pm 0.5$  °C) ( $p < 0.001$ ) (Table 4.1). A depth of cut of 0.5 mm produced a mean temperature of  $33.0 \pm 0.4$  °C whereas a depth of cut of 1.0 mm produced a mean temperature of  $40.5 \pm 0.4$  °C ( $p < 0.001$ ). At 0 degrees inclination, a cylinder tool produced a mean temperature of  $47.5 \pm 0.7$  °C; at the same inclination angle a sphere tool produced a mean temperature of  $35.4 \pm 0.7$  °C ( $p < 0.001$ ) (Figure 4.3).

Table 4.1: Summary of statistical analysis for process parameters that resulted in local minimums of temperature and vibration

<b>Local Minimums of Temperature and Vibration - Factors Fixed (Rotational Speed = 15,000 rpm, Feed Rate = 2 mm/s, Overlap = 50%)</b>											
<b>Multivariate Analysis - Main Effects</b>											
<i>Tool Type</i>		<i>Diameter</i>			<i>Tilt Angle</i>		<i>Inclination Angle</i>		<i>Depth of Cut</i>		
p<0.001		p=0.002			p<0.001		p<0.001		p<0.001		
<b>Univariate Analysis - Main Effects</b>											
<b>Temperature (°C)</b>					<b>Vibration (g-rms)</b>						
<i>Tool Type</i>	<i>Diameter</i>	<i>Tilt Angle</i>	<i>Inclination Angle</i>	<i>Depth of Cut</i>		<i>Tool Type</i>	<i>Diameter</i>	<i>Tilt Angle</i>	<i>Inclination Angle</i>	<i>Depth of Cut</i>	
p<0.001	p=0.057	p<0.001	p<0.001	p<0.001		p=0.903	p=0.990	p<0.001	p<0.001	p<0.001	
<b>Pairwise Comparison</b>											
<u>Level-1</u>	35.7±0.4	37.0±0.4	38.8±0.4	41.5±0.5	33.0±0.4		1.93±0.05	1.93±0.05	1.80±0.05	2.10±0.07	1.69±0.05
<u>Level-2</u>	37.8±0.4	36.5±0.4	34.8±0.4	29.3±0.5	40.5±0.4		1.93±0.05	1.93±0.05	2.07±0.05	1.80±0.07	2.17±0.05
<u>Level-3</u>	-	-	-	39.5±0.5	-		-	-	-	2.00±0.07	-

Table 4.1 outlines the MANOVA results for the reduced sample set that resulted from locking certain factors that led to local minimums for both temperature and vibration (rotational speed = 15,000 rpm, feed rate = 2 mm/s, overlap = 50%). The multivariate and univariate results are presented in the above table. Temperature and vibration measurements are outlined (mean ± 95% confidence interval) at each of the levels of the associated process parameter.





**Figure 4.3: Temperature measurements of the sphere and cylinder tools at varying inclination and tilt angles**

The above figure illustrates the sensitivity of the sphere and cylinder bits due to the angle of the tool with respect to the workpiece. The sphere tool produced a range of data (max-min) of 13.4 °C at varying inclination angle increments and tilt angles. The cylinder tool produced a range of 28.5 °C at various increments of inclination angle and tilt angle. Significant differences are denoted by \*,  $p < 0.05$ ; \*\*,  $p < 0.01$ ; \*\*\*,  $p < 0.001$ .

## 4.4 Local Maximums of Temperature and Vibration

### 4.4.1 Heuristic Filtering Result

Originally, the heuristic filtering method led to fixing the parameters of rotational speed, inclination angle and overlap at levels of 75,000 rpm, 0 degrees, and 0%. Since an overlap of 0% is rarely encountered practically (only on first the cut of a burring path), a 10% overlap path is more of practical interest. Therefore, overlap was fixed at 10% rather than 0%. The remaining parameters (tool type, diameter, tilt angle, feed rate, and depth of cut) were not fixed and comprised of the reduced sample set. Each of the parameters were found to produce statistically significant differences at the multivariate level ( $p < 0.001$ ) (Table 4.2).

### 4.4.2 Vibration

Increasing the feed rate from 2 to 6 mm/s resulted in an increase of  $1.23 \pm 0.21$  g-rms ( $p < 0.001$ ). A tilt angle of 0 degrees resulted in a mean vibration of  $6.58 \pm 0.21$  g-rms, whereas a tilt angle of 45 degrees resulted in a mean vibration of  $5.82 \pm 0.21$  g-rms ( $p < 0.001$ ).

### 4.4.3 Temperature

The sphere ( $32.4 \pm 0.6$  °C) bit produced lower mean temperatures compared to the cylinder bit ( $43.5 \pm 0.6$  °C) ( $p < 0.001$ ). A 45 degree tilt angle produced a mean temperature of  $8.8 \pm 0.8$  °C less than a 0 degree tilt ( $p < 0.001$ ).

Table 4.2: Summary of statistical analysis for process parameters that resulted in local maximums of temperature and vibration

<b>Local Maximums of Temperature and Vibration - Factors Fixed (Rotational Speed = 75,000 rpm, Inclination Angle = 0, Overlap = 10%)</b>											
<b>Multivariate Analysis - Main Effects</b>											
<i>Tool Type</i>		<i>Diameter</i>		<i>Tilt Angle</i>		<i>Feed Rate</i>		<i>Depth of Cut</i>			
p<0.001		p<0.001		p<0.001		p<0.001		p<0.001			
<b>Univariate Analysis - Main Effects</b>											
<b>Temperature (°C)</b>					<b>Vibration (g-rms)</b>						
<i>Tool Type</i>	<i>Diameter</i>	<i>Tilt Angle</i>	<i>Feed Rate</i>	<i>Depth of Cut</i>		<i>Tool Type</i>	<i>Diameter</i>	<i>Tilt Angle</i>	<i>Feed Rate</i>	<i>Depth of Cut</i>	
p<0.001	p<0.001	p<0.001	p=0.926	p<0.001		p=0.009	p=0.372	p<0.001	p<0.001	p=0.884	
<b>Pairwise Comparison</b>											
<u>Level-1</u>	32.4±0.6	36.6±0.6	42.3±0.6	37.9±0.6	36.1±0.6		6.01±0.21	6.27±0.21	6.58±0.21	5.59±0.21	6.19±0.21
<u>Level-2</u>	43.5±0.6	39.3±0.6	33.5±0.6	37.9±0.6	39.8±0.6		6.40±0.21	6.14±0.21	5.82±0.21	6.82±0.21	6.22±0.21
<u>Level-3</u>	-	-	-	-	-		-	-	-	-	-

Table 4.2 outlines the MANOVA results for the reduced sample set that resulted from locking certain factors that led to local maximums for both temperature and vibration (rotational speed = 75,000 rpm, inclination angle = 0 degrees, overlap = 10%). The multivariate and univariate results are outlined in the above table. Temperature and vibration measurements are also outlined (mean ± 95 % confidence interval) at each of the levels of the associated process parameter.

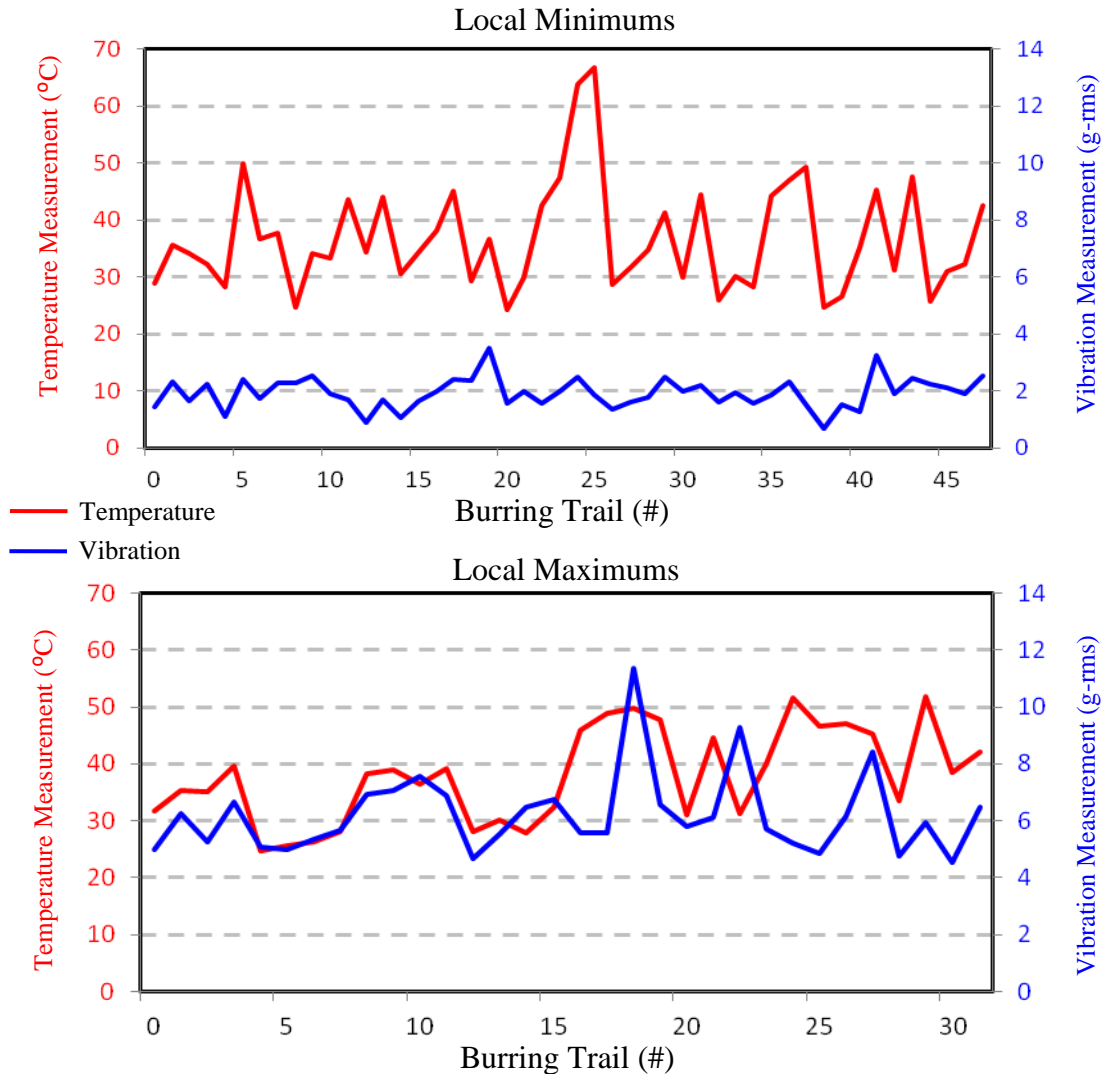


**Figure 4.4: Local minimums and maximums of temperature and vibration measurements**

*The outcome measurements (temperature and vibration) of all combinations of process parameters within the reduced sample sets that led to local minimums and maximums is shown above. Subsections within the combinations of process parameters that led to minimums in temperature ( $<30$  °C) and vibration ( $<3$  g-rms) can be found within the local minimums sample set. However, no combinations of parameters that minimize temperature and vibration can be found within the local maximums sample set. A full list of the corresponding burring trial numbers can be found in Appendix D.*

## 4.5 Absolute Maximums of Temperature

### 4.5.1 Heuristic Filtering Results

Fixing the parameters of tool type, inclination angle, and tilt angle at levels of cylinder, 0 degrees, and 0 degrees produced absolute maximums of temperature. The remaining parameters (diameter, rotational speed, feed rate, depth of cut, and overlap) were not fixed and comprised of the reduced sample set. Each of the parameters were found to produce statistically significant differences at the multivariate level ( $p < 0.001$ ) (Table 4.3).

### 4.5.2 Vibration

A rotational speed of 75,000 rpm increased the vibration by  $4.31 \pm 0.23$  g-rms ( $p < 0.001$ ) and  $1.38 \pm 0.23$  G-rms ( $p < 0.001$ ) compared to 15,000 and 45,000 rpm. Increasing the feed rate from 2 to 6 mm/s resulted in an increase of vibration of  $0.95 \pm 0.26$  g-rms ( $p < 0.001$ ).

### 4.5.3 Temperature

A 6 mm diameter tool ( $55.7 \pm 0.5$  °C) produced larger average temperatures than the 4 mm diameter tool ( $50.4 \pm 0.5$  °C) ( $p < 0.001$ ). A 6 mm/s feed rate decreased the mean temperature by  $4.5 \pm 0.5$  °C compared to a feed rate of 2 mm/s ( $p < 0.001$ ). A rotational speed of 75,000 rpm produced an average temperature of  $48.9 \pm 0.5$  °C; whereas, a rotational speed of 15,000 and 45,000 rpm produced average temperatures of  $56.4 \pm 0.5$  °C ( $p < 0.001$ ) and  $54.0 \pm 0.5$  °C ( $p < 0.001$ ).

Table 4.3: Summary of statistical analysis for process parameters that resulted in absolute maximums of temperature

<b>Absolute Maximums of Temperature - Factors Fixed (Tool Type = Cylinder, Inclination Angle = 0, Tilt Angle = 0)</b>											
<b>Multivariate Analysis - Main Effects</b>											
<i>Diameter</i>		<i>Rotational Speed</i>			<i>Feed Rate</i>		<i>Depth of Cut</i>		<i>Overlap</i>		
p<0.001		p<0.001			p<0.001		p<0.001		p<0.001		
<b>Univariate Analysis - Main Effects</b>											
<b>Temperature (°C)</b>					<b>Vibration (g-rms)</b>						
<i>Diameter</i>	<i>Rotational Speed</i>	<i>Feed Rate</i>	<i>Depth of Cut</i>	<i>Overlap</i>		<i>Diameter</i>	<i>Rotational Speed</i>	<i>Feed Rate</i>	<i>Depth of Cut</i>	<i>Overlap</i>	
p<0.001	p<0.001	p<0.001	p<0.001	p<0.001		p<0.001	p<0.001	p<0.001	p=0.008	p=0.012	
<b>Pairwise Comparison</b>											
<u>Level-1</u>	55.7±0.5	56.4±0.6	55.3±0.5	52.3±0.5	55.5±0.6		5.50±0.19	2.38±0.23	4.32±0.19	4.97±0.19	4.91±0.23
<u>Level-2</u>	50.4±0.5	54.0±0.6	50.8±0.5	53.9±0.5	53.0±0.6		4.08±0.19	5.30±0.23	5.26±0.19	4.61±0.19	4.96±0.23
<u>Level-3</u>	-	48.9±0.6	-	-	50.7±0.6		-	6.89±0.23	-	-	4.50±0.23

Table 4.3 outlines the MANOVA results for the reduced sample set that resulted from locking certain factors that led to absolute maximums of temperature (tool type = cylinder, inclination angle = 0 degrees, tilt angle = 0 degrees). The multivariate and univariate results are outlined in the above table. Temperature and vibration measurements are outlined (mean ± 95% confidence interval) at each of the levels of the associated process parameter.

## 4.6 Absolute Maximums of Vibration

### 4.6.1 Heuristic Filtering Results

The heuristic filtering method led to fixing the factors of rotational speed, feed rate, and overlap at levels of 75,000 rpm, 6 mm/s, and 10% which produced absolute maximums of vibration. The remaining factors (tool type, diameter, tilt angle, inclination angle, and depth of cut) were not fixed and comprised of the reduced sample set that was analyzed in the MANOVA. Each of the factors were found to produce statistically significant differences at the multivariate level ( $p < 0.001$ ) (Table 4.4).

### 4.6.2 Vibration

A cylinder tool decreased the average vibration by  $0.59 \pm 0.31$  g-rms compared to the sphere tool ( $p < 0.001$ ). A +40 degrees inclination decreased the average vibration by  $0.95 \pm 0.47$  g-rms ( $p < 0.001$ ) and  $0.34 \pm 0.47$  g-rms ( $p = 0.247$ ) compared to 0 and -40 degree inclination angles.

### 4.6.3 Temperature

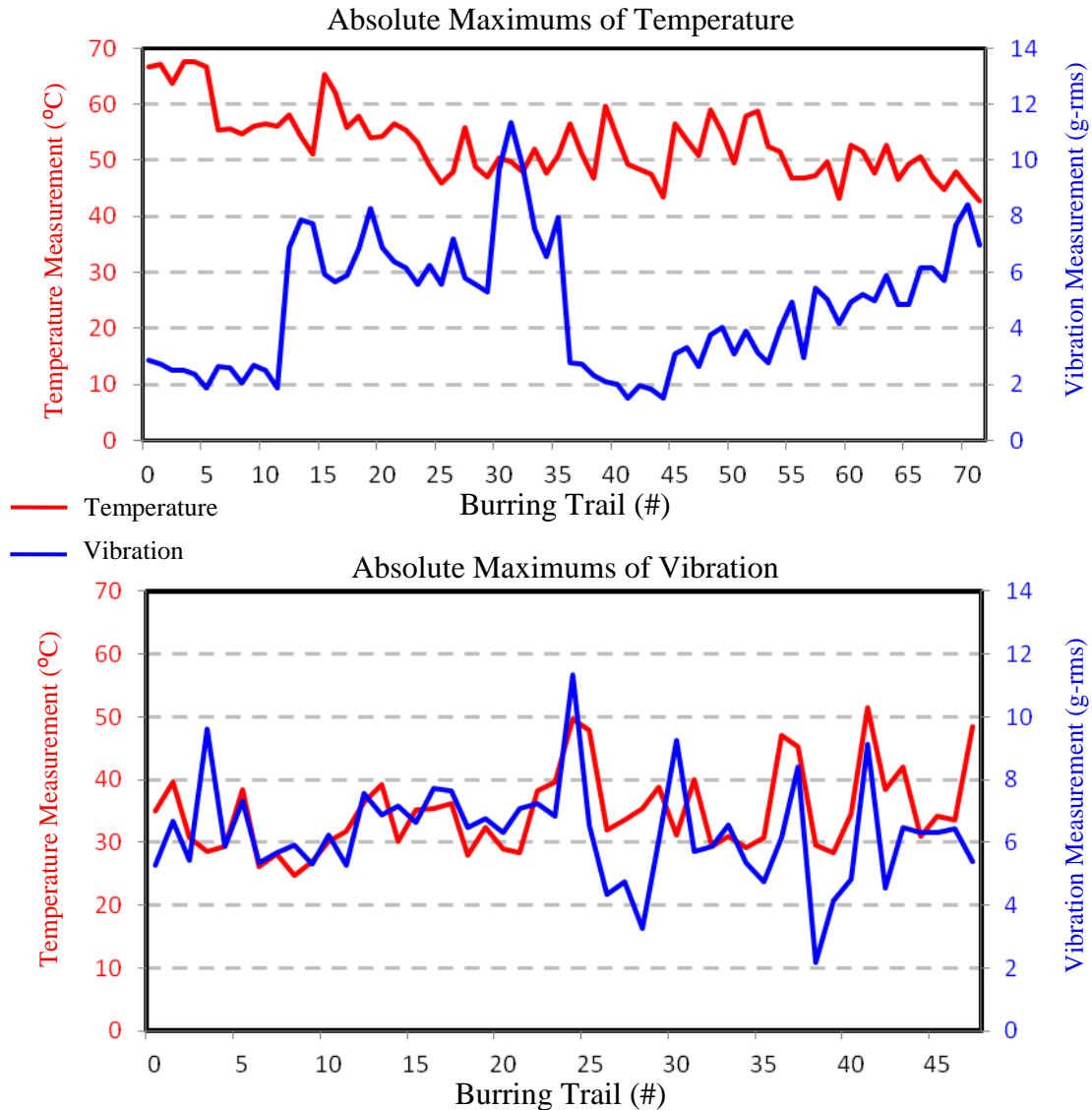
A sphere tool produced an average of  $4.8 \pm 0.6$  °C less than the cylinder tool ( $p < 0.001$ ). An inclination angle of +40 degrees produced an average temperature of  $30.2 \pm 0.6$  °C whereas a 0 and -40 degree inclination angles produced average temperatures of  $37.9 \pm 0.6$  °C ( $p < 0.001$ ) and  $36.4 \pm 0.6$  °C ( $p < 0.001$ ).

Table 4.4: Summary of statistical analysis for process parameters that resulted in absolute maximums of vibration

<b>Absolute Maximums of Vibration - Factors Fixed (Rotational Speed = 75,000 rpm, Feed Rate = 6 mm/s, Overlap = 10%)</b>											
<b>Multivariate Analysis - Main Effects</b>											
<i>Tool Type</i>		<i>Diameter</i>			<i>Tilt Angle</i>		<i>Inclination Angle</i>			<i>Depth of Cut</i>	
p<0.001		p<0.001			p<0.001		p<0.001			p<0.001	
<b>Univariate Analysis - Main Effects</b>											
<b>Temperature (°C)</b>					<b>Vibration (g-rms)</b>						
<i>Tool Type</i>	<i>Diameter</i>	<i>Tilt Angle</i>	<i>Inclination Angle</i>	<i>Depth of Cut</i>		<i>Tool Type</i>	<i>Diameter</i>	<i>Tilt Angle</i>	<i>Inclination Angle</i>	<i>Depth of Cut</i>	
p<0.001	p<0.001	p<0.001	p<0.001	p<0.001		p<0.001	p=0.063	p=0.041	p<0.001	p=0.013	
<b>Pairwise Comparison</b>											
<u>Level-1</u>	32.4±0.4	33.3±0.4	37.0±0.4	37.9±0.5	33.1±0.4		6.60±0.22	6.15±0.22	6.46±0.22	6.82±0.27	6.10±0.22
<u>Level-2</u>	37.2±0.4	36.3 ±0.4	32.6±0.4	30.2±0.5	36.5±0.4		6.00±0.22	6.45±0.22	6.14±0.22	5.87±0.27	6.50±0.22
<u>Level-3</u>	-	-	-	36.4±0.5	-		-	-	-	6.21±0.27	-

Table 4.4 outlines the MANOVA results for the reduced sample set that resulted from locking certain factors that led to absolute maximums for vibration (rotational speed = 75,000 rpm, feed rate = 6 mm/s, overlap = 10%). The multivariate and univariate results are outlined in the above table. Temperature and vibration measurements are outlined (mean ± 95% confidence interval) at each of the levels of the associated process parameter.





**Figure 4.5: Absolute maximums of temperature and vibration**

The outcome measurements (temperature and vibration) of all combinations of process parameters within the reduced sample sets that led to maximums of temperature and vibration is shown above. By choosing an inclination and tilt angle of 0 degrees, coupled with a cylinder tool; an average temperature of  $53 \pm 6$  °C was induced regardless of the selection of other parameters. Likewise, fixing the burring process at a rotational speed of 75,000 rpm, feed rate of 6 mm/s and overlap of 10% resulted in an average vibration  $6.3 \pm 1.6$  g-rms. A full list of the corresponding burring trial numbers can be found in Appendix D.

## 4.7 Chapter Summary

The experimental matrix which was comprised of each outcome measurement for all combinations of parameters was narrowed down to reduced sample sets. This was done to aid in the selection of process parameters associated with the bone burring process.

Selecting a rotational speed of 15,000 rpm with a 2 mm/s feed rate and 50% overlap was found to provide optimal process parameters that led regions of minimums of temperature ( $<30\text{ }^{\circ}\text{C}$ ) and vibration ( $<3\text{ g-rms}$ ). Selection of a rotational speed of 75,000 rpm, inclination angle of  $0^{\circ}$ , and an overlap of 10%, resulted in a condition where no combination of the remaining parameters produced low temperature and low vibration. This was also indicated by the larger average magnitudes of the main effects pairwise in comparing the optimal to suboptimal parameter set (Table 4.1 and Table 4.2).

The findings that certain sets of parameters can produce optimal or suboptimal outcome measurements with statistical significance, fully supports the second hypothesis. Additionally, the initial trends of increasing the material removal rate increases the process outcomes mostly agreed as indicated by the pairwise comparison trends in Table 4.1 and Table 4.2. However, the only factor that contradicted this hypothesis, was that although a higher feed rate resulted in higher dynamic effects, it did not necessarily result in higher temperatures as indicated by the results in Table 4.3. This contradiction is believed to be due to the reduced time to allow for heat conduction between the tool-workpiece interface previously established by Shin *et al.*[40].

Additionally, Chapter 4 investigated certain parameters that should not be jointly constrained, if the objective is to avoid high temperatures or high dynamic effects.

Selection of a cylinder tool with 0 inclination and 0 tilt angle resulted in temperatures of greater than 40 °C regardless of how the remaining process parameters were selected. Selecting a rotational speed of 75,000 rpm, feed rate of 6 mm/s, and overlap of 10% resulted in high vibrations for combinations of remaining parameters ( $6.3 \pm 1.6$  g-rms). To allow for the design of the tool path trajectory to have the fewest constraints, these parameters should be avoided, as they do not offer any advantages in the context of avoiding high temperatures and high vibrations.

A sensitivity analysis of the tool's response to changes in angles was also performed. The analysis found that the cylinder produced larger differences in inclination angles and tilt angles. The cylinder tool produced the highest temperatures at a 0 degree inclination angle. Therefore, to use the cylinder tool safely, the tool should enter the burring process with a positive or negative inclination angle; although preference would be given to a positive angle as it produced the lowest temperature and vibration as indicated by Figure 4.3.

By performing the large experimental matrix with 864 unique parameter combinations, a select few have been distinguished to be optimal in providing low temperature generation as well as low dynamic effects. The sawbone analog was useful in this analysis because its uniformity allowed for the identification of process trends, while its availability made the large number of trials possible. While the absolute levels of temperature and vibrations are likely different in real bone, it is reasonable to anticipate that these same trends will be relevant, given that the trends are a function of the process parameters. However, it is valuable to know the absolute levels of temperature and vibration for

burring real bone, and so moving forward, the selection of optimal process parameters should be validated on cancellous bone specimens.

## Chapter 5 - Experimental Validation of Process Parameters on Porcine Cadaver Model

***OVERVIEW:** The aim of the current chapter was to quantify the effects of various process parameters using five outcome measurements (cutting force in three directions, vibration, and temperature) on a porcine cadaver specimen. The burring process was performed on cancellous bone located at the distal porcine femur. Specimen and data preparation are discussed within this chapter. Additionally, a method adapted from Chapter 3 to normalize the temperature to the center of the tool, was performed using the porcine specimen as a workpiece. Two sets of parameters were investigated which involved an optimal and suboptimal set of parameters. A statistical analysis (repeated measures multivariate analysis of variance) was conducted to quantify the main-effects and interactions between the process parameters.*

### 5.1 Parameter Selection

A handful of parameters from the experimental matrix in Chapter 3, were selected to be performed on a porcine specimen. The structural properties of bone vary between subjects due to various factors which include: age, gender, and diet [5]. Even within a subject, the structural properties vary dependent on anatomical location and external mechanical stimuli. Due to the variability of the structural properties between and within subjects, it is important to evaluate the process parameters used in Chapter 3 on a

workpiece that exhibits the same differences of mechanical properties compared to a consistent sawbone specimen.

The porcine specimen provides a realistic representation of the workpiece that would be encountered in bone burring process in a clinical setting. As the amount of cancellous bone is limited by the volume of the epiphysis, only select combinations of parameters from Chapters 3 and 4 were selected for porcine testing. Parameters that led to local minimums of temperature and vibration were viewed as optimal parameters in which to perform the bone burring process. A select combination of parameters that led to local maximums of temperature and vibration were selected as suboptimal parameters and allowed for comparisons to be drawn between the combination sets.

Two sets of parameter combinations were constructed which constituted of the optimal and suboptimal sets, as shown in Table 5.1 and Table 5.2. The optimal data set comprised of fixing the parameters to a rotational speed of 15,000 rpm, feed rate of 2 mm/s and overlap of 50%. The fixed parameters were chosen based on the findings within Chapter 4, which investigated combinations of parameters that led to local minimums for temperature and vibration. The diameter of the tool was also fixed at 6 mm, as the diameter of tool was found not to produce a statistical significant difference in the outcome measurements of temperature and vibration. Additionally, as a fully immersed burring path is required in the experimental methodology to produce a consistent overlap of burring paths, the measurements of a fully immersed (0% overlap) path were analyzed and included in the parameter set.

The second combination of parameters or the suboptimal set, was selected based on the parameters that led to local maximums of temperature and vibration as found in Chapter 4. The fixed parameter set included: a rotational speed of 75,000 rpm, inclination angle of 0 degrees, and overlap of 10%. The diameter of the tool was also fixed at 6 mm to be consistent with the previous parameter set as well as the diameter of the tool was found not to have produced a statistical significant difference in the outcome measurement of temperature as reported in Chapter 4. Based on the goal to produce a parameter set that results in maximizing temperature and vibration; tilt angle of the tool was additionally fixed at 0 degrees. The 0 degree tilt angle led to increases of temperature and vibration of  $8.8 \pm 0.8$  °C and  $0.76 \pm 0.4$  g-rms compared to the 45 degree tilt angle (Table 4.2). A fully immersed (0% overlap) burring path was also included within the combinations of parameters as it was required to be performed, due to the experimental procedure. A full summary of the optimal and suboptimal parameter set can be found in Table 5.1 and Table 5.2.

Table 5.1: Optimal combination of process parameters

	Tool Type	Tilt Angle (°)	Inclination Angle (°)	Depth of Cut (mm)	Overlap (%)
<u>Level-1</u>	Sphere	0	0	0.5	0
<u>Level-2</u>	Cylinder	45	+40	1.0	50
<u>Level-3</u>	-	-	-40	-	-

*Note: Constrained parameters included: 6 mm diameter tool, rotational speed of 15,000 rpm, and feed rate of 2 mm/s*

Table 5.2: Suboptimal combination of process parameters

	Tool Type	Feed Rate (mm/s)	Depth of Cut (mm)	Overlap (%)
<u>Level-1</u>	Sphere	2	0.5	0
<u>Level-2</u>	Cylinder	6	1.0	10

*Note: Constrained parameters included: 6 mm diameter tool, rotational speed of 75,000 rpm, inclination angle of 0 degrees, and tilt angle of 0 degrees*

## 5.2 Specimen and Data Preparation

### 5.2.1 Specimen Selection

Six fresh-frozen porcine femurs were used to evaluate the selected process parameters associated with the bone burring process. Porcine bone has previously been used as a workpiece substitute in machining processes to evaluate the process parameters [60, 61]. Specifically, a porcine femur was selected as a surrogate for human cancellous bone as they are readily available and inexpensive. Macroscopically, a porcine femur provides a relatively large cross sectional area of cancellous bone located within the epiphysis. A larger volume of cancellous bone is desirable as it allows for more parameters to be performed within the same specimen. Due to the subtractive machining process of bone burring, the cancellous bone can only be machined a set number of times determined by the process parameters. Microscopically, a porcine femur also provides a cancellous bone structure that is similar to humans [62]. Although, no previous published study was found that measured the bone mineral density of the distal epiphysis of a porcine femur; Clyde *et al.* reported that the total bone mineral density of the entire femur ranges from 0.288 to 0.369 g/cm<sup>3</sup> [63]. The bone density agrees well with the sawbone selected in Chapter 3, which had a density of 0.320 g/cm<sup>3</sup>.



### 5.2.2 Specimen Preparation

The porcine femurs were obtained from a local butcher shop and stored frozen at a temperature of -20 °C. On the day of testing, the porcine femur was thawed to room temperature. These methods were shown not to affect the mechanical properties of the bone, and also used in previous experimental procedures involving porcine bones [64-66]. The specimens were denuded of soft tissue and the femur was transected using a hack saw approximately 25 mm at the distal end of the femur (Figure 5.1). The transected slice was orientated at an angle to reveal the maximum area of cancellous bone for bone burring. The femur was then additionally sectioned (approximately 10 cm in length) at the distal end to allow for cementation of the specimen. The specimen was cemented in place using a custom fabricated jig that ensured parallel sides of the block to be clamped in place using the experimental apparatus developed in Chapter 2.

### 5.2.3 Bone Removal Burring Testing and Data Preparation

The potted porcine femur specimen was clamped in place and the exposed cancellous bone was premachined by the experimental apparatus. The bone was premachined to ensure a parallel plane between the workpiece and tool in order to provide consistency in material removal while varying the process parameters. After the bone was premachined to ensure the plane was parallel (approximately 1 mm deep from original cut), burring trials were performed. When the exposed cancellous bone did not allow for any more burring trials to be performed, the plane was resurfaced to ensure accuracy. This was performed until all combinations of parameters were tested.

Quantifying the outcome measurements (temperature, vibration, and cutting force) were based on the protocol discussed in Chapter 2. A sample run involving the experimental apparatus burring a portion of cancellous bone is found in Figure 5.2. The engaged state of the tool (entry and exit points) were determined using the cutting force measurements. One modification to the protocol as discussed in Chapter 2, was that only one half of the diameter of the tool (3 mm) was added to the entry and exit portions of the cut for clipping of data to ensure the stable state of the cut. Half the diameter of the tool was used rather than the full diameter due to the reduced length available in a porcine specimen compared to the sawbone workpiece. Another modification to the protocol outlined in Chapter 2 was the calculation of the average temperature. The maximum value of temperature does not necessarily occur at the end of the trial as seen with a sawbone workpiece. Therefore the temperature was averaged over the entire burring run. An average length of 20 mm of cancellous bone was used.

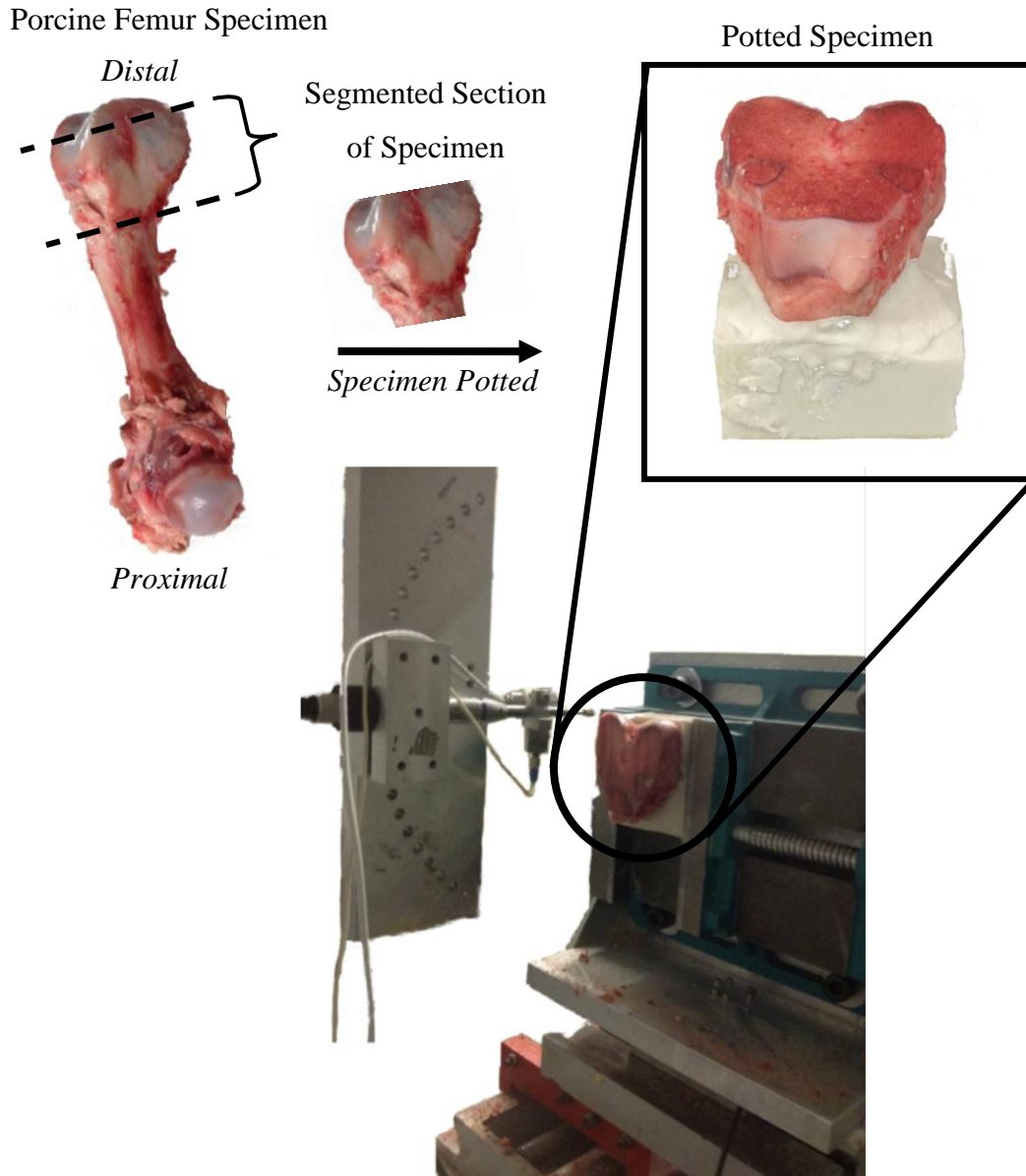


**Figure 5.1: Preparation of specimen**

*Porcine femurs were acquired from a local butcher shop and denuded of all soft tissue. The specimens were then segmented at the distal end of the femur to reveal cancellous bone for burring. The specimen was then potted using dental cement. The specimen was fixed in place using the grips on the apparatus to allow for experimental measurements during burring.*

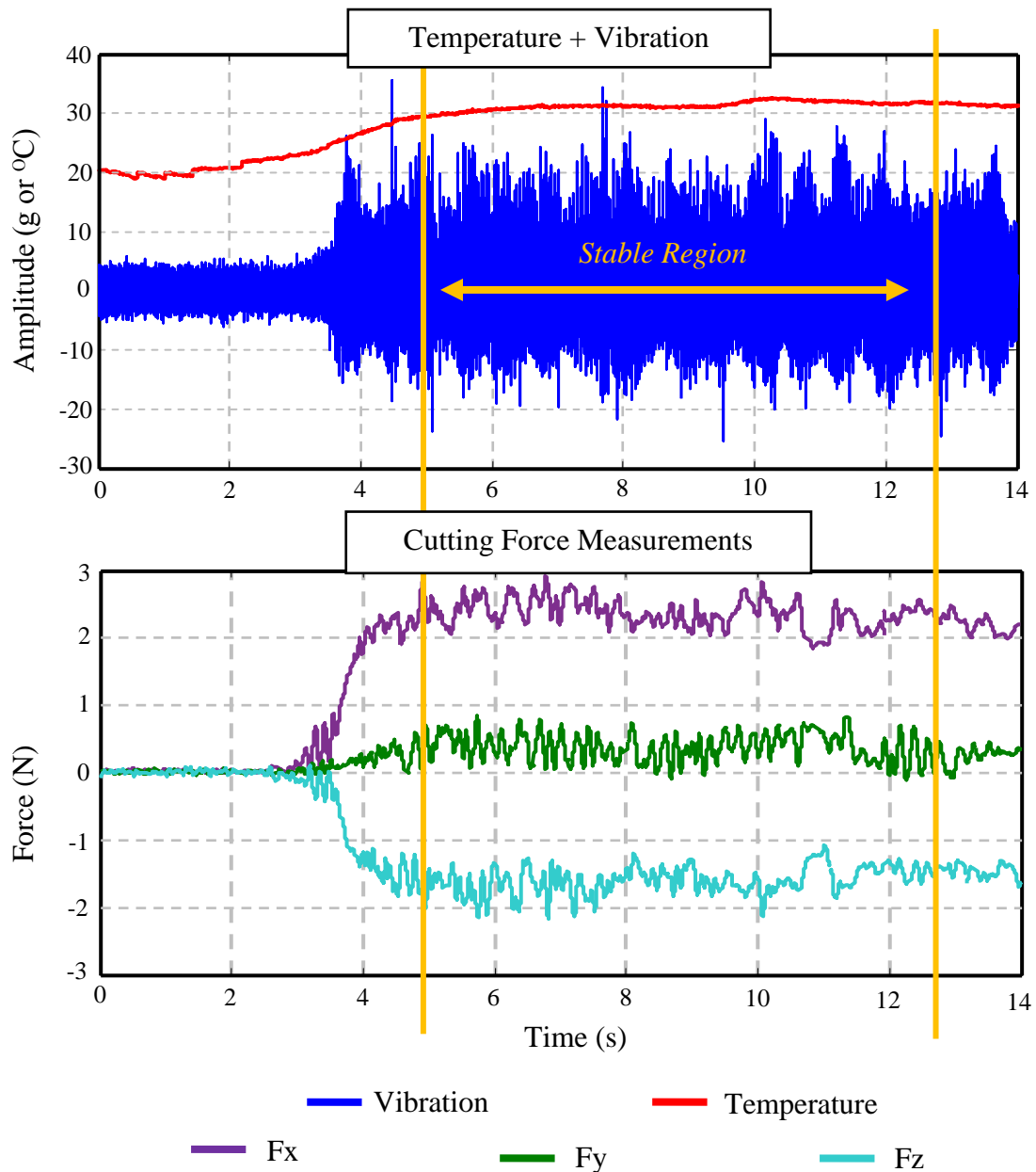


**Figure 5.2: Simultaneous measurements of outcome variables while burring porcine cancellous bone**

*A sample output of the outcome measurements (temperature, vibration, and cutting force) is shown above. The stable state of the cut, defined as 3 mm (1/2 diameter of tool) away from the entry and exit points, indicated by orange lines on the graph above. The stable state of the cut was used for computing the means of the outcome measurements and allow for a statistical analysis to be performed.*

#### 5.2.4 Feed Rate Normalization

To normalize the temperature measurements to the center of the tool the protocol discussed in section 3.1.1 was used. The infrared pyrometer was positioned at three lagging distances (with five repeated measurements) to quantify the cooling due to the lagging temperature measurements.

Results of the feed rate normalization experiment can be found in Figure 5.3.

An exponential curve was fitted to the experimental temperature measurements at both feed rates. The lines of best fit showed strong correlation ( $R^2 > 0.807$ ) for both feed rates. Extrapolating these curves to the center of the tool, it was found that the 2 mm/s feed rate (29.7 °C) resulted in a higher change in temperature than a 6 mm/s feed rate (20.1 °C) for the selected process parameters.

Moving forward, the cooling curves quantified in the feed rate normalization experiment were applied to the temperature measurements. The temperature at the center of the tool was then extrapolated based on the cooling time associated with the feed rate. By normalizing the temperature to the center of the tool, separate feed rates could be compared.

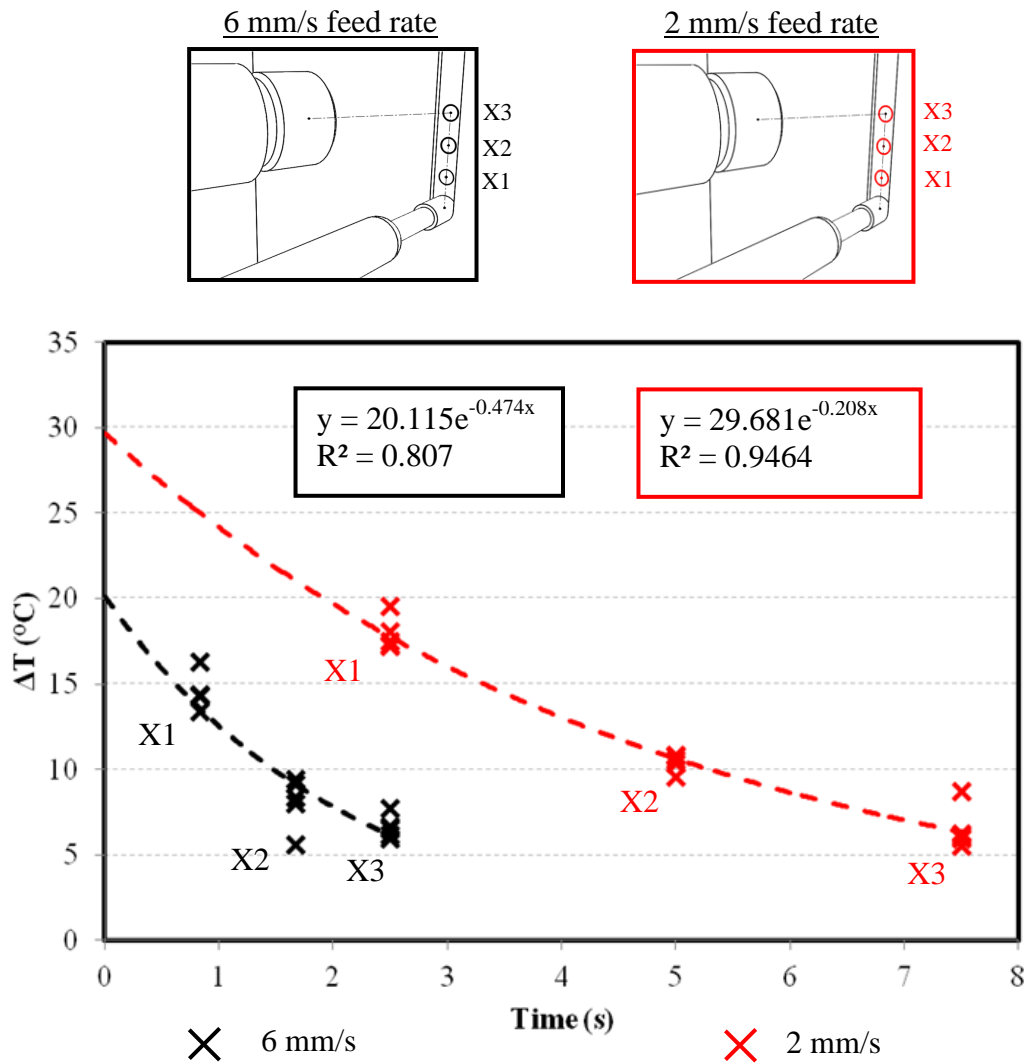


**Figure 5.3: Feed rate normalization for porcine bone**

Results from the feed rate normalization experiment are shown above. X1, X2, and X3 are plotted along with their respective feed rates, 2mm/s (red) and 6 mm/s (black). An exponential line of best fit was applied to both feed rates; the equation and  $R^2$  values can be found within the outlined boxes above. The lines of best fit were used to extrapolate the temperature at the theoretical contact point between the tool and workpiece.

### 5.3 Outcome Measurements & Statistical Analysis

Cutting force was quantified as the arithmetic mean over the course of a burring trial in the X, Y, and Z direction. The dynamic effects were quantified as the root-mean-square value over the course of a burring trial. The temperature experienced by the workpiece was quantified using the average of the measurements over the burring trial.

A fully balanced experimental design was conducted using the combination of parameters within the optimal and suboptimal parameter set. A repeated measures MANOVA with five outcome measurements was performed. The repeated measures MANOVA was performed using SPSS 22.0 (SPSS Inc., Chicago, IL). A univariate ANOVA was also conducted on each of the outcome measurements. To quantify the main effects of the process parameters on the outcome measurements, a pairwise comparison was performed. An alpha of 0.05 ( $p < 0.05$ ) was used. All results are reported as the population mean  $\pm$  95% confidence interval.

### 5.4 Effects of Process Parameters on Outcome Measurements - Optimal Set

The descriptive statistics of the outcome measurements for the optimal data set is found in Table 5.3. The results of the multivariate, univariate, and pairwise comparison of the main effects can be found in Table 5.5.

#### 5.4.1 Cutting Force

Increasing depth of cut from 0.5 to 1.0 mm increased the average forces by  $F_x = 0.6 \pm 0.2$  N ( $p < 0.001$ ),  $F_y = 0.2 \pm 0.1$  N ( $p < 0.001$ ), and  $F_z = 0.6 \pm 0.2$  N ( $p < 0.001$ ). A +40 inclination

angle ( $F_x=0.8\pm0.1$  N,  $F_y=0.3\pm0.1$  N,  $F_z=-0.5\pm0.1$  N) reduced forces in all directions compared to 0 degree inclination ( $F_x=1.9\pm0.6$  N ( $p=0.014$ ),  $F_y=0.6\pm0.1$  N ( $p=0.021$ ),  $F_z=-0.9\pm0.1$  N ( $p=0.002$ )) and decreased forces in the X and Z direction compared to a -40 degree inclination ( $F_x=1.6\pm0.2$  N ( $p<0.001$ ),  $F_y=-0.2\pm0.1$  N ( $p<0.001$ ),  $F_z=-1.2\pm0.1$  N ( $p=0.001$ )).

#### 5.4.2 Vibration

Increasing depth of cut from 0.5 ( $2.7\pm0.2$  g-rms) to 1.0 mm ( $3.5\pm0.3$  g-rms) increased the vibration of the tool during burring trials ( $p=0.001$ ). An overlap of 50% compared to 0% decreased the average vibration by  $0.7\pm0.2$  g-rms ( $p<0.001$ ).

#### 5.4.3 Temperature

Increasing depth of cut from 0.5 ( $32.1\pm1.5$  °C) to 1.0 mm ( $38.4\pm2.7$  °C) increased the average temperature experienced by the workpiece ( $p=0.002$ ). An inclination angle of +40 degrees lowered the temperature by  $10.7\pm2.0$  °C ( $p<0.001$ ) and  $10.1\pm4.2$  °C ( $p=0.001$ ) compared to a 0 degree and -40 degree inclination angle, respectively. A cylinder tool with 0 degree inclination and tilt angle resulted in  $50.8\pm6.8$  °C compared to a sphere tool which resulted in  $33.5\pm4.3$  °C with the same parameters ( $p=0.008$ ).

### 5.5 Effects of Process Parameters on Outcome Measurements - Suboptimal Set

The descriptive statistics of the outcome measurements for the suboptimal data set is found in Table 5.4. The results of the multivariate, univariate, and pairwise comparison of the main effects can be found in Table 5.6.



Table 5.3: Descriptive statistics of outcome measurements - optimal set

	Temperature (°C)	Vibration (g-rms)	F <sub>x</sub> (N)	F <sub>y</sub> (N)	F <sub>z</sub> (N)
Average Measurement	35.0±7.9	3.1±0.9	1.4±0.9	0.2±0.5	-0.8±0.6
Maximum Value	55.9±7.6	5.5±1.0	4.6±1.7	1.4±0.5	-0.13±0.1
Minimum Value	24.4±1.0	1.7±0.2	0.1±0.2	-1.1±0.2	-2.6±0.7

*Note: Values are presented as mean ± 1 standard deviation*

Table 5.4: Descriptive statistics of outcome measurements - suboptimal set

	Temperature (°C)	Vibration (g-rms)	F <sub>x</sub> (N)	F <sub>y</sub> (N)	F <sub>z</sub> (N)
Average Measurement	42.3±10.7	6.9±1.1	1.7±0.7	0.4±0.2	-0.4±0.2
Maximum Value	59.8±6.4	10.4±2.9	3.4±1.3	0.8±0.6	-0.2±0.1
Minimum Value	28.5±1.8	6.0±0.8	0.9±0.2	0.2±0.1	-0.8±0.3

*Note: Values are presented as mean ± 1 standard deviation*

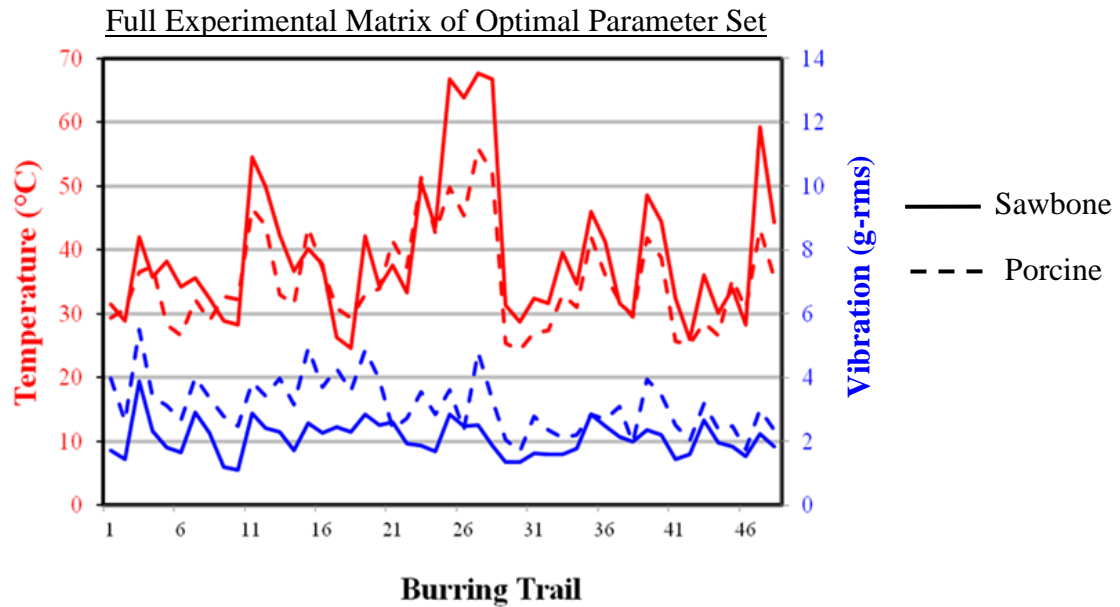


**Figure 5.4: Temperature and vibration measurements of sawbone vs. porcine - optimal parameter set**

*Outcome measurements of temperature (red) and vibration (blue) are plotted for all combinations of the optimal set of parameters (shown above). Comparison of sawbone (solid line - averaged value of 3 repeated runs) and porcine bone (dashed lined - averaged value of 6 specimens) is shown. Combinations of parameters that result in local minimums in temperature ( $<40^{\circ}\text{C}$ ) and vibration ( $<4$  g-rms) are present when burring a porcine bone with the optimal parameter set. The force results and parameters that lead to the burring trials can be found in Appendix E.*

Table 5.5: Summary of statistical analysis for process parameters that resulted in local minimums of temperature and vibration

<b>Local Minimums of Temperature and Vibration - Factors Fixed (Diameter = 6 mm, Rotational Speed = 15,000 rpm, Feed Rate = 2mm/s)</b>											
<b>Multivariate Analysis - Main Effects</b>											
<i>Tool Type</i>		<i>Tilt Angle</i>		<i>Inclination Angle</i>		<i>Depth of Cut</i>		<i>Overlap</i>			
p=0.147		p=0.061		p<0.001		p=0.271		p=0.046			
<b>Univariate Analysis - Main Effects</b>											
<b>Temperature (°C)</b>						<b>Vibration (g-rms)</b>					
<i>Tool Type</i>	<i>Tilt Angle</i>	<i>Inclination Angle</i>	<i>Depth of Cut</i>	<i>Overlap</i>		<i>Tool Type</i>	<i>Tilt Angle</i>	<i>Inclination Angle</i>	<i>Depth of Cut</i>	<i>Overlap</i>	
p=0.853	p=0.539	p<0.001	p=0.002	p<0.001		p=0.006	p=0.393	p<0.001	p=0.001	p<0.001	
<b>Pairwise Comparison</b>											
<u>Level-1</u>	35.4±2.5	35.6±2.7	39.0±1.7	32.1±1.5	36.6±1.7		3.5±0.3	3.1±0.2	3.6±0.3	2.7±0.2	3.5±0.3
<u>Level-2</u>	35.1±2.8	34.9±1.6	28.4±0.7	38.4±2.7	34.0±1.8		2.7±0.3	3.2±0.3	3.1±0.3	3.5±0.3	2.8±0.2
<u>Level-3</u>	-	-	38.4±3.5	-	-		-	-	2.7±0.2	-	-

Table 5.5 outlines the repeated measures MANOVA results for the reduced sample set that resulted from locking certain factors that led to local minimums for both temperature and vibration (diameter = 6 mm, rotational speed = 15,000 rpm, feed rate = 2mm/s). The multivariate and univariate results are presented in the above table. Additionally, the pairwise comparison of the main effects and outcome measurements of temperature and vibration are outlined (mean ± 95% confidence interval).

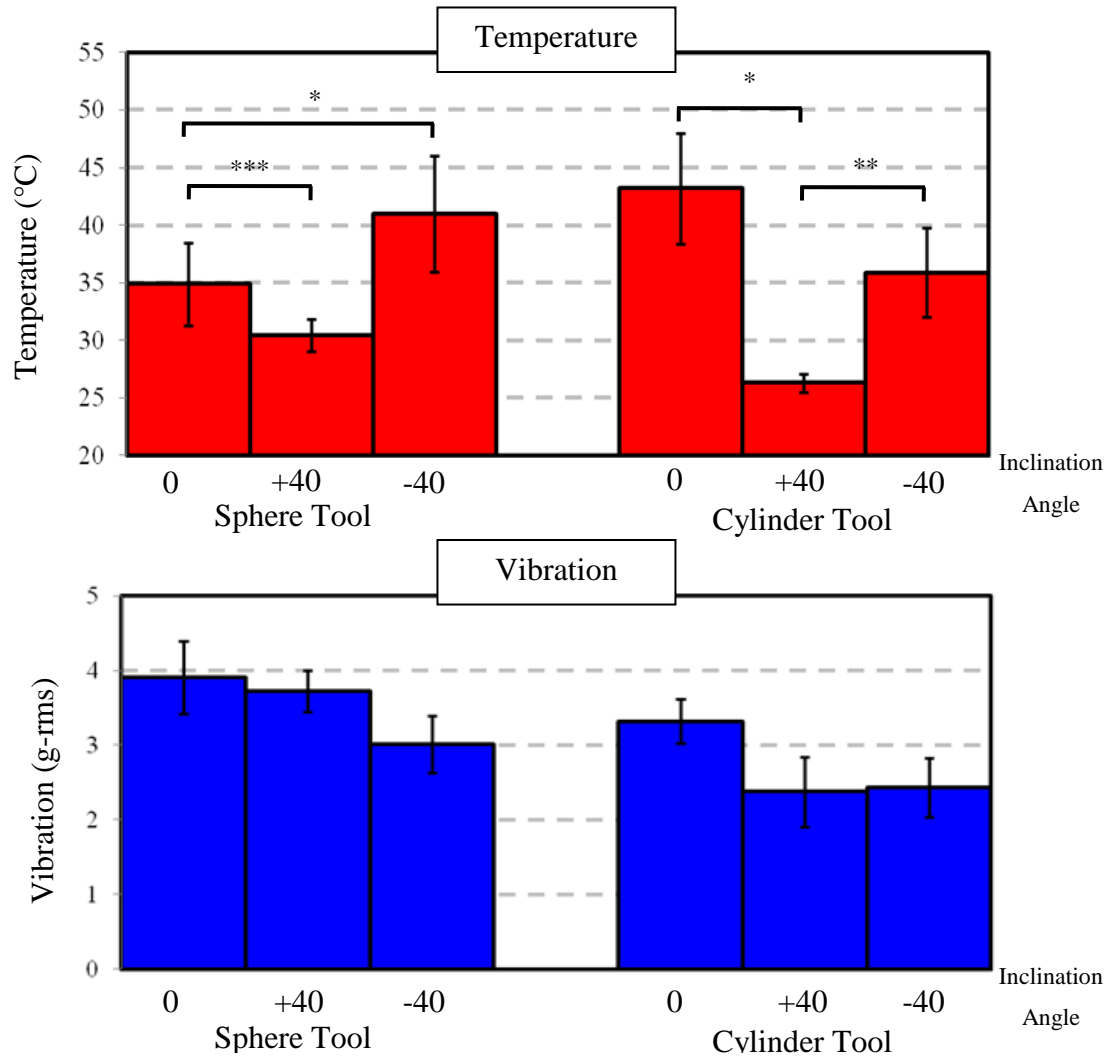


**Figure 5.5: Sensitivity of tool type to changes in inclination angles**

*The effects of varying the inclination angle and tool type are illustrated above with outcome measurements of temperature (red) and vibration (blue). A -40 degree inclination angle resulted in the highest temperatures with the sphere tool; whereas, a 0 degree inclination angle resulted in highest temperatures with the cylinder tool. Vibrations were on average less than 4 g-rms regardless of the tool and inclination angle. Significant differences are denoted by \*,  $p < 0.05$ ; \*\*,  $p < 0.01$ ; \*\*\*,  $p < 0.001$ .*

### 5.5.1 Cutting Force

A depth of cut of 1.0 mm ( $F_x=1.8\pm0.5$  N,  $F_y=0.5\pm0.1$  N,  $F_z=-0.5\pm0.1$  N) produced higher magnitudes of forces than a 0.5 mm depth of cut ( $F_x=1.6\pm0.5$  N,  $F_y=0.4\pm0.1$  N,  $F_z=-0.3\pm 0.0$  N) ( $p=0.321$ ,  $p=0.041$ ,  $p=0.007$ ). A feed rate of 6 mm/s ( $F_x=2.1\pm0.6$  N,  $F_y=0.5\pm0.2$  N,  $F_z=-0.5\pm0.1$  N) produced higher forces compared to a slower feed rate of 2 mm/s ( $F_x=1.4\pm0.3$  N,  $F_y=0.3\pm0.1$  N,  $F_z=-0.3\pm0.1$  N) ( $p=0.007$ ,  $p=0.007$ ,  $p=0.001$ ).

### 5.5.2 Vibration

Increasing depth of cut from 0.5 to 1.0 mm increased the vibration by  $0.6\pm0.7$  g-rms ( $p=0.060$ ). Increasing the feed rate from 2 ( $6.5\pm0.6$  g-rms) to 6 mm/s ( $7.3\pm0.7$  g-rms) increased the average vibration experienced by the tool during the burring process ( $p=0.021$ ).

### 5.5.3 Temperature

Increasing the feed rate from 2 to 6 mm/s decreased the average temperature by  $7.8\pm2.2$  °C ( $p=0.012$ ). A cylinder tool produced an average temperature of  $51.4\pm3.2$  °C; whereas a sphere tool resulted in an average temperature of  $33.1\pm2.7$  °C ( $p=0.002$ ).

### Full Experimental Matrix of Suboptimal Set of Parameters

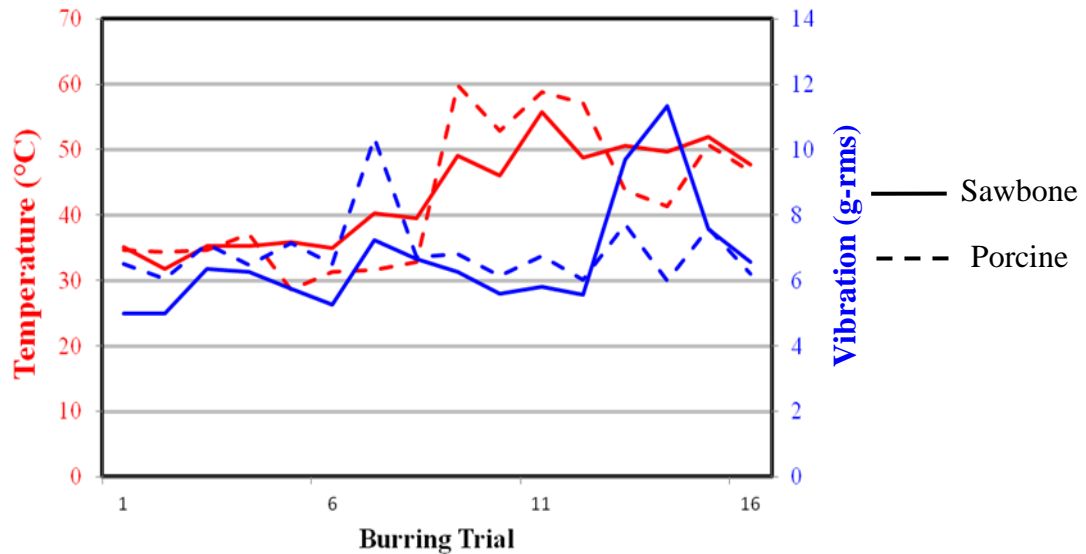


**Figure 5.6: Temperature and vibration measurements of sawbone vs. porcine - suboptimal parameter set**

*Outcome measurements of temperature (red) and vibration (blue) are plotted for all combinations of the suboptimal set of parameters (outlined above). Comparison of sawbone (solid line - averaged value of 3 repeated runs) and porcine bone (dashed lined - averaged value of 6 specimens) is shown. Combinations of parameters that resulted in local minimums in temperature ( $<40^{\circ}\text{C}$ ) and vibration ( $<4$  g-rms) are not present when burring a porcine bone with the suboptimal parameter set. The force results and parameters that lead to the burring trials can be found in Appendix E.*

Table 5.6: Summary of statistical analysis for process parameters that resulted in local maximums of temperature and vibration

<b>Local Maximums of Temperature and Vibration - Factors Fixed (Diameter = 6 mm, Rotational Speed = 75,000 rpm, Inclination Angle = 0 degrees, Tilt Angle = 0 degrees)</b>									
<b>Multivariate Analysis - Main Effects</b>									
<i>Tool Type</i>		<i>Feed Rate</i>			<i>Depth of Cut</i>			<i>Overlap</i>	
p=0.068		p=0.203			p=0.435			p=0.379	
<b>Univariate Analysis - Main Effects</b>									
<b>Temperature (°C)</b>					<b>Vibration (g-rms)</b>				
<i>Tool Type</i>	<i>Feed Rate</i>	<i>Depth of Cut</i>	<i>Overlap</i>		<i>Tool Type</i>	<i>Feed Rate</i>	<i>Depth of Cut</i>	<i>Overlap</i>	
p<0.001	p<0.001	p=0.163	p=0.230		p=0.137	p=0.003	p=0.108	p=0.002	
<b>Pairwise Comparison</b>									
<u>Level-1</u>	33.1±2.7	46.2±2.7	40.9±2.2	42.8±2.8		7.1±0.9	6.5±0.6	6.6±0.6	7.5±0.8
<u>Level-2</u>	51.4±3.2	38.4±2.8	43.7±4.2	41.7±2.6		6.7±0.6	7.3±0.7	7.2±0.7	6.3±0.6

Table 5.6 outlines the repeated measures MANOVA results for the reduced sample set that resulted from locking certain factors that led to local maximums for both temperature and vibration (diameter = 6 mm, rotational speed = 75,000 rpm, inclination angle = 0 degrees, tilt angle = 0 degrees). The multivariate and univariate results are presented in the above table. Additionally, the pairwise comparison of the main effects and outcome measurements of temperature and vibration are outlined (mean ± 95% confidence interval).

## 5.6 Chapter Summary

The aim of these experiments was to validate the previously tested process parameters on a porcine femur workpiece. The optimal combination of parameters produced certain combinations that led to minimums in temperature ( $<40^{\circ}\text{C}$ ) and vibration ( $<4$  g-rms). Similar to the sawbone results, the cylinder, when oriented normal to the workpiece, produced the highest temperatures ( $>50^{\circ}\text{C}$ ), which could possibly cause bone necrosis. In fact, burnishing of the porcine specimens was observed under these conditions. The trends within the optimal set of parameters were also similar to the trends established in Chapter 4, as increasing depth of cut and overlap led to increases in temperature and vibration. Additionally, an inclination angle of  $+40$  degrees produced the lowest average temperature compared to other inclination angles (Table 4.1, Table 5.3).

The suboptimal parameter set did not produce any combinations that led to minimums in temperature ( $<40^{\circ}\text{C}$ ) and vibration ( $<4$  g-rms). The suboptimal parameter set produced higher average temperatures ( $7.1^{\circ}\text{C}$ ) and vibration levels ( $4.1$  g-rms) compared to the optimal parameter set. Increasing depth of cut and overlap led to an increase in temperature and vibration, which supports the observations from the earlier sawbone trials. The sphere bit ( $33.1\pm 2.7^{\circ}\text{C}$ ) also produced much lower temperatures than the cylinder bit ( $51.4\pm 3.2$ ) within this parameter set. However, the large difference was mainly due to the choice of the orientation of the tool with respect to the workpiece. The sphere produced lower temperatures at  $0$  inclination and  $0$  tilt, as seen in Figure 5.5, and would be a superior choice to avoid necrosis if the burring process was limited to this orientation.



These findings supported the third hypothesis, such that optimal and suboptimal parameters produced similar results in cancellous bone. As well the trends previously established in Chapters 3 and 4, were transferrable for burring in a cadaveric specimen.

The trends found within burring cancellous porcine bone also agree well with published burring studies [40-42, 46]. Temperature trends of thicker depths of cut coupled with slower feed rates result in high temperatures established by Shin *et al.*, agreed well with the findings within this study (Table 5.4) [40]. Although the magnitudes are much lower compared to the findings by Shin *et al.*, this was due to the fact that a denser cortical bone was used as the workpiece in the author's experiment [40]. The trends produced within the force measurements (increased depth of cut and feed rate result in higher forces) are also in line with previous findings by Dillon *et al.* [41]. The magnitude of the average forces in all directions (<5 N) are also similar to previously published studies using a high speed rotational tool for bone removal purposes [41, 42, 46].

The experimental results indicate that the cylinder tool should not be placed at a normal orientation to the workpiece as it results in high temperatures for both sets of parameters (optimal =  $50.8 \pm 6.8$  °C, suboptimal =  $51.4 \pm 3.2$  °C). A +/- inclination angle would be ideal; however, this increases the difficulty in the design of a tool path trajectory due to the complex channel geometries, which result in rotations of the cylinder tool.

Thus, the optimal parameters are a 6 mm diameter sphere tool with a rotational speed of 15,000 rpm, a 2 mm/s feed rate, and a 50% overlap. This combination allows for different depth of cuts (0.5 and 1.0 mm tested), inclination angles (0, +40, and -40 tested) and tilt

angles (0 and 45 tested), to be encountered during the burring process, while still producing temperatures less than 42.0 °C and vibrations less than 4.1 g-rms.

## Chapter 6 - General Discussion and Conclusions

***OVERVIEW:** This chapter reviews the objectives and hypotheses defined in Chapter 1, and presents a brief summary of the experimental work taken to achieve the objectives. The strengths and limitations of this work are discussed, and finally, potential future work for investigating the bone burring process is proposed.*

### 6.1 Summary and General Discussion

Experimental quantification of the bone removal characteristics associated with bone burring proves useful in applications across various fields that have implemented, or have the potential to implement, a high speed rotary tool for bone burring. High temperature generation caused during bone burring in some surgical procedures has been shown to cause osteonecrosis, which may cause joint replacement loosening [35, 36, 53]. The selection of burring process parameters becomes relevant as the selected parameters subsequently determine the process outcomes. The body of work presented contributes to the preexisting knowledge already associated with characterizing the bone burring process. First, a developed experimental apparatus was designed that allowed for control of various process parameters and monitored the outcome measurements: temperature, vibration, and cutting force in three directions, simultaneously during bone burring (Chapter 2). A full factorial analysis with eight process parameters and five outcome measurements was performed using the developed apparatus, using a sawbone analog as the workpiece (Chapter 3). Optimal and suboptimal sets of process parameters were

identified in Chapter 4. Finally, using the developed apparatus from Chapter 2, and selected parameters through findings in Chapters 3 and 4, the burring process was further evaluated on porcine cadaveric specimens in Chapter 5.

Previous studies within the context of bone burring have focused on assessing the process primarily in regards to temperature or cutting force independently [40-42, 45]. Unique to the experimental apparatus presented in Chapter 2, was the ability to capture dynamic effects of the tool during burring in order to simultaneously measure the temperature and cutting force of the process. As well, the developed apparatus provided the ability to precisely control the multiple process parameters (depth of cut, feed rate, cutting overlap, inclination angle, and tilt angle). Findings within Chapter 2 proved the feasibility of capturing the process outcomes through various integrated transducers. The system proved to be repeatable, standard deviations of  $F_x = 0.08$  N,  $F_y = 0.01$  N,  $F_z = 0.09$  N, vibration = 0.36 g-rms, and temperature = 1.4 °C. Additionally, a signal-to-noise ratio greater than 5 dB was found for each of the directional cutting forces. The high signal-to-noise ratio coupled with high repeatability of the system matched previous experimental studies, supporting the first hypothesis. Additionally, the experimental tests outlined in Appendix C, further supported the accuracy of these results.

Chapter 3 provided further insight into the magnitude of influence that the process parameters had on the outcome measurements; an eight-way fully balanced MANOVA with five outcome measurements was conducted. Statistically significant differences were found with nearly every process parameter at the multivariate and univariate level for each outcome measurement. The volume of statistically significant differences was attributed to the highly controlled experimental apparatus and its sensitivity to detect

small effect sizes due to small adjustments in the process parameters. High repeatability, coupled with high signal-to-noise ratio was desirable in the developmental phase in Chapter 2; however, it resulted in difficulty in indentifying key sets of parameters for selection of an optimal tool configuration. Although Chapter 3 supported the second hypothesis, such that statistically significant differences were found; no such indication into optimal and suboptimal parameters was obtained through the methods performed in Chapter 3 alone.

Building off of Chapter 3, Chapter 4 evaluated the tradeoffs that were present and selected process parameters based on clinical relevance. The force magnitudes were low (<3 N) and as a result, they were disregarded in the selection process because the magnitude of the measurements were deemed to not be clinically relevant, regardless of the selection of process parameters. Chapter 4 sought to select parameters based on the criteria that led to: local minimums in temperature and vibration, local maximums in temperature and vibration, maximums in temperature only, and maximums in vibration only. Selection of a 15,000 rpm rotational speed, 2 mm/s feed rate, and 50% cutting overlap, led to an optimal tool configuration that avoided high temperatures and vibrations within the remaining unconstrained parameters. Although it was earlier established (Chapter 3) that the process parameters can statistically alter the process outcomes, Chapter 4 was able to fully support the second hypothesis in selection of optimal and suboptimal parameters.

Chapter 5 further provided insight into the influence of process parameters, by validating the optimal and suboptimal sets on a porcine cadaveric bone model. The optimal set of parameters established in the sawbone burring trials, also produced favorable results in

reducing temperature and vibration compared to the suboptimal set. Additionally, similar trends were found within the porcine model that were previously established with the sawbone analog (Figure 5.4 and Figure 5.6). Increasing the depth of cut and feed rate, as well as constraining the inclination angle to 0 degrees, resulted in an increase of temperature and vibration. The relationship between trends between the sawbone analog and porcine cancellous bone, as well as the similarities exhibited between optimal and suboptimal parameters, supported the third and final hypothesis.

Comparing the trends observed agree well with previous findings [40-42]. Increasing depth of cut and decreasing feed rate resulted in an increasing temperature, which was also found by Shin *et al.* [40]. Dillon *et al.* found that increasing depth of cut, tilt angle, and feed rate resulted in increased forces, which was found in this work as well [41]. The overall rationale of this project was to perform a full factorial analysis to evaluate all of the process parameters and selected levels within, to provide a thorough understanding of the characteristics associated with bone burring. The current experimental results align with previously established trends. Moreover, additional characteristics of the process parameters were established in Chapters 3 and 5, including vibration.

Overall, the optimal tool configuration is a 6 mm sphere tool with a rotational speed of 15,000 rpm, 2 mm/s feed rate, and overlap of 50%. This choice of fixed parameters allows for the remaining parameters to be varied, while still avoiding high temperatures or high vibrations. Specifically, depths of cut (0.5 and 1.0 mm tested), inclination angles (0, +40, and -40° tested) and tilt angles (0 and 45° tested), may be selected, or randomly encountered while still achieving optimal temperature and vibrations. The ability to allow for different angles and depths of cut to be encountered is an important flexibility in the

design of the tool path trajectories for robotic burring applications, and for manual burring procedures in which these parameters are difficult to control.

## 6.2 Strengths and Limitations

A significant strength of this work is the large amount of independent and dependent variables included within the experimental protocol, which is notably more thorough than any previously published work. The full factorial analysis examined the effects and interdependencies of the process parameters associated with bone burring without aliasing any effects that may be present in a fractional designed study. A significant contribution to experimentally quantifying the bone burring process was achieved through completion of the second objective.

Evaluating the process parameters on a sawbone analog (Chapter 3 and Chapter 4) can be seen as a limitation due to the inherent differences between the foam polyurethane sawbone compared to cancellous bone. However, as natural bone's structural properties vary within and between subjects, a consistent workpiece for means of evaluation of the process parameters provided low variability needed to statistically compare the effects of various process parameters. Through choice of a consistent workpiece, the differences evoked within the statistical analysis are due to variations in the process parameters rather than differences in the workpiece. Although it is anticipated, and demonstrated in Chapter 5, that magnitudes of the outcome variables are different in sawbone compared to cancellous bone, the process trends established in the sawbone trials are characteristic of the burring process, which are then transferable to cancellous bone.

A main strength of this study, was measuring the dynamic effects of the tool itself, which is relevant to ergonomics and to robotic systems that rely on force measurement in their feedback controllers.

### 6.3 Future Work

Throughout the course of this work, further objectives became apparent to fully characterize the bone burring process. Chapter 2 discussed the methods of quantifying the dynamic effects of the tool, through use of the root-mean-square vibration. One drawback of this metric is that it does not provide insight into the frequencies of the dynamic effects, which could prove useful in detecting chatter or resonant frequencies. Principle and harmonic frequencies of the rotational speed of the tool were present in the results of Chapter 2. Whether additional chatter frequencies can be observed within the frequency domain is unknown. A highly controlled study involving a select few process parameters that result in chatter free and chatter present conditions would be useful in detecting a frequency that may be unique to the chatter vibration. As well, and more importantly, it would be interesting to examine the effects of chatter on other outcome measurements, such as force and temperature, and the performance of burring trials with high chatter.

Finally, another possible application of these methods is to generate synthesized burring haptic feedback in the design of high fidelity surgical simulations. An important mode of immersive feedback is the acoustics of the burring process. It is believed that the same frequencies generated due to the machining process would be present in the sound profile [67]. While not reported in the body of this thesis, a pilot study was conducted to investigate the feasibility of using a microphone to synthesize the acoustics associated



with bone burring. This work is presented in Appendix G to form the basis for future work.

## 6.4 Conclusion

Bone burring is ideally performed using a spherical burr. Cylinder burrs should be avoided unless it can be insured that the nose of the burr does not engage the bone. Using a spherical burr, the optimal configuration is to use a 6 mm sphere burr at 15,000 rpm with a 2 mm/s feed rate and a 50% overlap. This combination is the safest in terms of avoiding high temperatures and high vibrations. Moreover, it provides the flexibility to variably penetrate the bone, and to tilt the tool in various angles relative to the bone, without sacrificing low temperature and vibration.

## References

- [1] D. R. Carter and W. C. Hayes, "The compressive behavior of bone as a two-phase porous structure," *The Journal of Bone & Joint Surgery*, vol. 59, pp. 954-962, 1977.
- [2] J. Galante, W. Rostoker, and R. D. Ray, "Physical properties of trabecular bone," *Calcified tissue research*, vol. 5, pp. 236-246, 1970.
- [3] J. Wolff, P. Maquet, and R. Furlong, *The Law of Bone Remodelling*: Springer-Verlag, 1986.
- [4] M. Nordin and V. H. Frankel, *Basic Biomechanics of the Musculoskeletal System*: Lippincott Williams & Wilkins, 2001.
- [5] J. D. Currey, *Bones: Structure and Mechanics*: Princeton University Press, 2002.
- [6] J. Y. Rho, R. B. Ashman, and C. H. Turner, "Young's modulus of trabecular and cortical bone material: ultrasonic and microtensile measurements," *J Biomech*, vol. 26, pp. 111-9, Feb 1993.
- [7] v. G. H. H. Lenthe, A. Hermus, H. W. J. R. Huiskes, and v. d. J. P. W. J. Bergh, "The prospects of estimating trabecular bone tissue properties from the combination of ultrasound, dual-energy X-ray absorptiometry, microcomputed tomography, and microfinite element analysis," *Journal of Bone and Mineral Research*, vol. 16, p. 550, 2001.
- [8] C. R. Ethier and C. A. Simmons, *Introductory Biomechanics: From Cells to Organisms*: Cambridge University Press, 2007.
- [9] D. M. L. Cooper, C. D. L. Thomas, J. G. Clement, A. L. Turinsky, C. W. Sensen, and B. Hallgrímsson, "Age-dependent change in the 3D structure of cortical porosity at the human femoral midshaft," *Bone*, vol. 40, pp. 957-965, 2007.
- [10] V. Bentolila, T. M. Boyce, D. P. Fyhrie, R. Drumb, T. M. Skerry, and M. B. Schaffler, "Intracortical remodeling in adult rat long bones after fatigue loading," *Bone*, vol. 23, pp. 275-281, 1998.
- [11] P. Roschger, S. Rinnerthaler, J. Yates, G. A. Rodan, P. Fratzl, and K. Klaushofer, "Alendronate increases degree and uniformity of mineralization in cancellous bone and decreases the porosity in cortical bone of osteoporotic women," *Bone*, vol. 29, pp. 185-191, 2001.
- [12] J. Lundskog, "Heat and bone tissue. An experimental investigation of the thermal properties of bone and threshold levels for thermal injury," *Scand J Plast Reconstr Surg*, vol. 9, pp. 1-80, 1972.

- [13] A. Eriksson, T. Albrektsson, B. Grane, and D. McQueen, "Thermal injury to bone," *International Journal of Oral Surgery*, vol. 11, pp. 115-121, 1982.
- [14] A. R. Eriksson and T. Albrektsson, "Temperature threshold levels for heat-induced bone tissue injury: A vital-microscopic study in the rabbit," *The Journal of prosthetic dentistry*, vol. 50, pp. 101-107, 1983.
- [15] W. R. Krause, D. W. Bradbury, J. E. Kelly, and E. M. Lunceford, "Temperature elevations in orthopaedic cutting operations," *Journal of Biomechanics*, vol. 15, pp. 267-275, 1982.
- [16] C. M. Callahan, B. G. Drake, D. A. Heck, and R. S. Dittus, "Patient outcomes following unicompartmental or bicompartamental knee arthroplasty," *The Journal of arthroplasty*, vol. 10, pp. 141-150, 1995.
- [17] J. R. Kirwan, H. L. F. Currey, M. A. R. Freeman, S. Snow, and P. J. Young, "Overall long-term impact of total hip and knee joint replacement surgery on patients with osteoarthritis and rheumatoid arthritis," *Rheumatology*, vol. 33, pp. 357-360, 1994.
- [18] P. Dieppe, H. D. Basler, J. Chard, P. Croft, J. Dixon, M. Hurley, *et al.*, "Knee replacement surgery for osteoarthritis: effectiveness, practice variations, indications and possible determinants of utilization," *Rheumatology (Oxford, England)*, vol. 38, p. 73, 1999.
- [19] D. L. Burgess, M. S. McGrath, P. M. Bonutti, D. R. Marker, R. E. Delanois, and M. A. Mont, "Shoulder Resurfacing," *The Journal of Bone & Joint Surgery*, vol. 91, pp. 1228-1238, 2009.
- [20] T. P. Vail, "Hip resurfacing," *The Journal of the American Academy of Orthopaedic Surgeons*, vol. 19, p. 236, 2011.
- [21] H. Hildmann and H. Sudhoff, *Middle Ear Surgery*: Springer Berlin Heidelberg, 2006.
- [22] J. E. Lang, S. Mannava, A. J. Floyd, M. S. Goddard, B. P. Smith, A. Mofidi, *et al.*, "Robotic systems in orthopaedic surgery," *The Journal of bone and joint surgery. British volume*, vol. 93, p. 1296, 2011.
- [23] S.-J. Lim, S.-M. Kim, B.-H. Lim, Y.-W. Moon, and Y.-S. Park, "Comparison of manual rasping and robotic milling for short metaphyseal-fitting stem implantation in total hip arthroplasty: a cadaveric study," *Computer Aided Surgery*, vol. 18, pp. 33-40, 2012.
- [24] S. Nishihara, N. Sugano, T. Nishii, H. Miki, N. Nakamura, and H. Yoshikawa, "Comparison Between Hand Rasping and Robotic Milling for Stem Implantation in Cementless Total Hip Arthroplasty," *The Journal of Arthroplasty*, vol. 21, pp. 957-966, 2006.

- [25] W. L. Bargar, "Robots in Orthopaedic Surgery: Past, Present, and Future," *Clinical orthopaedics and related research*, vol. PAP, 2007.
- [26] H. A. Paul, W. L. Bargar, B. Mittlestadt, B. Musits, R. H. Taylor, P. Kazanzides, *et al.*, "Development of a surgical robot for cementless total hip arthroplasty," *Clinical orthopaedics and related research*, pp. 57-66, 1992.
- [27] L. H. Frich, N. C. Jensen, A. Odgaard, C. M. Pedersen, J. O. Sjøbjerg, and M. Dalstra, "Bone strength and material properties of the glenoid," *Journal of Shoulder and Elbow Surgery*, vol. 6, pp. 97-104, 1997.
- [28] T. Hananouchi, N. Sugano, T. Nishii, N. Nakamura, H. Miki, A. Kakimoto, *et al.*, "Effect of robotic milling on periprosthetic bone remodeling," *Journal of Orthopaedic Research*, vol. 25, pp. 1062-1069, 2007.
- [29] A. D. Pearle, D. Kendoff, V. Stueber, V. Musahl, and J. A. Repicci, "Perioperative management of unicompartmental knee arthroplasty using the MAKO robotic arm system (MAKOplasty)," *American journal of orthopedics (Belle Mead, N.J.)*, vol. 38, p. 16, 2009.
- [30] D. H. Nawabi, M. A. Conditt, A. S. Ranawat, N. J. Dunbar, J. Jones, S. Banks, *et al.*, "Haptically guided robotic technology in total hip arthroplasty: A cadaveric investigation," *Proceedings of the Institution of Mechanical Engineers, Part H: Journal of Engineering in Medicine*, vol. 227, pp. 302-309, 2013.
- [31] M. Jakopc, F. Rodriguez y Baena, S. J. Harris, P. Gomes, J. Cobb, and B. L. Davies, "The hands-on orthopaedic robot "acrobot": Early clinical trials of total knee replacement surgery," *IEEE Transactions on Robotics and Automation*, vol. 19, pp. 902-911, 2003.
- [32] A. R. W. Barrett, B. L. Davies, M. P. S. F. Gomes, S. J. Harris, J. Henckel, M. Jakopc, *et al.*, "Computer-assisted hip resurfacing surgery using the Acrobot® Navigation System," *Proceedings of the Institution of Mechanical Engineers*, vol. 221, p. 773, 2007.
- [33] A. Danilchenko, R. Balachandran, J. L. Toennies, S. Baron, B. Munske, J. M. Fitzpatrick, *et al.*, "Robotic mastoidectomy," *Otology & neurotology : official publication of the American Otological Society, American Neurotology Society [and] European Academy of Otology and Neurotology*, vol. 32, pp. 11-16, 2011.
- [34] P. A. Federspil, B. Plinkert, and P. K. Plinkert, "Experimental Robotic Milling in Skull-Base Surgery," *Computer Aided Surgery*, vol. 8, pp. 42-48, 2003.
- [35] P. A. McCann, P. P. Sarangi, R. P. Baker, A. W. Blom, and R. Amirfeyz, "Thermal damage during humeral reaming in total shoulder resurfacing," *International journal of shoulder surgery*, vol. 7, p. 100, 2013.

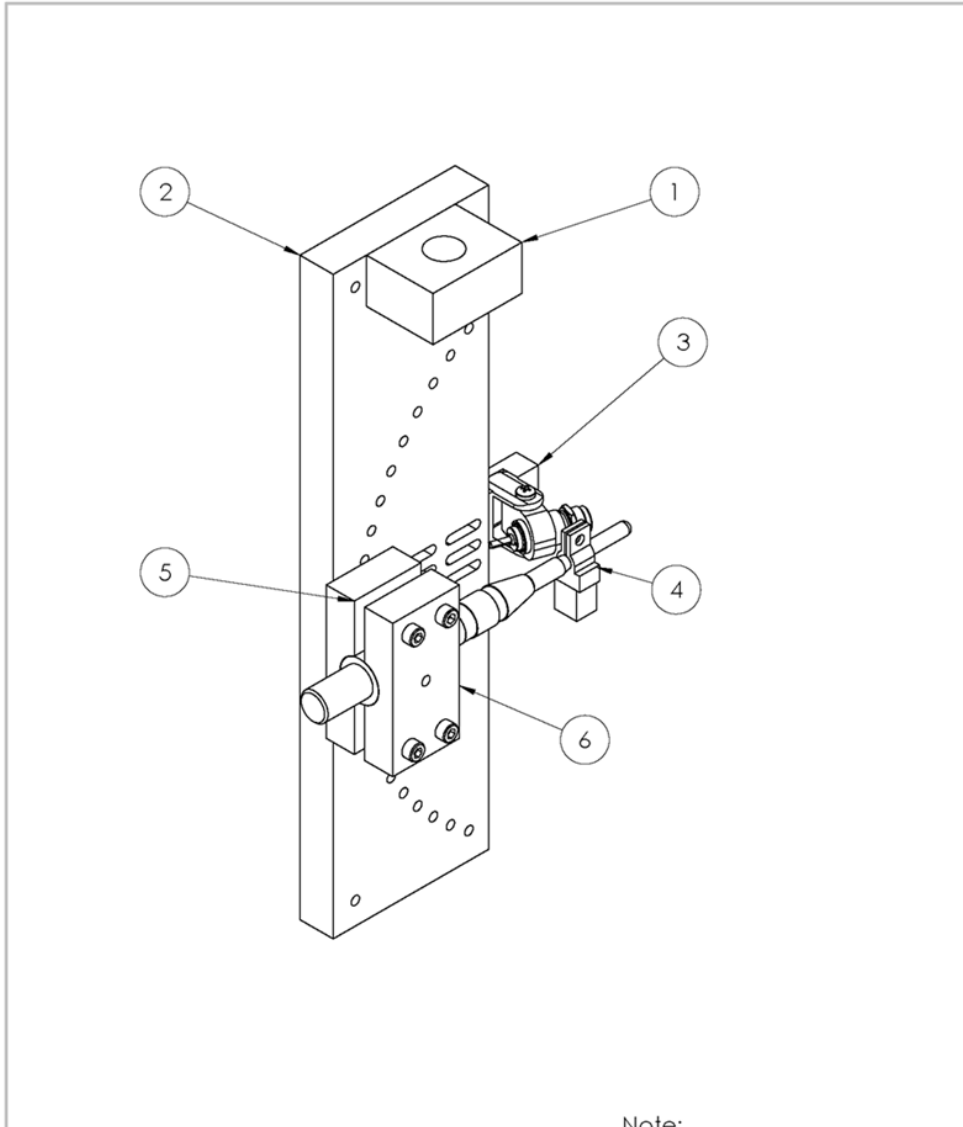
- [36] S. Olson, J. M. Clinton, Z. Working, J. R. Lynch, W. J. Warne, W. Womack, *et al.*, "Thermal Effects of Glenoid Reaming During Shoulder Arthroplasty in Vivo," *The Journal of Bone & Joint Surgery*, vol. 93, pp. 11-19, 2011.
- [37] S. J. Calder, M. R. Barnes, and W. M. Harper, "Reduction of temperatures generated by the triple reamer within the femoral head," *Injury*, vol. 26, pp. 183-185, 1995.
- [38] G. R. G. Oscar, F. L. Mombiela, F. Consuelo Jiménez de la, M. G. Aránguez, D. V. Escribano, and J. V. Martín, "The Influence of the Size and Condition of the Reamers on Bone Temperature During Intramedullary Reaming," *The Journal of Bone & Joint Surgery*, vol. 86, pp. 994-999, 2004.
- [39] K. Denis, G. Van Ham, J. Vander Sloten, R. Van Audekercke, G. Van der Perre, J. De Schutter, *et al.*, "Influence of bone milling parameters on the temperature rise, milling forces and surface flatness in view of robot-assisted total knee arthroplasty," *International Congress Series*, vol. 1230, pp. 300-306, 2001.
- [40] H. C. Shin and Y. S. Yoon, "Bone temperature estimation during orthopaedic round bur milling operations," *Journal of Biomechanics*, vol. 39, pp. 33-39, 2006.
- [41] N. P. Dillon, L. B. Kratchman, M. S. Dietrich, R. F. Labadie, I. I. I. R. J. Webster, and T. J. Withrow, "An Experimental Evaluation of the Force Requirements for Robotic Mastoidectomy," *Otology & Neurotology*, vol. 34, pp. e93-e102, 2013.
- [42] M. Arbabtafti, M. Moghaddam, A. Nahvi, M. Mahvash, B. Richardson, and B. Shirinzadeh, "Physics-Based Haptic Simulation of Bone Machining," *IEEE Transactions on Haptics*, vol. 4, pp. 39-50, 2011.
- [43] P. A. Federspil, U. W. Geithoff, D. Henrich, and P. K. Plinkert, "Development of the First Force-Controlled Robot for Otoneurosurgery," *The Laryngoscope*, vol. 113, pp. 465-471, 2003.
- [44] M. Nogler, M. Krismer, C. Haid, M. Ogon, C. Bach, and C. Wimmer, "Excessive heat generation during cutting of cement in the Robodoc hip-revision procedure," *Acta Orthopaedica*, vol. 72, pp. 595-599, 2001.
- [45] C. Plaskos, A. Hodgson, and P. Cinquin, "Modelling and Optimization of Bone-Cutting Forces in Orthopaedic Surgery," in *Medical Image Computing and Computer-Assisted Intervention - MICCAI 2003*. vol. 2878, R. Ellis and T. Peters, Eds., ed: Springer Berlin Heidelberg, 2003, pp. 254-261.
- [46] N. Sugita, T. Nakano, Y. Nakajima, K. Fujiwara, N. Abe, T. Ozaki, *et al.*, "Dynamic controlled milling process for bone machining," *Journal of Materials Processing Tech*, vol. 209, pp. 5777-5784, 2009.

- [47] R. L. Poole, S. C. Lea, J. E. Dyson, A. C. C. Shortall, and A. D. Walmsley, "Vibration characteristics of dental high-speed turbines and speed-increasing handpieces," *Journal of dentistry*, vol. 36, pp. 488-493, 2008.
- [48] E. Rytönen, E. Sorainen, P. Leino-Arjas, and S. Solovieva, "Hand-arm vibration exposure of dentists," *International archives of occupational and environmental health*, vol. 79, pp. 521-527, 2006.
- [49] A. Calvo, R. Deboli, C. Preti, and A. De Maria, "Daily exposure to hand arm vibration by different electric olive beaters," *Journal of Agricultural Engineering*, vol. 45, pp. 103-110, 2014.
- [50] D. Edwards and G. Holt, "Hand-arm vibration exposure from construction tools: results of a field study," *Construction Management and Economics*, vol. 24, pp. 209-217, 2006.
- [51] L. A. Kurtz, P. Vi, and D. K. Verma, "Occupational exposures to hand-arm vibration, whole-body vibration, and noise among crane operators in construction: a pilot study," *Journal of occupational and environmental hygiene*, vol. 9, p. D117, 2012.
- [52] M. P. Groover, *Fundamentals of modern manufacturing: materials, processes, and systems* vol. 4th. Chichester; Hoboken, N.J: Wiley, 2010.
- [53] F. A. Matsenlii, J. Clinton, J. Lynch, A. Bertelsen, and M. L. Richardson, "Glenoid Component Failure in Total Shoulder Arthroplasty," *The Journal of Bone & Joint Surgery*, vol. 90, pp. 885-896, 2008.
- [54] J. Lee, O. B. Ozdoganlar, and Y. Rabin, "An experimental investigation on thermal exposure during bone drilling," *Medical engineering & physics*, vol. 34, p. 1510, 2012.
- [55] M. T. Hillery and I. Shuaib, "Temperature effects in the drilling of human and bovine bone," *Journal of Materials Processing Tech*, vol. 92, pp. 302-308, 1999.
- [56] G. Augustin, T. Zigman, S. Davila, T. Udiljak, T. Staroveski, D. Brezak, *et al.*, "Cortical bone drilling and thermal osteonecrosis," *Clinical biomechanics (Bristol, Avon)*, vol. 27, pp. 313-325, 2012.
- [57] I. O. f. S. (ISO), "ISO 5349:2001 - Mechanical Vibration," in *Measurement and Evaluation of Human Exposure to Hand-Transmitted Vibration*, ed. Geneva: ISO.
- [58] ASTM, "Standard Specification for Rigid Polyurethane Foam for Use as a Standard Material for Testing Orthopaedic Devices and Instruments," vol. F1839-08, ed: ASTM International, West Conshohocken, PA, 2012, 2012.
- [59] H. Y. Kim, "Statistical notes for clinical researchers: assessing normal distribution (2) using skewness and kurtosis," *Restor Dent Endod*, vol. 38, pp. 52-4, Feb 2013.

- [60] S. den Dunnen, L. Mulder, G. M. M. J. Kerkhoffs, J. Dankelman, and G. J. M. Tuijthof, "Waterjet drilling in porcine bone: the effect of the nozzle diameter and bone architecture on the hole dimensions," *Journal of the mechanical behavior of biomedical materials*, vol. 27, pp. 84-93, 2013.
- [61] S.-J. Kim, J. Yoo, Y.-S. Kim, and S.-W. Shin, "Temperature change in pig rib bone during implant site preparation by low-speed drilling," *Journal of Applied Oral Science*, vol. 18, pp. 522-527, 2010.
- [62] J. Aerssens, S. Boonen, G. Lowet, and J. Dequeker, "Interspecies differences in bone composition, density, and quality: potential implications for in vivo bone research," *Endocrinology*, vol. 139, pp. 663-70, Feb 1998.
- [63] M. C. Pierce, A. Valdevit, L. Anderson, N. Inoue, and D. L. Hauser, "Biomechanical Evaluation of Dual-Energy X-Ray Absorptiometry for Predicting Fracture Loads of the Infant Femur for Injury Investigation: An In Vitro Porcine Model," *Journal of orthopaedic trauma*, vol. 14, pp. 571-576, 2000.
- [64] R. R. Pelker, G. E. Friedlaender, T. C. Markham, M. M. Panjabi, and C. J. Moen, "Effects of freezing and freeze-drying on the biomechanical properties of rat bone," *Journal of orthopaedic research : official publication of the Orthopaedic Research Society*, vol. 1, p. 405, 1984.
- [65] J. T. Nurmi, H. SievÄänen, P. Kannus, M. JÄärvinen, and L. N. J. r. Teppo, "Porcine Tibia Is a Poor Substitute for Human Cadaver Tibia for Evaluating Interference Screw Fixation," *The American Journal of Sports Medicine*, vol. 32, pp. 765-771, 2004.
- [66] H. Bonney, B. J. Colston, and A. M. Goodman, "Regional variation in the mechanical properties of cortical bone from the porcine femur," *Medical Engineering and Physics*, vol. 33, pp. 513-520, 2011.
- [67] S. Smith and T. Delio, "Sensor-Based Chatter Detection and Avoidance by Spindle Speed Selection," *Journal of Dynamic Systems, Measurement, and Control*, vol. 114, pp. 486-492, 1992.
- [68] V. Shaikh, *Mist and Microstructure Characterization in End Milling AISI 1018 Steel Using Microlubrication*, 2013.
- [69] A. Mayers, *Introduction to Statistics and SPSS in Psychology*: Pearson Education, Limited, 2013.
- [70] R. Mee, *A Comprehensive Guide to Factorial Two-Level Experimentation*: Springer, 2009.

# Appendix A: Developed Experimental Apparatus Component Drawings

**Note:** All dimensions are in millimeters (mm).

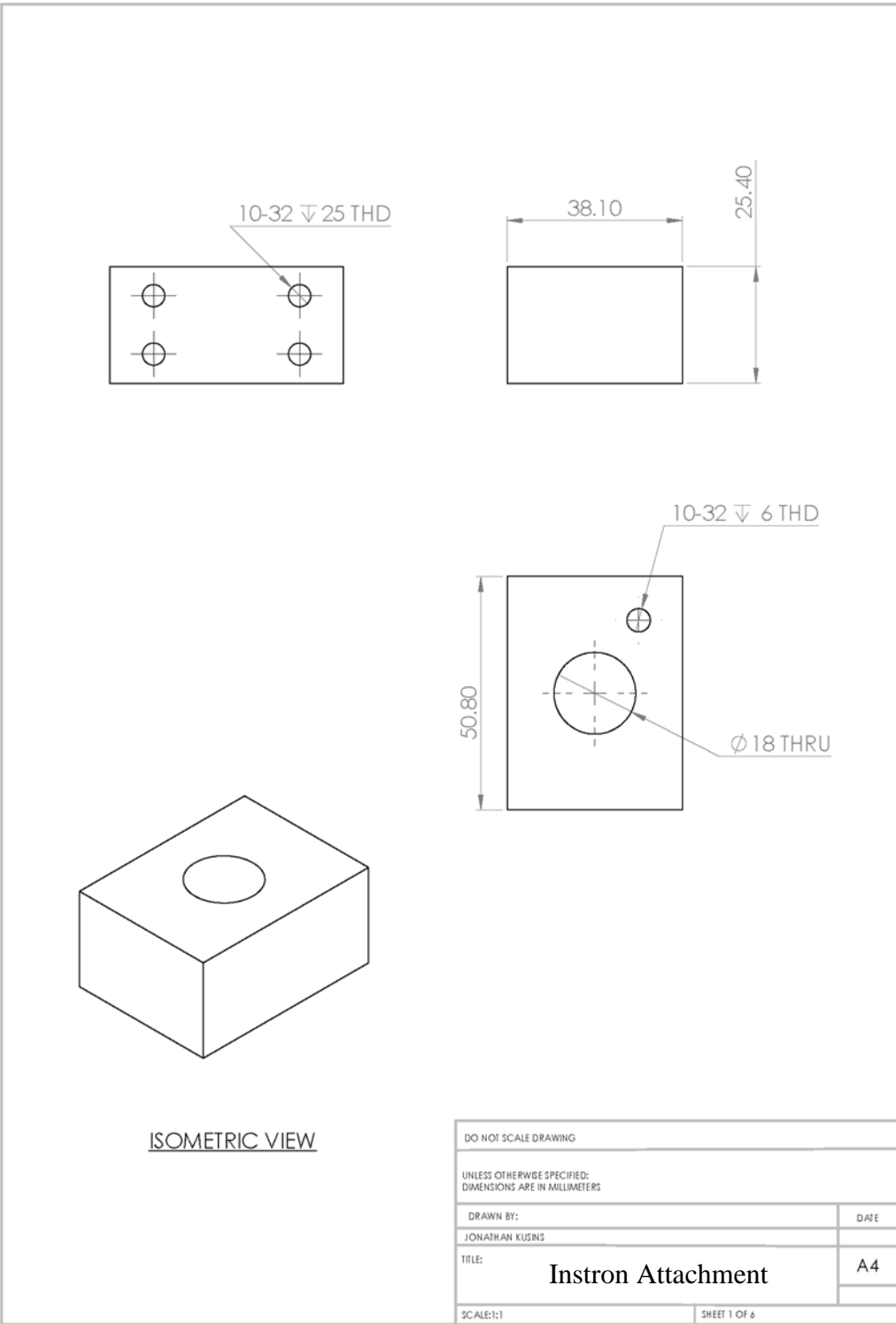


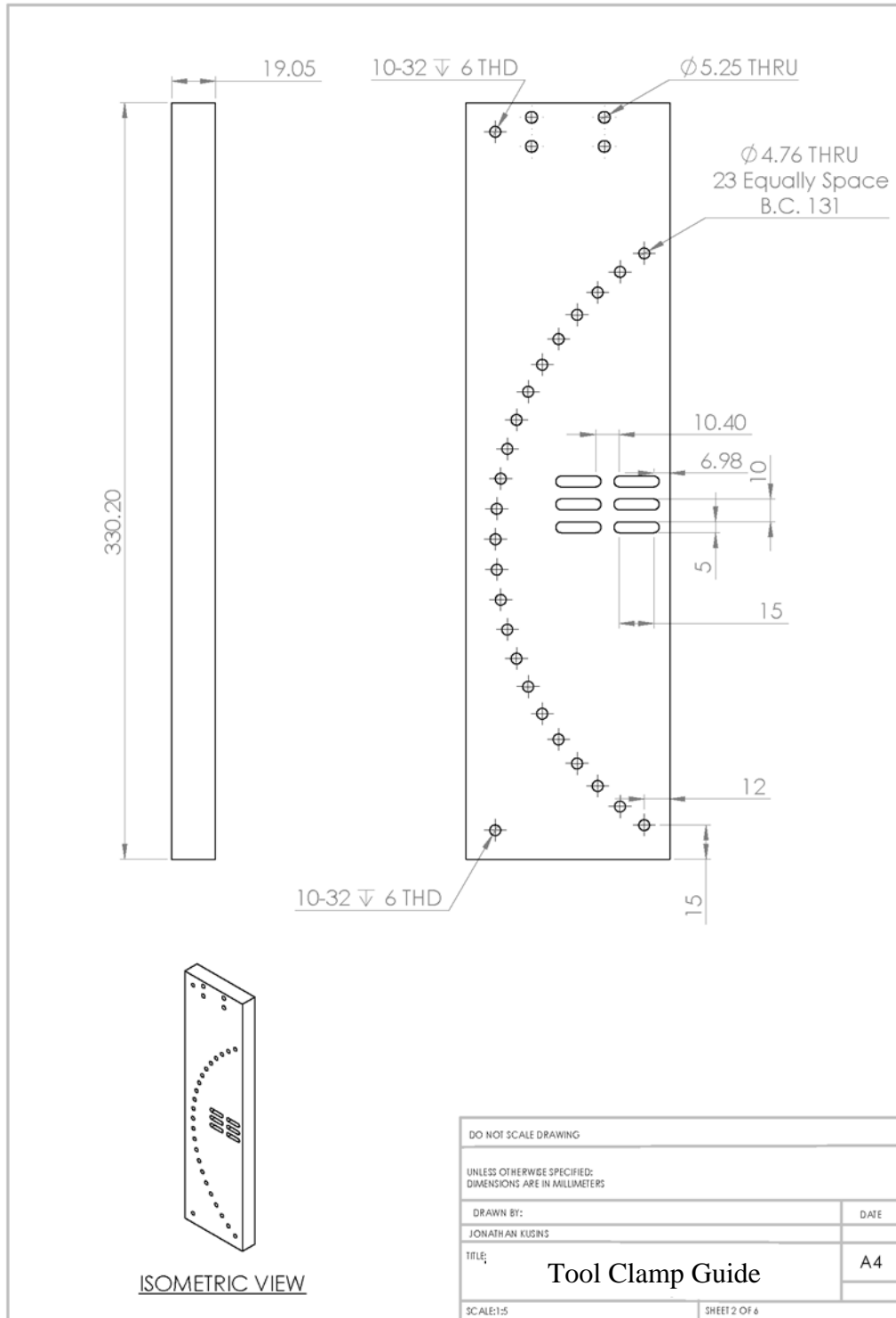
Note:  
Parts to be manufactured are indicated in bill of materials

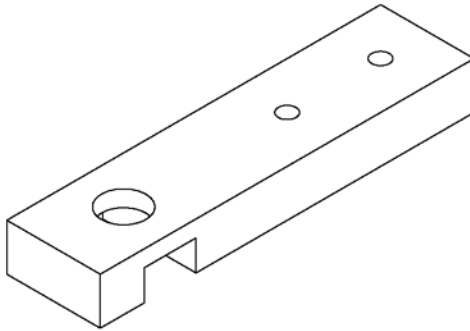
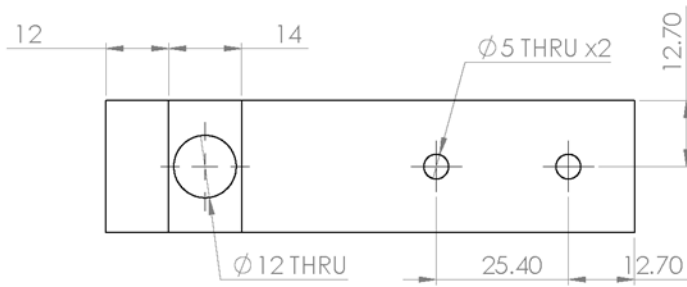
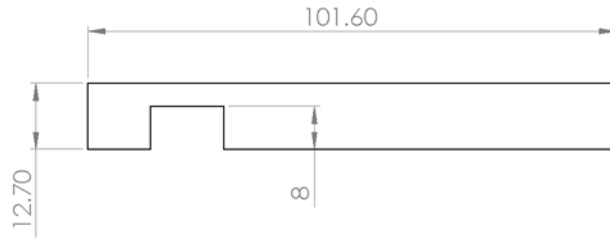
ITEM NO.	PART NUMBER	Original/QTY.
1	Instron Attachment	1
2	Tool Clamp Guide	1
3	IR Place Holder	1
4	Shaft Collar	1
5	Tool Clamp Left	1
6	Tool Clamp Right	1

DO NOT SCALE DRAWING	
UNLESS OTHERWISE SPECIFIED: DIMENSIONS ARE IN MILLIMETERS	
DRAWN BY: JONATHAN KUSINS	DATE
TITLE: <b>Tool Holder</b>	A4
SCALE:1:5	SHEET 1 OF 1



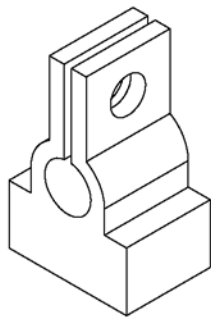
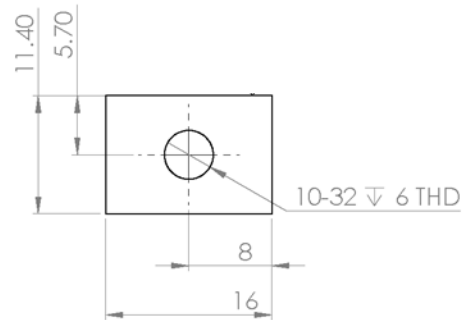
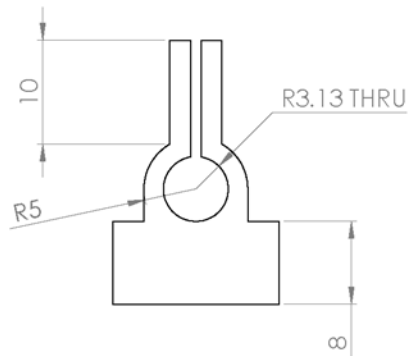
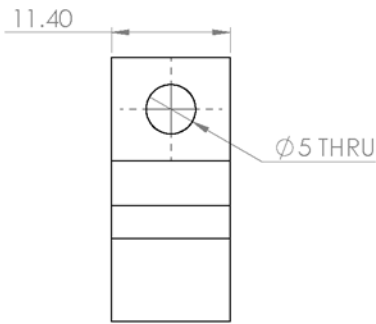






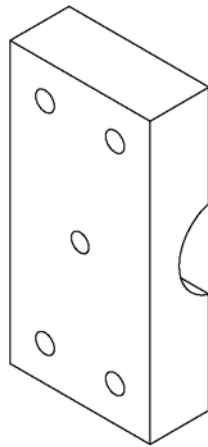
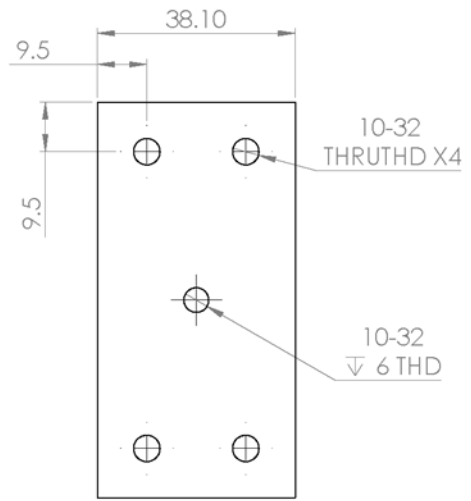
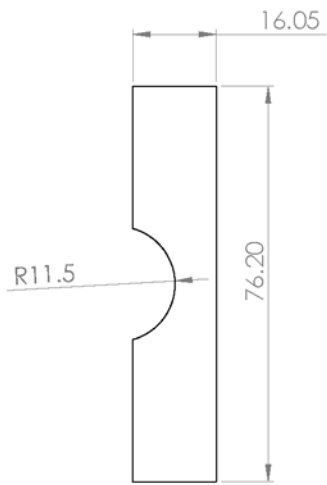
ISOMETRIC VIEW

DO NOT SCALE DRAWING	
UNLESS OTHERWISE SPECIFIED: DIMENSIONS ARE IN MILLIMETERS	
DRAWN BY: JONATHAN KUSINS	DATE
TITLE: <b>IR Place Holder</b>	A4
SCALE:1:2	SHEET 3 OF 6



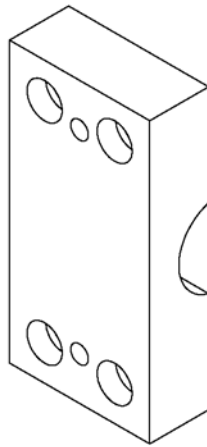
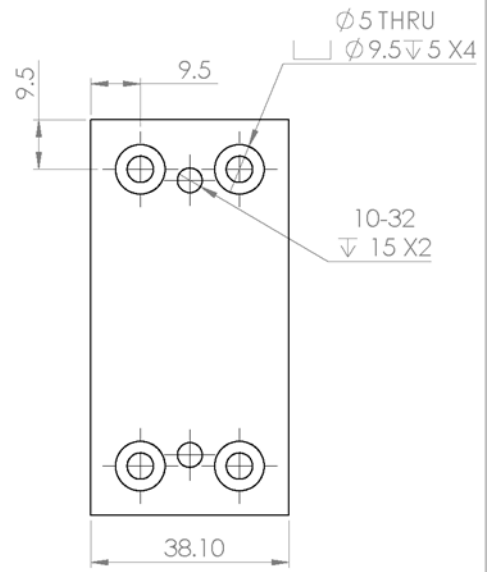
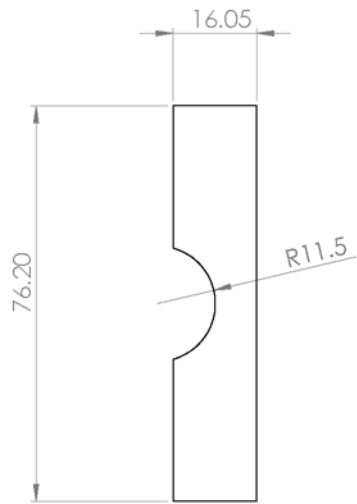
ISOMETRIC VIEW

DO NOT SCALE DRAWING	
UNLESS OTHERWISE SPECIFIED: DIMENSIONS ARE IN MILLIMETERS	
DRAWN BY: JONATHAN KUSINS	DATE
TITLE: <b>Shaft Collar</b>	A4
SCALE:2:1	SHEET 4 OF 6



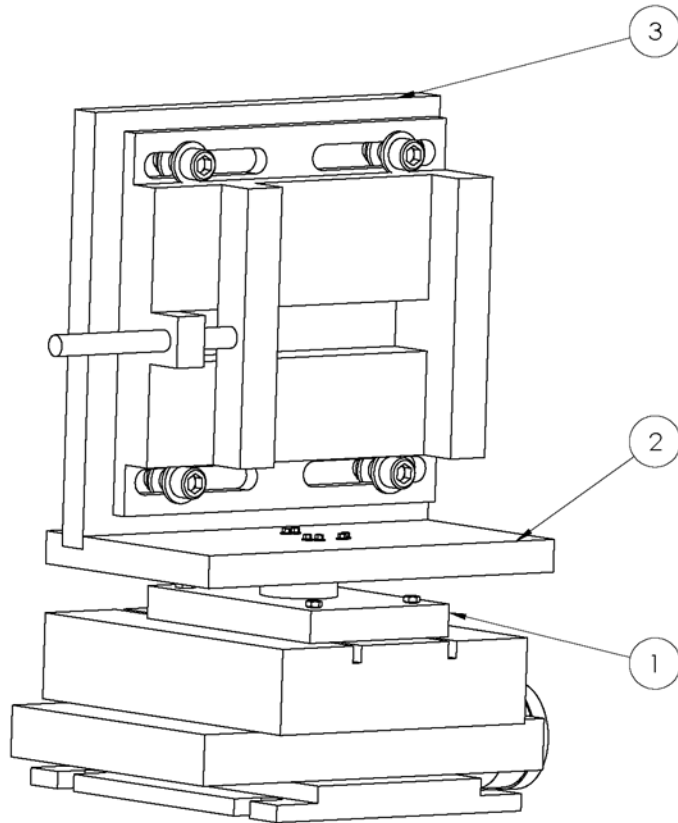
ISOMETRIC VIEW

DO NOT SCALE DRAWING	
UNLESS OTHERWISE SPECIFIED: DIMENSIONS ARE IN MILLIMETERS	
DRAWN BY: JONATHAN KUSINS	DATE
TITLE: <b>Tool Clamp Left</b>	A4
SCALE:1:1	SHEET 5 OF 6



ISOMETRIC VIEW

DO NOT SCALE DRAWING	
UNLESS OTHERWISE SPECIFIED: DIMENSIONS ARE IN MILLIMETERS	
DRAWN BY: JONATHAN KUSINS	DATE
TITLE: <b>Tool Clamp Right</b>	A4
SCALE:1:1	SHEET 4 OF 6

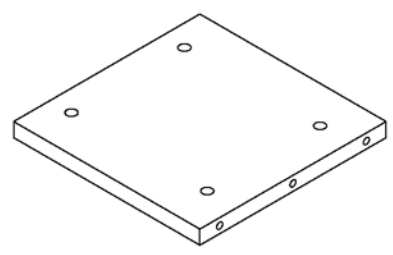
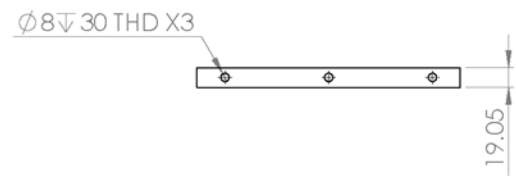
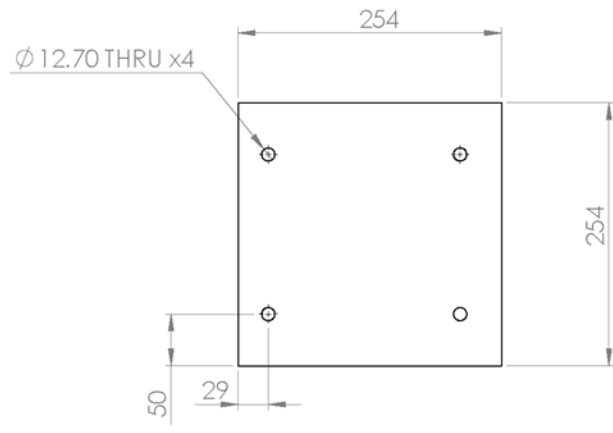


Note:  
Parts to be manufactured are indicated in bill of materials

ITEM NO.	PART NUMBER	QTY.
1	Vise Holder	1
2	Vise to Mini	1
3	Mini to XY	1

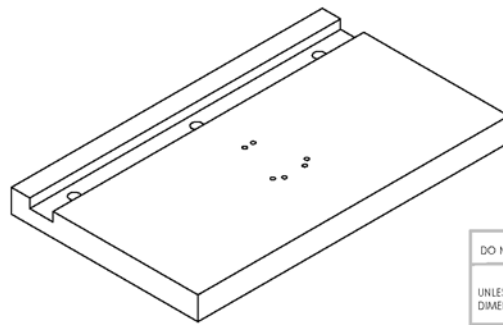
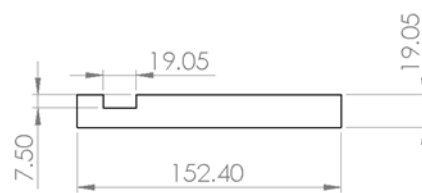
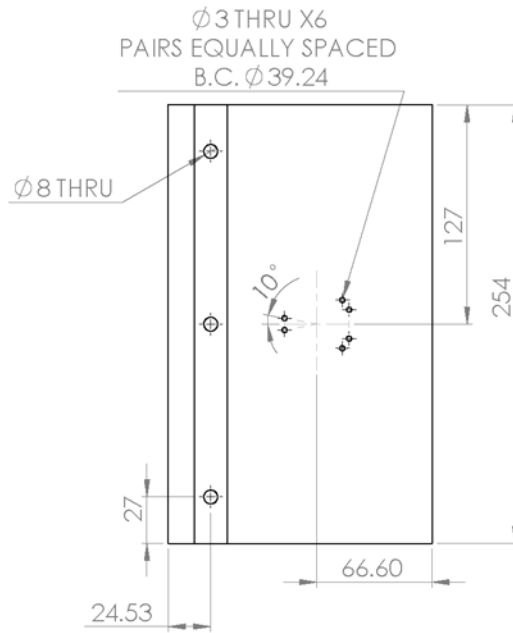
DO NOT SCALE DRAWING	
UNLESS OTHERWISE SPECIFIED: DIMENSIONS ARE IN MILLIMETERS	
DRAWN BY: JONATHAN KUSINS	DATE
TITLE: <b>Work Piece</b>	A4
SCALE:1:10	SHEET 1 OF 1



ISOMETRIC VIEW

DO NOT SCALE DRAWING	
UNLESS OTHERWISE SPECIFIED: DIMENSIONS ARE IN MILLIMETERS	
DRAWN BY: JONATHAN KUSINS	DATE
TITLE: <b>Vise Holder</b>	A4
SCALE:1:5	SHEET 1 OF 3

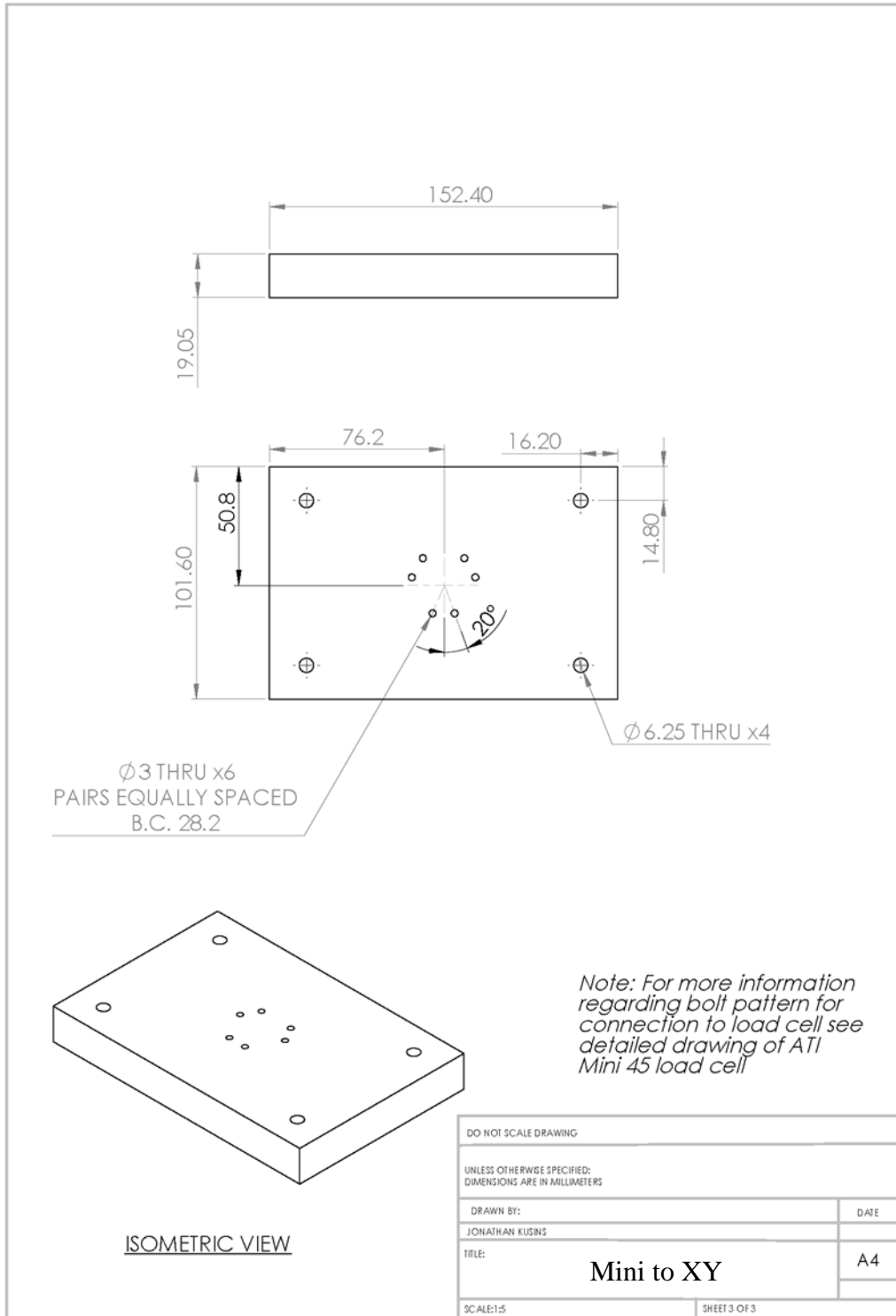




ISOMETRIC VIEW

*Note: For more information regarding bolt pattern for connection to load cell see detailed drawing of ATI Mini 45 load cell*

DO NOT SCALE DRAWING	
UNLESS OTHERWISE SPECIFIED: DIMENSIONS ARE IN MILLIMETERS	
DRAWN BY: JONATHAN KUSINS	DATE
TITLE: <b>Vise to Mini</b>	A4
SCALE:1:5	SHEET 2 OF 3



## Appendix B: Supplementary Specification Sheets

Listed following are specification sheets for the accelerometer (42A16), load cell, and infrared pyrometer supplied by the manufacturer.

### Load Cell Specification Sheet

#### 4.8.3 Mini45 Titanium Physical Properties

##### Standard (US)

Single-Axis Overload	
Fxy	±670 lbf
Fz	±1400 lbf
Txy	±590 lbf-in
Tz	±720 lbf-in
Stiffness (Calculated)	
X-axis & Y-axis forces (Kx, Ky)	2.5x10 <sup>5</sup> lb/in
Z-axis force (Kz)	3.3x10 <sup>5</sup> lb/in
X-axis & Y-axis torque (Ktx, Kty)	8.6x10 <sup>4</sup> lbf-in/rad
Z-axis torque (Ktz)	1.8x10 <sup>5</sup> lbf-in/rad
Resonant Frequency	
Fx, Fy, Tz	5800 Hz
Fz, Tx, Ty	4600 Hz
Physical Specifications	
Weight*	0.22 lb
Diameter*	1.77 in
Height*	0.69 in

##### Metric (SI)

Single-Axis Overload	
Fxy	±3000 N
Fz	±6400 N
Txy	±67 Nm
Tz	±81 Nm
Stiffness (Calculated)	
X-axis & Y-axis forces (Kx, Ky)	4.3x10 <sup>7</sup> N/m
Z-axis force (Kz)	5.7x10 <sup>7</sup> N/m
X-axis & Y-axis torque (Ktx, Kty)	9.7x10 <sup>3</sup> Nm/rad
Z-axis torque (Ktz)	2.0x10 <sup>4</sup> Nm/rad
Resonant Frequency	
Fx, Fy, Tz	5800 Hz
Fz, Tx, Ty	4600 Hz
Physical Specifications	
Weight*	0.0998 kg
Diameter*	45 mm
Height*	17.5 mm

\* Specifications include standard interface plates.

## Accelerometer (42A16) Specification Sheet

Aerospace  
Energy  
Test and measurement

# Isotron® accelerometer Model 42A

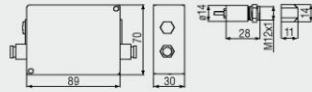
## Specifications

The following performance specifications conform to ISA-RP-37.2 and are typical values, referenced at +75°F (+24°C), 4 mA, and 100 Hz, unless otherwise noted. Calibration data, traceable to National Institute of Standards and Technology (NIST), is supplied.

Dynamic characteristics	Units	42A13	42A14	42A16	42A18	42A19
Range	g	±500	±200	±50	±10	±5
Sensitivity						
±5%	mV/g	10	25	100	500	1000
±10%	mV/g					
Frequency response						
Resonance frequency						
Typical	kHz	35	35	35	30	30
Minimum	kHz	30	30	30	25	25
Amplitude response						
±5%	Hz			1 to 10 000		
±10%	Hz			1 to 12 000		
Phase response						
±5°	Hz			5 to 10 000		
Sensitivity deviation over temperature						
-67°F to +257°F [-55°C to +125°C]	%	5	5	5	10	10
Transverse sensitivity	%			≤5		
Amplitude linearity	%			<1		
<b>Electrical characteristics</b>						
Output polarity				Acceleration directed into base produces positive output		
DC output bias voltage						
Room temperature +75°F (+24°C)	Vdc			+11.4 to +13.0		
-67°F to +257°F [-55°C to +125°C]	Vdc			+8.0 to +15.5		
Output impedance	Ω			<100		
Noise floor						
Broadband						
1 Hz to 10 kHz	µg rms	300	200	100	60	40
Spectral						
1 Hz	µg/√Hz	250	150	80	30	30
10 Hz	µg/√Hz	30	25	10	5	5
100 Hz	µg/√Hz	6	4	3	1.3	1.3
1000 Hz	µg/√Hz	3	2	1	0.6	0.4
Grounding method				Signal ground isolated from case		
Power requirements						
Supply voltage	Vdc			+24 to +30		
Supply current	mA			+2 to +20		
Warm-up time [1]	s	2	3	5	10	15
<b>Environmental characteristics</b>						
Temperature range, operating				-67°F to +257°F [-55°C to +125°C]		
Humidity				Hermetically sealed		
Vibration limit [sinusoidal motion] [2]	g	1000	1000	1000	600	600
Shock limit [3]	g pk			5000		
Base strain sensitivity at 250 µstrain	g/µstrain			0.001		
<b>Physical characteristics</b>						
Dimensions				See outline drawing		
Weight, maximum	gram [oz]	8 [0.28]	8 [0.28]	8 [0.28]	10 [0.35]	10 [0.35]
Case material				Titanium		
Connector				10-32 threaded coaxial		
Mounting method				Threaded stud		
Mounting stud torque, recommended						
10-32 and M6 studs	lbf-in [Nm]			18 [2]		
M5 stud	lbf-in [Nm]			13 [1.5]		
1/4-28 stud	lbf-in [Nm]			30 [3.5]		
<b>Calibration data supplied</b>						
Sensitivity	mV/g					
Frequency response				50 Hz to 10 kHz		
Amplitude response	%					
DC output bias voltage	Vdc					

**MEGGITT**  
smart engineering for  
extreme environments

## Infrared Pyrometer (CT-SF02-C3) Specification Sheet



### Product identification

**CT - SF02 - C3**  
 Cable length [1m / 3m (standard) / 8m / 15m]  
 Focus [SF02 / SF15 / SF22]  
 thermoMETER CT

27

Model	CT-SF02-C3	CT-SF15-C3	CT-SF22-C3
Optical resolution	2:1	15:1	22:1
Temperature range <sup>1</sup>	-50°C to 600°C	-50°C to 600°C	-50°C to 975°C
Spectral range	8 to 14μm		
System accuracy <sup>2</sup>	< 1% or < 1°C		
Repeatability <sup>2</sup>	< 0.5% or < 0.5°C		
Temperature resolution	< 0.1°C		
Response time	150ms (95%)		
Emissivity/gain <sup>1</sup>	0.100 to 1.100		
Transmissivity/gain <sup>1</sup>	0.100 to 1.100		
Signal processing <sup>1</sup>	peak hold, valley hold, average; extended hold function with threshold and hysteresis		
Certificate of calibration	optional		
Outputs/analog	channel 1 channel 2 optional	0/4 to 20mA, 0 to 5/10V, thermocouple J, K sensor temperature (-20 to 180°C as 0 to 5V or 0 to 10V), alarm output relay: 2 x 60VDC/ 42VAC <sub>opt</sub> ; 0.4A; optically isolated	
Outputs/digital	optional	USB, RS232, RS485, CAN, Profibus DP, Ethernet	
Output impedances	current output voltage output	mA max. 500Ω (with 8 to 36VDC) mV min. 100kΩ load impedance thermocouple 20Ω	
Inputs	programmable functional inputs for external emissivity adjustment, ambient temperature compensation, trigger (reset of hold functions)		
Cable length	1m, 3m (standard), 8m, 15m		
Power supply	8 to 36VDC; max. 100mA		
Environmental rating	IP 65 (NEMA-4)		
Ambient temperature	sensor controller	-20°C to 130°C	-20°C to 180°C
Storage temperature	sensor controller	-40°C to 130°C	-40°C to 180°C
Relative humidity	10 - 95%, non condensing		
Vibration	sensor	IEC 68-2-6: 3G, 11 to 200Hz, any axis	
Shock	sensor	IEC 68-2-27: 50G, 11ms, any axis	
Weight	sensor: 40g; controller: 420g		

<sup>1</sup> adjustable via controller or software

<sup>2</sup> ± ambient temperature 23 ± 5°C; whichever is greater

### Accessories page 46 - 49

- ▶ CF lense
- ▶ Protective window
- ▶ Mounting bracket / Mounting bolt
- ▶ Air purge collar
- ▶ Right angle mirror
- ▶ Rail mount adapter for controller
- ▶ Massive housing
- ▶ Protective tube
- ▶ Laser sighting tool
- ▶ Digital-Interface kit
- ▶ Relay output module
- ▶ Accessory-Kit for use of the CT in hazardous locations
- ▶ Software CompactConnect
- ▶ Certificate of calibration

## Appendix C: Supplementary Testing Files

A series of developmental experiments were performed to ensure accurate measurements for the various transducers. The performed tests included:

- Noise testing of all transducers
- Depth of cut calibration
- Load cell measurement verification
- Effect of time between successive burring trials on temperature measurements
- Alignment of pyrometer

Noise testing was performed on each transducer, to view the noise characteristics that are inherent to the transducers. The depth of cut calibration was performed as through development, it was discovered that the developed apparatus required a means to adjust the workpiece plane for consistent and accurate depths of cut. Load cell verification testing was performed against an offline measurement performed by means of static weights to ensure accurate measurements post processing of the signal. Finally, throughout the development phase, it was apparent a means to align the infrared pyrometer was needed to ensure accurate placement and subsequently measurements of the temperature of the workpiece. From the results of the developmental experiments it can be reasonably concluded that the developed apparatus obtained accurate outcome measurements. Additional information regarding each individual test is detailed in the following pages.

## Noise Testing

Noise testing was performed to determine the noise of the transducers at an idle state. Measurements of the three transducers (accelerometer, IR pyrometer, and load cell) were recorded for a duration of 10 seconds and are reported below. The mean value as well as the scatter ( $\pm 1$  standard deviation) is shown for each of the outcome measurements.

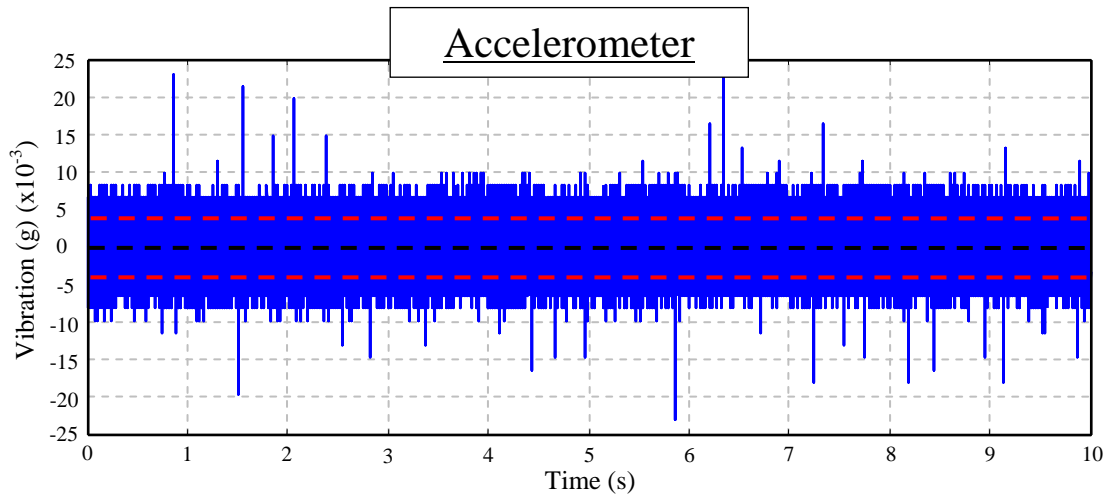


**Figure C.1: Noise characterization of accelerometer**

The noise measurements of the accelerometer are shown above. A mean noise (black dashed line) of 0 g was found with a standard deviation (red dashed line) of 0.004 g.

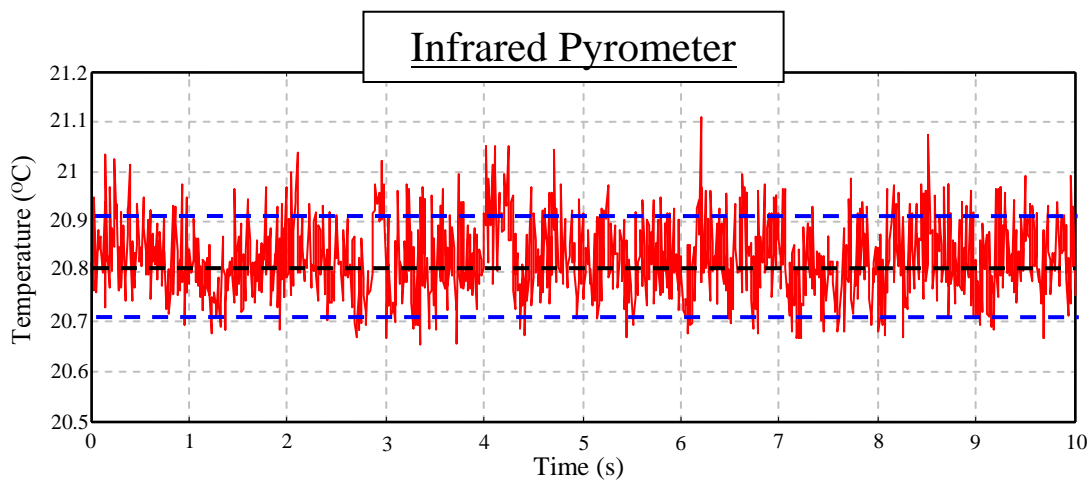


**Figure C.2: Noise characterization of pyrometer**

The noise measurements of the infrared pyrometer are shown above. A mean temperature (black dashed line) of 20.8 °C was found with a standard deviation (red dashed line) of 0.1°C.

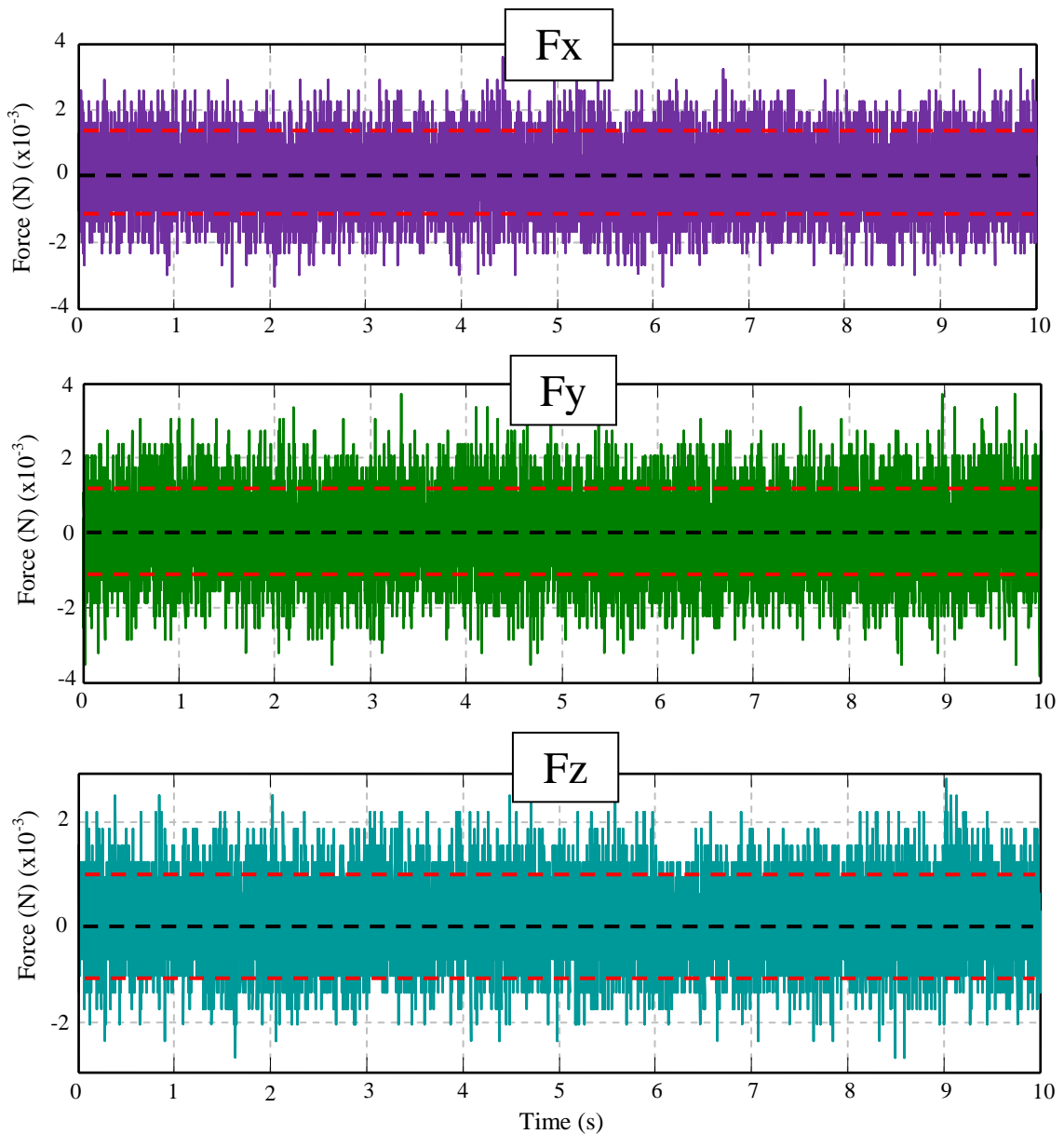


**Figure C.3: Noise measurements of 3 DOF load cell**

The noise measurements of the forces ( $F_x$ ,  $F_y$ , and  $F_z$ ) obtained from the load cell are shown above. A mean noise (black dashed line) of 0 N with a standard deviation (red dashed line) of 0.001 N was found in the x-direction. A mean noise (black dashed line) of  $0 \pm 0.001$  N was found in the y-direction and  $0 \pm 0.001$  N was found in the z-direction.



### Depth of Cut Calibration

Throughout the design process; it was observed that the workpiece clamp did not produce a consistent depth of cut throughout the burring trial as indicated by the cutting force results recorded. The associated errors arose due to the planes between the burring bit and workpiece were not aligned, resulting in the depth of cut to change throughout the burring path. The error was viewed in the outcome measurements as seen in Figure C.4 as the recorded force measurements increased as the burring bit progresses throughout its trajectory. It is apparent that the forces do not reach a steady state as originally anticipated.

To overcome the varying depth of cut, a means to adjust the workpiece plane was designed. A series of nuts, bolts, and washers were used to control the back of the vise grips essentially acting as stilts. Subsequently, the plane of the workpiece could be adjusted using the pitch of the screw, as depicted in Figure C.5. The leveling process was performed manually and locked in place when the outcome measurements were deemed adequate.

Initial results from the unlevelled workpiece clamp are presented in Figure C.4. Additionally, the design and components of the adjustable experimental apparatus , and the cutting force results obtained, once the leveling process was complete, are shown in Figure C.5.

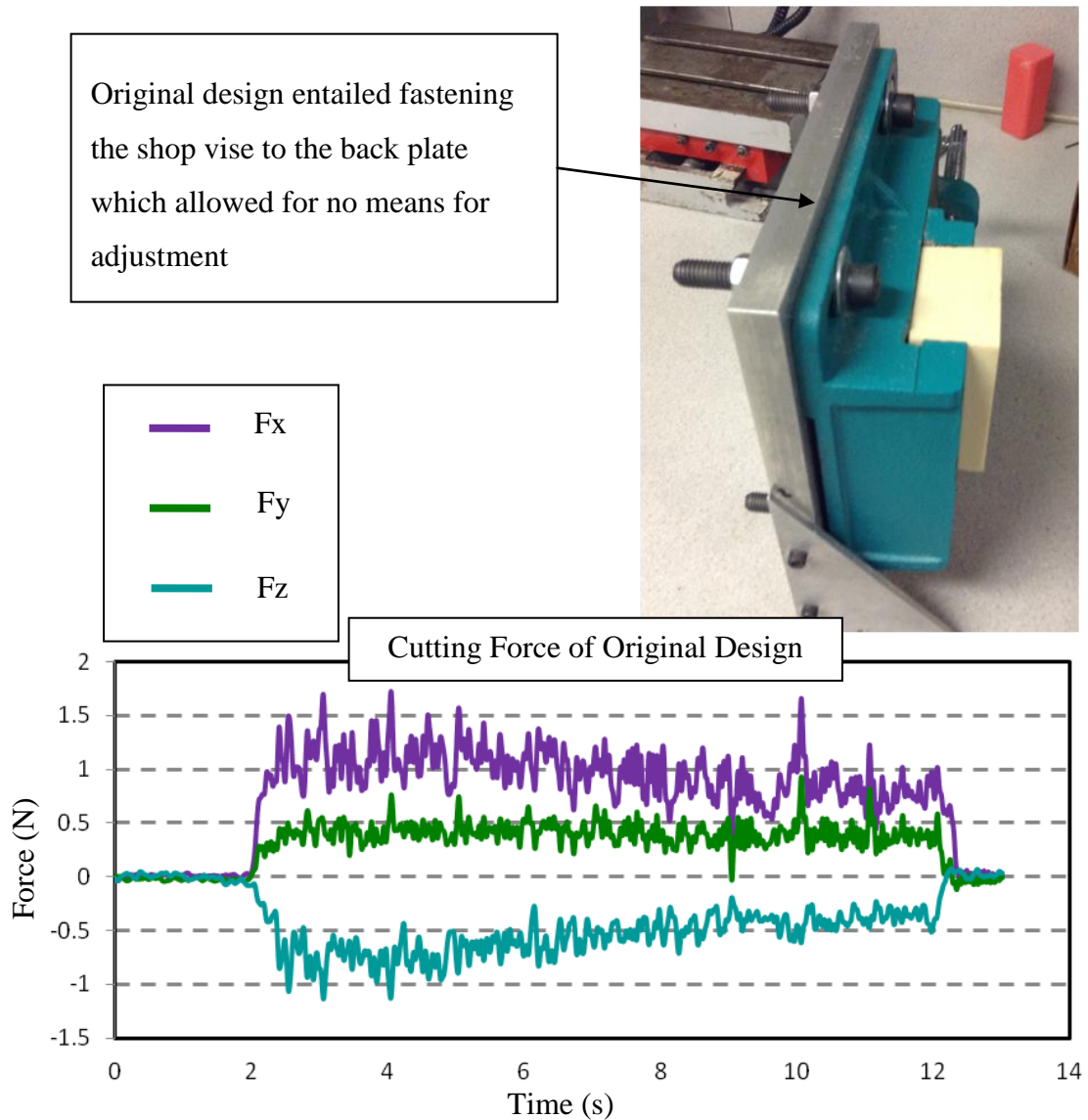


**Figure C.4: Force measurements of original designed workpiece clamp**

*The cutting force ( $F_x$ ,  $F_y$ , and  $F_z$ ) measurements obtained from the load cell using the original design of the workpiece clamp are shown above. Viewing the cutting force results, it is apparent that the force varies from entry to exit points of the burr. The variation in the outcome measurements is due to the varying depth of cut, confirmed visually, throughout the burring process.*

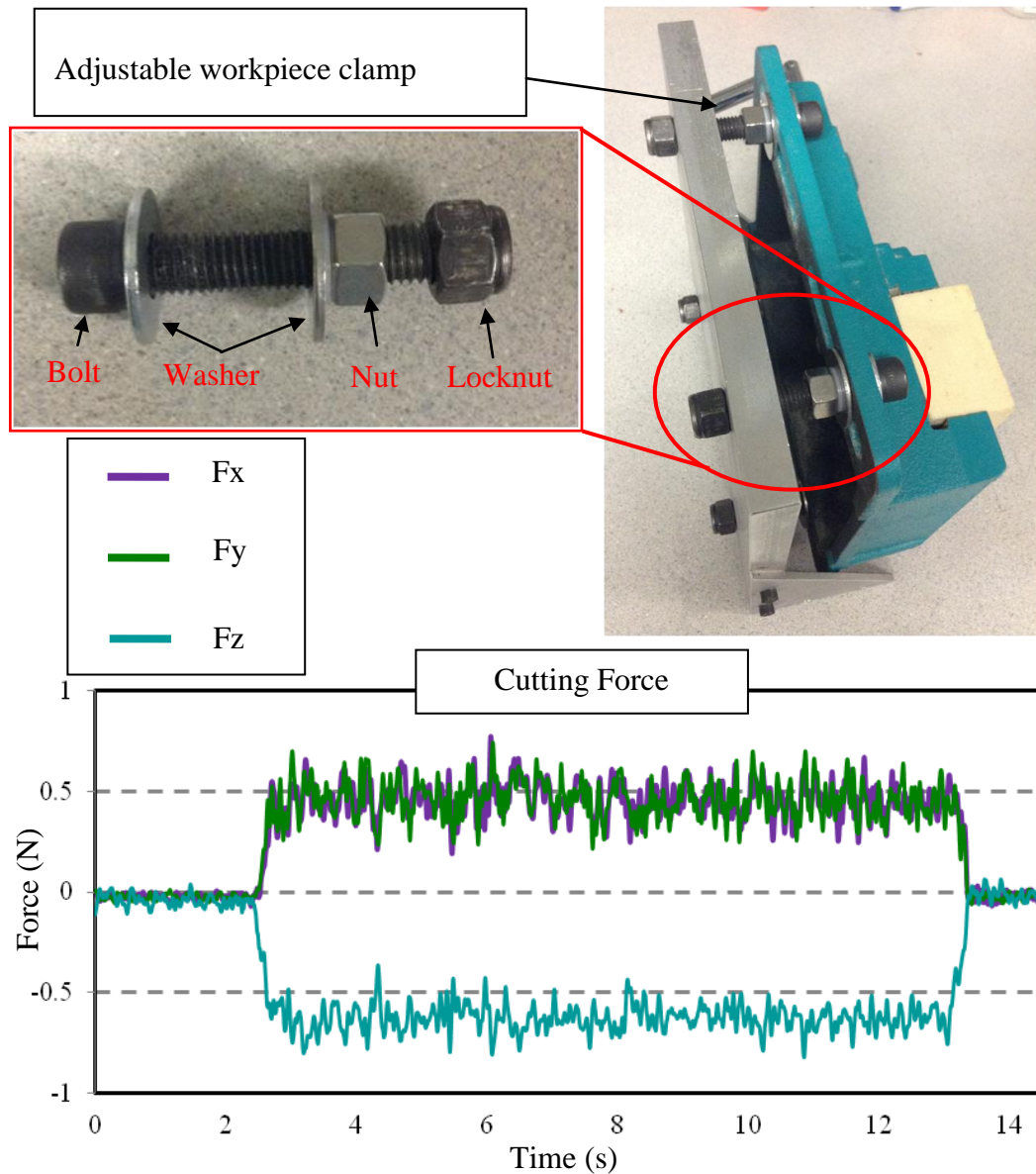


**Figure C.5: Force measurements with adjustable clamp**

The cutting force ( $F_x$ ,  $F_y$ , and  $F_z$ ) measurements obtained from the load cell using the redesigned adjustable workpiece clamp are shown above. Viewing the cutting force results, it is apparent that the forces are more consistent compared to the previous design between the entry and exit points of the burr. Moving forward into the experimental analysis (Chapter 3 and onward), the redesigned workpiece clamp was used.

### Load Cell Verification

The measurement of the load cell was calibrated against offline measurement performed by means of comparable static weights (200 grams, 400 grams, 600 grams) and the results are presented. The same parameters were used in each burring trial to allow for comparisons between runs.

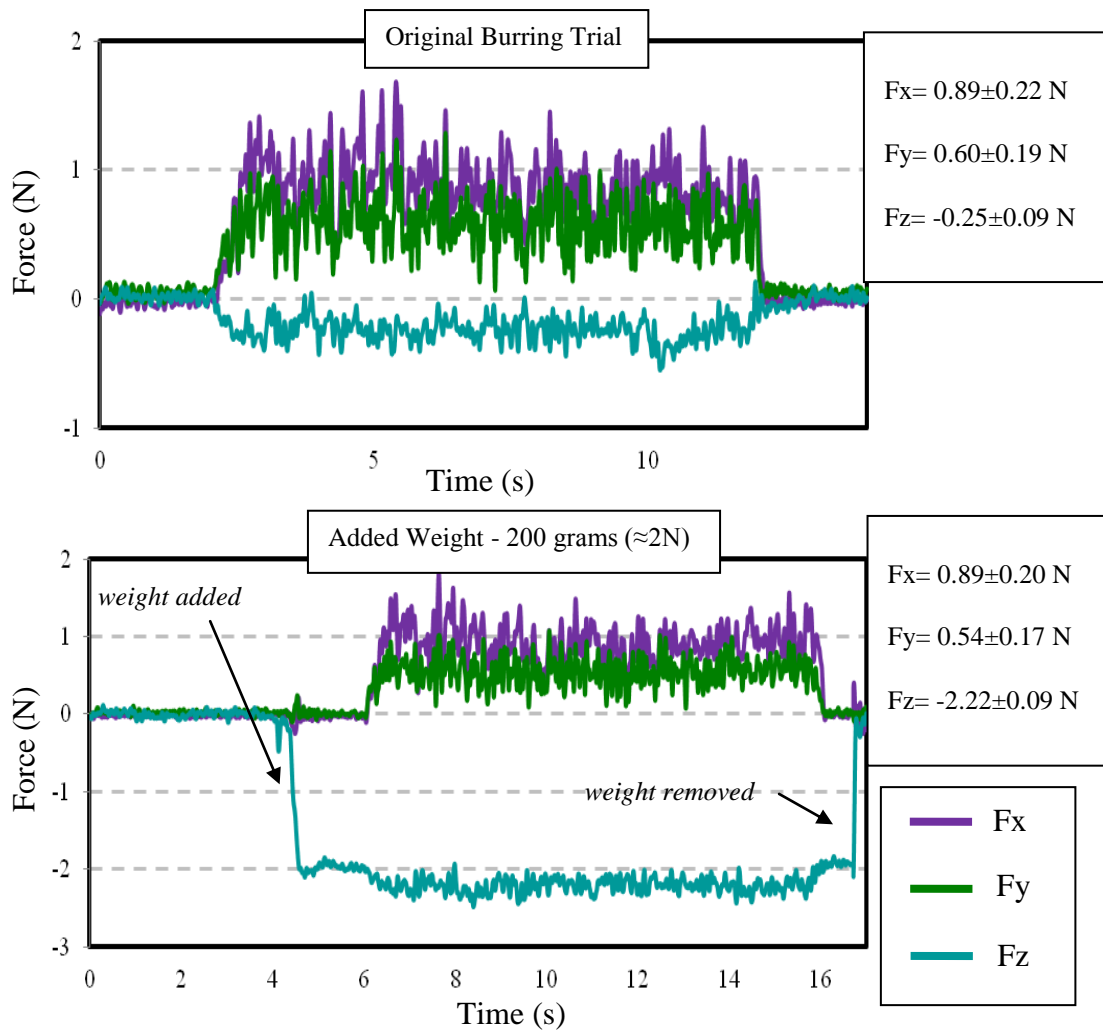


**Figure C.6: Sample outputs from load cell verification tests (0, 2N)**

*Outcome measurements of the cutting force ( $F_x$ ,  $F_y$ , and  $F_z$ ) for the original and 200 grams burring trial are shown above. The original burring trial was performed as a means of comparison for the subsequent trails. The 200 grams added trial was performed using a static weight that was added to the system.*

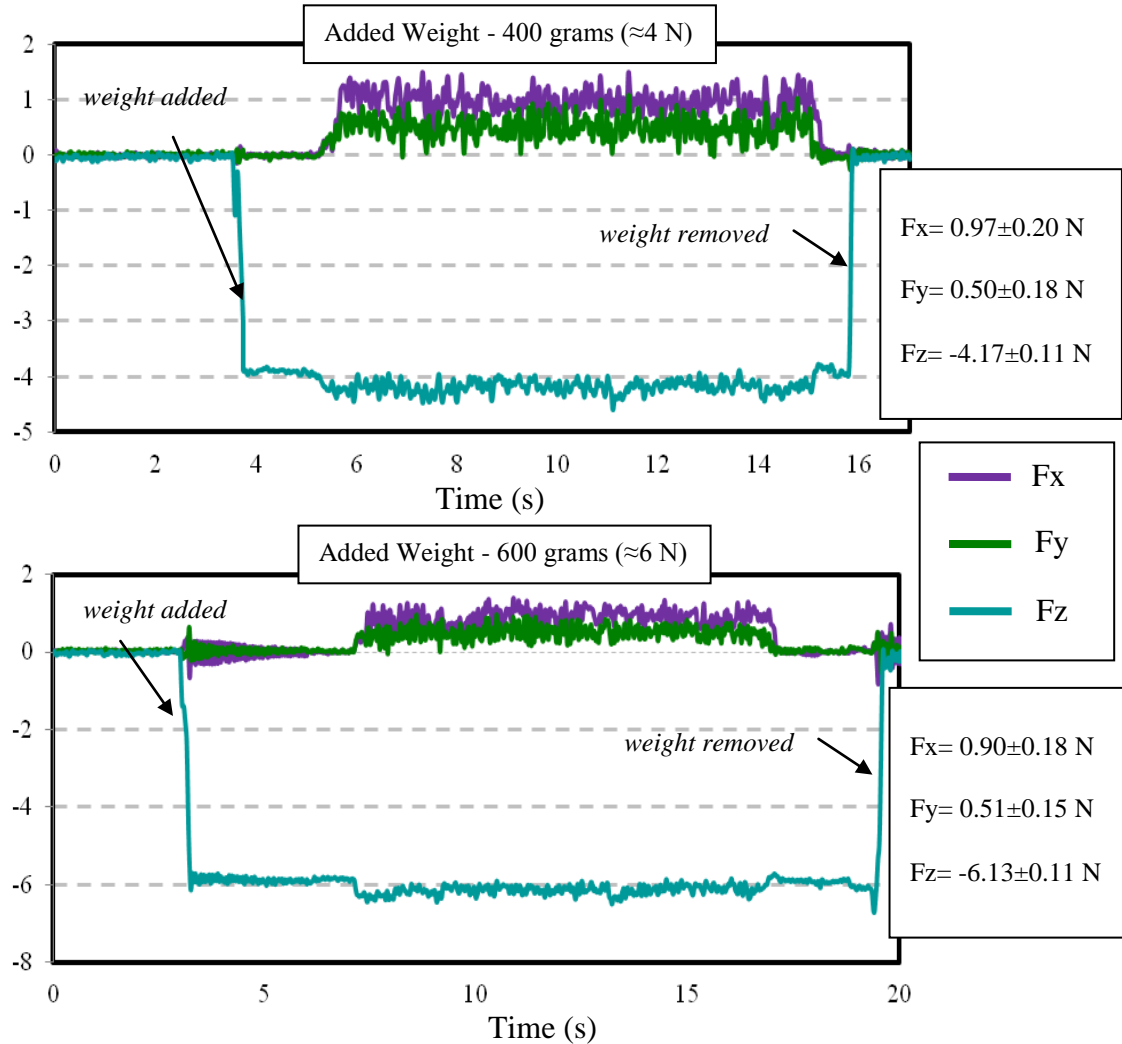


**Figure C.7: Sample outputs from load cell verification tests (4N, 6 N)**

*Outcome measurements of the cutting force ( $F_x$ ,  $F_y$ , and  $F_z$ ) for the  $\approx 4\text{N}$  and  $\approx 6\text{N}$  burring trial are shown above. Both trials further indicate that the developed apparatus is measuring correctly, due to its ability to measure the static weights along with the cutting force.*

The results of the load cell calibration were performed to ensure accurate measurements of the load cell. The results recorded, show high repeatability in the X and Y direction as the weights were added only in the Z direction. The Z direction is also able to account for the added static weight in each condition, further indicating that the load cell is recording the physical quantity correctly.

Effect of Time Between Successive Burring Paths on Temperature

The effect of time between successive burring trails on the outcome measurement of temperature was examined. The reason this experimental protocol was performed, was to ensure that the burring bit cooled long enough before a subsequent burring trial. As a large number of burring trials were to be performed within the experimental analysis, to reduce the time involved associated with data collection, the shortest time between successive burring trials without altering the outcome measurement of time should be optimized. Consistent process parameters were used within this trial. An original run was performed with the tool at room temperature. Cooling time was varied at three different increments, 30 seconds, 1.5 minutes, and 10 minutes. The shortest cooling time to allow for less than 0.5 °C was ideal. The results from the experimental measurements are shown in Table C.1.

**Table C.1: Temperature measurements for time delay between subsequent trails**

Cooling Time	Measured Temperature (°C)
Original Run	40.1±0.4
30 seconds	41.4±0.3
1.5 minutes	40.4±0.3
10 minutes	40.0±0.2

From the results obtained through the experimental measurements, it was found that 1.5 minutes was an appropriate time to allow for cooling of the tool between burring trials. Therefore, for data collection, the least amount of time needed between successive trials was 1.5 minutes.

### Alignment of Pyrometer

As an infrared pyrometer relies on a non-contact means of measuring temperature; ensuring the pyrometer's measurement spot is in the correct location is essential in obtaining an accurate measurement. To ensure that the pyrometer measurement spot was placed in the correct position on the workpiece three steps were taken. The steps performed to ensure correct positioning include:

1. A channel was burred into the workpiece.
2. The pyrometer was aligned in the burred channel using a custom designed 3d printed jig, that matched the infrared pyrometers' beam pattern.
3. The position was validated against inducing a heat gradient into the burred channel using a heated wire (width of the burring channel).

The steps outlined above are summarized in Figure C.8. The steps to realign the infrared pyrometer were repeated only when the tilt angle was varied. The infrared pyrometer was only varied with varying tilt angle, as the infrared pyrometer was aligned to the center of the tool with a 0 degree tilt angle. However, as the tilt angle changes to 45 degrees, the face that provides the cutting changes from the face of the burr, to the edge of the burr. Therefore, if the infrared pyrometer was not realigned, the infrared pyrometer would still be aligned to the center of the tool, which may be outside the burred channel.

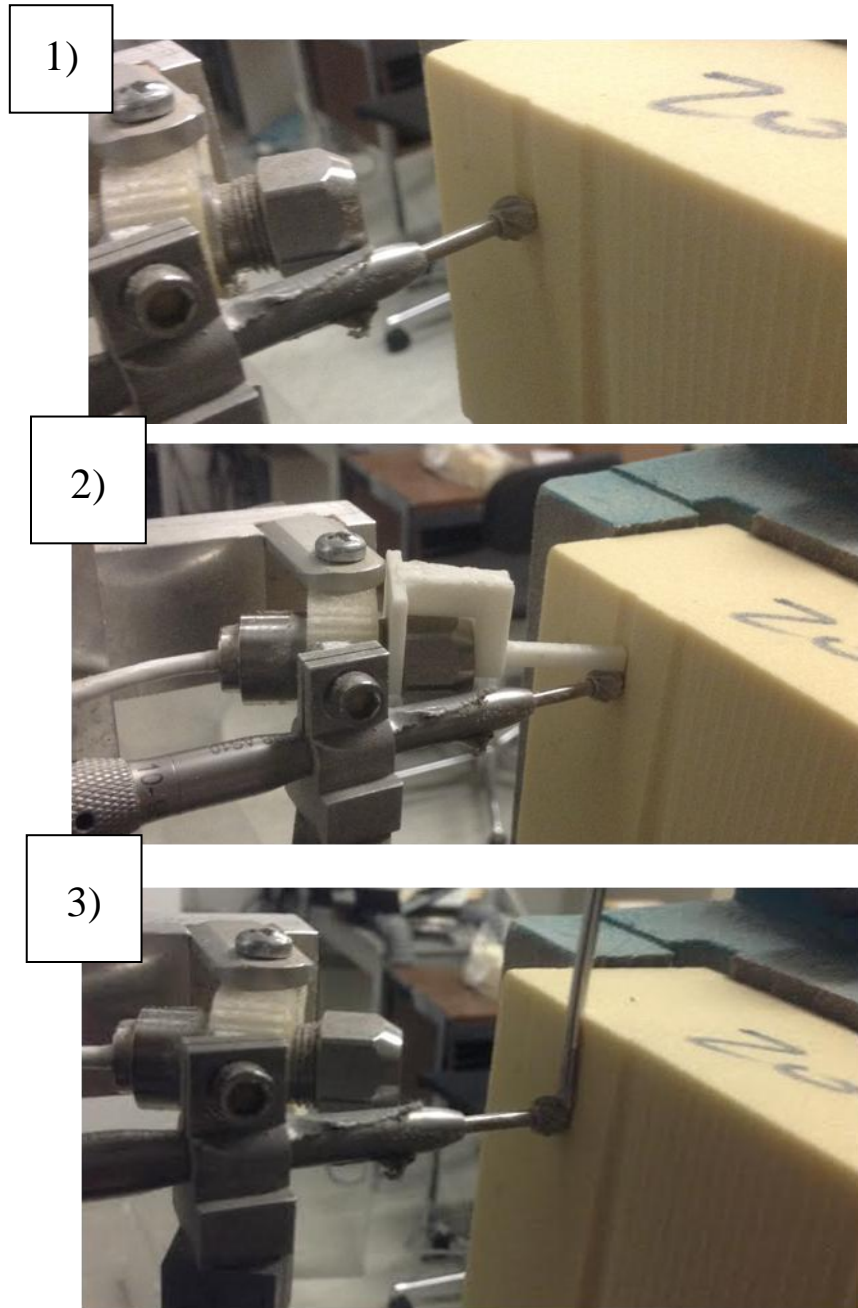


**Figure C.8: Alignment of pyrometer**

*Three steps taken to align the pyrometer. First, a channel was burred into the workpiece. Secondly, the infrared pyrometer was aligned using a 3d printed jig. Finally, to validate the placement of the pyrometer, a heated wire was used to induce a heat gradient in the workpiece.*



## **Appendix D: Statistical Analysis Guide**

Various statistical methods are employed within the current project to evaluate the effects of process parameters in a bone burring application. An experimental approach was taken that included varying the process parameters and quantifying the experimental measurands through transducers. Statistical methods were then used to view the significance of the results and provide rationale for selection of various process parameters. The typical procedure for performing the statistical analysis, adapted from a similar study involving machining, followed three steps [68]:

1. a multivariate analysis of variance (MANOVA)
2. an univariate analysis of variance (ANOVA) on each outcome measurement
3. a pairwise comparison of the main effects and interactions

All statistical analyses conducted within this thesis was performed using IBM's Statistical Package for Social Sciences (SPSS), Version 22.0 (SPSS Inc., Chicago, IL).

A multivariate analysis of variance (MANOVA) was used to study the effects of one or more independent variables on more than one dependent variable. The strength of the MANOVA is to protect against Type 1 errors (false positive) that may occur if only multiple ANOVAs were performed on the same data set. The first step of the MANOVA is to test the overall hypothesis that no difference exist in the means for different groups of dependent variables. A typical output of a MANOVA analysis reports significant values for four different types of tests: Hotelling's T-squared test, Wilk's lambda, Pillai-Bartlett test, and Roy's greatest character root. For the sake of relevance to this thesis, Wilk's lambda and Pillai-Bartlett tests will be used. Wilk's lambda test is the most

common and widely used traditional test and is utilized when there are more than two groups formed by the independent variables [69]. Pillai-Bartlett test is also employed when the dependent variables fail to meet the assumption of equality of variance-covariance as assessed by Box's M test.

An analysis of variance (ANOVA) was subsequently applied to each of the outcome measurements comprised of the experimental data set. An ANOVA tests for statistical differences between the means of two or more groups. An ANOVA can report statistical differences between groups due to the varying levels of one independent variable (main effects) or multiple variables (interactions). For a repeated measures model, a typical output will report significance for four different types of tests: sphericity assumed, Greenhouse-Geisser, Hunynh-Feldt, and lower-bound [69]. Within this thesis, the sphericity assumed test is applied if the data set satisfies Mauchly's test of sphericity. If the data set violates Mauchly's test of sphericity, Greenhouse-Geisser test was applied.

Although MANOVA and ANOVA tests are useful for determining the process parameters that lead to statistically significant differences in the means of the outcome measurements, no indication of the magnitude of the effect is given. Therefore, pairwise comparisons and post hoc analyses were performed to analyze the extent of the effect of varying the process parameters. Post hoc analyses were performed on independent variables that had two or more levels to examine which levels were statistically significant. If the independent variable only had two levels, a post hoc analysis was not needed as statistical significance was already reported by the ANOVA.

The design of experiment is also important in constructing an appropriate data set for the statistical analysis. There exists two different types of experimental design for a multivariate statistical analysis: full factorial or fraction factorial design [70]. A full factorial analysis is the most effective at determining the main effects as well as interactions among the process parameters as it covers every combination of the independent variables. However, the main drawback of the full factorial analysis is the resources (cost and time) involved. The main contributor to cost in a machining experiment, would be the cost due to the amount of workpieces needed to carry out the experiment. A fractional factorial design reduces the amount of observations or machining trials typically required by selecting certain process parameters and evaluating the effects within the selected subsections. However, the main drawback of the fractional factorial design approach is that not all combinations of parameters are tested, and certain "synergistic" process parameters may be missed due to the experimental design [70]. The full factorial design and multivariate approach taken within this thesis, was drawn from a previous machining study with the similar objective of optimizing the process parameters albeit in a different application for end milling AISI 1018 steel [68].

## Appendix E: Burring Trials and Associated Force Results from Results Presented in Chapter 4

The following tables are the combinations of process parameters from the burring trials presented in Figure 4.4 and Figure 4.5. The burring trial # and the associated cutting force magnitudes in the X,Y, and Z direction are summarized in the following tables (Table E.1 to Table E.4).

Table E.1: Reduced sample set #1: local minimums of temperature and vibration

Burring Trial #	Tool Type	Diameter (mm)	Tilt Angle (°)	Inclination Angle (°)	Depth of Cut (mm)	F <sub>x</sub> (N)	F <sub>y</sub> (N)	F <sub>z</sub> (N)
0	Sphere	6	0	0	0.5	0.53	0.24	-0.04
1	Sphere	6	0	0	1.0	0.65	0.45	-0.19
2	Sphere	6	0	+40	0.0	0.32	0.27	-0.03
3	Sphere	6	0	+40	1.0	0.41	0.38	-0.13
4	Sphere	6	0	-40	0.0	0.19	-0.07	-0.08
5	Sphere	6	0	-40	1.0	0.88	-0.05	-0.32
6	Sphere	6	45	0	0.5	0.46	0.17	-0.46
7	Sphere	6	45	0	1.0	0.60	0.35	-0.72
8	Sphere	6	45	+40	0.0	0.21	0.11	-0.11
9	Sphere	6	45	+40	1.0	0.36	0.38	-0.34
10	Sphere	6	45	-40	0.0	0.28	-0.08	-0.16
11	Sphere	6	45	-40	1.0	0.57	-0.15	-0.50
12	Sphere	4	0	0	0.5	0.44	0.23	-0.05
13	Sphere	4	0	0	1.0	0.56	0.35	-0.13
14	Sphere	4	0	+40	0.0	0.13	0.11	-0.03
15	Sphere	4	0	+40	1.0	0.18	0.22	-0.09
16	Sphere	4	0	-40	0.0	0.59	-0.08	-0.10
17	Sphere	4	0	-40	1.0	0.83	0.08	-0.32
18	Sphere	4	45	0	0.5	0.27	0.13	-0.27
19	Sphere	4	45	0	1.0	0.33	0.51	-0.36
20	Sphere	4	45	+40	0.0	0.14	0.14	-0.14
21	Sphere	4	45	+40	1.0	0.17	0.23	-0.22
22	Sphere	4	45	-40	0.0	0.31	-0.06	-0.25
23	Sphere	4	45	-40	1.0	0.57	0.05	-0.55
24	Cylinder	6	0	0	0.5	1.46	0.54	-0.12
25	Cylinder	6	0	0	1.0	1.46	0.55	0.22

26	Cylinder	6	0	+40	0.0	0.08	0.10	-0.01
27	Cylinder	6	0	+40	1.0	0.12	0.15	-0.06
28	Cylinder	6	0	-40	0.0	0.32	-0.14	-0.14
29	Cylinder	6	0	-40	1.0	0.65	-0.29	-0.27
30	Cylinder	6	45	0	0.5	0.13	0.11	-0.08
31	Cylinder	6	45	0	1.0	0.46	0.50	-0.48
32	Cylinder	6	45	+40	0.0	0.04	0.04	-0.05
33	Cylinder	6	45	+40	1.0	0.09	0.12	-0.13
34	Cylinder	6	45	-40	0.0	0.13	0.01	-0.12
35	Cylinder	6	45	-40	1.0	0.36	0.05	-0.35
36	Cylinder	4	0	0	0.5	1.44	0.51	-0.15
37	Cylinder	4	0	0	1.0	1.44	0.56	-0.15
38	Cylinder	4	0	+40	0.0	0.06	0.09	-0.03
39	Cylinder	4	0	+40	1.0	0.07	0.12	-0.06
40	Cylinder	4	0	-40	0.0	0.33	-0.13	-0.17
41	Cylinder	4	0	-40	1.0	0.71	-0.23	-0.31
42	Cylinder	4	45	0	0.5	0.17	0.16	-0.15
43	Cylinder	4	45	0	1.0	0.60	0.74	-0.38
44	Cylinder	4	45	+40	0.0	0.04	0.02	-0.07
45	Cylinder	4	45	+40	1.0	0.08	0.07	-0.11
46	Cylinder	4	45	-40	0.0	0.20	0.03	-0.21
47	Cylinder	4	45	-40	1.0	0.50	0.08	-0.62

Table E.2: Reduced sample set #2: local maximums of temperature and vibration

Burring Trial #	Tool Type	Diameter (mm)	Tilt Angle (°)	Feed Rate (mm/s)	Depth of Cut (mm)	F <sub>x</sub> (N)	F <sub>y</sub> (N)	F <sub>z</sub> (N)
0	Sphere	6	0	2	0.5	0.25	0.12	-0.09
1	Sphere	6	0	2	1.0	0.28	0.12	-0.15
2	Sphere	6	0	6	0.0	0.34	0.16	-0.11
3	Sphere	6	0	6	1.0	0.46	0.25	-0.30
4	Sphere	6	45	2	0.0	0.15	0.04	-0.15
5	Sphere	6	45	2	1.0	0.17	0.04	-0.17
6	Sphere	6	45	6	0.5	0.22	0.05	-0.22
7	Sphere	6	45	6	1.0	0.38	0.27	-0.47
8	Sphere	4	0	2	0.5	0.19	0.11	-0.04
9	Sphere	4	0	2	1.0	0.15	0.10	-0.03
10	Sphere	4	0	6	0.0	0.27	0.13	-0.08
11	Sphere	4	0	6	1.0	0.31	0.15	-0.14
12	Sphere	4	45	2	0.0	0.10	0.04	-0.12
13	Sphere	4	45	2	1.0	0.12	0.16	-0.13
14	Sphere	4	45	6	0.5	0.18	0.14	-0.21

15	Sphere	4	45	6	1.0	0.18	0.23	-0.25
16	Cylinder	0	0	0	0.0	0.46	0.19	-0.06
17	Cylinder	0	0	0	1.0	0.47	0.19	-0.10
18	Cylinder	0	0	1	0.0	0.65	0.27	-0.10
19	Cylinder	0	0	1	1.0	0.71	0.24	-0.14
20	Cylinder	0	1	0	0.0	0.05	0.04	-0.05
21	Cylinder	0	1	0	1.0	0.14	0.16	-0.18
22	Cylinder	0	1	1	0.0	0.08	0.08	-0.03
23	Cylinder	0	1	1	1.0	0.20	0.18	-0.30
24	Cylinder	1	0	0	0.0	0.47	0.18	-0.06
25	Cylinder	1	0	0	1.0	0.43	0.19	-0.11
26	Cylinder	1	0	1	0.0	0.62	0.24	-0.10
27	Cylinder	1	0	1	1.0	0.58	0.25	-0.13
28	Cylinder	1	1	0	0.0	0.06	0.06	-0.04
29	Cylinder	1	1	0	1.0	0.16	0.21	-0.17
30	Cylinder	1	1	1	0.0	0.11	0.13	-0.09
31	Cylinder	1	1	1	1.0	0.27	0.34	-0.30

Table E.3: Reduced sample set #3: absolute maximum for temperature

Burring Trial #	Diameter (mm)	Rotary Speed (rpm)	Feed Rate (mm/s)	Depth of Cut (mm)	Overlap (%)	Fx (N)	Fy (N)	Fz (N)
0	6	15,000	2	0.5	0	1.55	0.52	-0.23
1	6	15,000	2	0.5	10	1.54	0.52	-0.23
2	6	15,000	2	0.5	50	1.46	0.54	-0.12
3	6	15,000	2	1.0	0	1.58	0.57	-0.28
4	6	15,000	2	1.0	10	1.57	0.57	-0.27
5	6	15,000	2	1.0	50	1.46	0.55	0.22
6	6	15,000	6	0.5	0	2.07	0.77	-0.36
7	6	15,000	6	0.5	10	2.02	0.77	-0.34
8	6	15,000	6	0.5	50	2.00	0.82	-0.15
9	6	15,000	6	1.0	0	2.09	0.75	-0.37
10	6	15,000	6	1.0	10	2.11	0.78	-0.36
11	6	15,000	6	1.0	50	2.08	0.83	-0.18
12	6	45,000	2	0.5	0	0.67	0.25	-0.13
13	6	45,000	2	0.5	10	0.67	0.25	-0.11
14	6	45,000	2	0.5	50	0.66	0.27	-0.07
15	6	45,000	2	1.0	0	0.68	0.26	-0.15
16	6	45,000	2	1.0	10	0.68	0.28	-0.17
17	6	45,000	2	1.0	50	0.68	0.31	-0.06
18	6	45,000	6	0.5	0	0.93	0.40	-0.22
19	6	45,000	6	0.5	10	0.94	0.39	-0.20

20	6	45,000	6	0.5	50	0.89	0.41	-0.11
21	6	45,000	6	1.0	0	1.00	0.38	-0.21
22	6	45,000	6	1.0	10	1.00	0.39	-0.21
23	6	45,000	6	1.0	50	0.96	0.43	-0.09
24	6	75,000	2	0.5	0	0.46	0.18	-0.07
25	6	75,000	2	0.5	10	0.46	0.19	-0.06
26	6	75,000	2	0.5	50	0.47	0.20	-0.04
27	6	75,000	2	1.0	0	0.47	0.19	-0.09
28	6	75,000	2	1.0	10	0.47	0.19	-0.10
29	6	75,000	2	1.0	50	0.47	0.21	-0.04
30	6	75,000	6	0.5	0	0.66	0.26	-0.09
31	6	75,000	6	0.5	10	0.65	0.27	-0.10
32	6	75,000	6	0.5	50	0.63	0.28	-0.04
33	6	75,000	6	1.0	0	0.70	0.25	-0.14
34	6	75,000	6	1.0	10	0.71	0.24	-0.14
35	6	75,000	6	1.0	50	0.67	0.28	-0.03
36	4	15,000	2	0.5	0	1.44	0.46	-0.27
37	4	15,000	2	0.5	10	1.45	0.49	-0.23
38	4	15,000	2	0.5	50	1.44	0.51	-0.15
39	4	15,000	2	1.0	0	1.45	0.48	-0.28
40	4	15,000	2	1.0	10	1.45	0.51	-0.27
41	4	15,000	2	1.0	50	1.44	0.56	-0.15
42	4	15,000	6	0.5	0	2.05	0.65	-0.32
43	4	15,000	6	0.5	10	2.01	0.65	-0.30
44	4	15,000	6	0.5	50	1.95	0.64	-0.18
45	4	15,000	6	1.0	0	1.88	0.74	-0.47
46	4	15,000	6	1.0	10	1.93	0.80	-0.42
47	4	15,000	6	1.0	50	1.88	0.80	-0.26
48	4	45,000	2	0.5	0	0.61	0.23	-0.10
49	4	45,000	2	0.5	10	0.61	0.22	-0.11
50	4	45,000	2	0.5	50	0.64	0.25	-0.08
51	4	45,000	2	1.0	0	0.59	0.23	-0.13
52	4	45,000	2	1.0	10	0.62	0.25	-0.16
53	4	45,000	2	1.0	50	0.65	0.28	-0.09
54	4	45,000	6	0.5	0	0.91	0.31	-0.17
55	4	45,000	6	0.5	10	0.87	0.30	-0.18
56	4	45,000	6	0.5	50	0.90	0.34	-0.09
57	4	45,000	6	1.0	0	0.86	0.32	-0.21
58	4	45,000	6	1.0	10	0.83	0.34	-0.20
59	4	45,000	6	1.0	50	0.86	0.38	-0.11
60	4	75,000	2	0.5	0	0.45	0.17	-0.07
61	4	75,000	2	0.5	10	0.47	0.18	-0.06
62	4	75,000	2	0.5	50	0.47	0.19	-0.03

63	4	75,000	2	1.0	0	0.39	0.17	-0.09
64	4	75,000	2	1.0	10	0.43	0.19	-0.11
65	4	75,000	2	1.0	50	0.41	0.20	-0.08
66	4	75,000	6	0.5	0	0.62	0.23	-0.09
67	4	75,000	6	0.5	10	0.62	0.24	-0.10
68	4	75,000	6	0.5	50	0.62	0.25	-0.06
69	4	75,000	6	1.0	0	0.57	0.24	-0.14
70	4	75,000	6	1.0	10	0.58	0.25	-0.13
71	4	75,000	6	1.0	50	0.56	0.24	-0.06

Table E.4: Reduced sample set #4: absolute maximum for vibration

Burring Trial #	Tool Type	Diameter (mm)	Tilt Angle (°)	Inclination Angle (°)	Depth of Cut (mm)	F <sub>x</sub> (N)	F <sub>y</sub> (N)	F <sub>z</sub> (N)
0	Sphere	6	0	0	0.5	0.34	0.16	-0.11
1	Sphere	6	0	0	1.0	0.46	0.25	-0.30
2	Sphere	6	0	+40	0.5	0.18	0.11	-0.04
3	Sphere	6	0	+40	1.0	0.24	0.15	-0.11
4	Sphere	6	0	-40	0.5	0.29	-0.13	-0.15
5	Sphere	6	0	-40	1.0	0.81	-0.08	-0.56
6	Sphere	6	45	0	0.5	0.22	0.05	-0.22
7	Sphere	6	45	0	1.0	0.38	0.27	-0.47
8	Sphere	6	45	+40	0.0	0.16	0.12	-0.15
9	Sphere	6	45	+40	1.0	0.26	0.14	-0.23
10	Sphere	6	45	-40	0.0	0.24	-0.06	-0.19
11	Sphere	6	45	-40	1.0	0.44	-0.11	-0.55
12	Sphere	4	0	0	0.5	0.27	0.13	-0.08
13	Sphere	4	0	0	1.0	0.31	0.15	-0.14
14	Sphere	4	0	+40	0.5	0.11	0.07	-0.04
15	Sphere	4	0	+40	1.0	0.16	0.11	-0.11
16	Sphere	4	0	-40	0.5	0.29	-0.06	-0.16
17	Sphere	4	0	-40	1.0	0.46	-0.12	-0.26
18	Sphere	4	45	0	0.5	0.18	0.14	-0.21
19	Sphere	4	45	0	1.0	0.18	0.23	-0.25
20	Sphere	4	45	+40	0.0	0.10	0.08	-0.12
21	Sphere	4	45	+40	1.0	0.11	0.12	-0.16
22	Sphere	4	45	-40	0.0	0.19	-0.06	-0.18
23	Sphere	4	45	-40	1.0	0.34	0.01	-0.49
24	Cylinder	6	0	0	0.5	0.65	0.27	-0.10
25	Cylinder	6	0	0	1.0	0.71	0.24	-0.14
26	Cylinder	6	0	+40	0.5	0.07	0.05	-0.03
27	Cylinder	6	0	+40	1.0	0.17	0.13	-0.13
28	Cylinder	6	0	-40	0.5	0.28	-0.16	-0.16



29	Cylinder	6	0	-40	1.0	0.62	-0.34	-0.41
30	Cylinder	6	45	0	0.5	0.08	0.08	-0.03
31	Cylinder	6	45	0	1.0	0.20	0.18	-0.30
32	Cylinder	6	45	+40	0.0	0.08	0.05	-0.07
33	Cylinder	6	45	+40	1.0	0.14	0.09	-0.14
34	Cylinder	6	45	-40	0.0	0.17	0.02	-0.22
35	Cylinder	6	45	-40	1.0	0.24	0.03	-0.30
36	Cylinder	4	0	0	0.5	0.62	0.24	-0.10
37	Cylinder	4	0	0	1.0	0.58	0.25	-0.13
38	Cylinder	4	0	+40	0.5	0.10	0.09	-0.10
39	Cylinder	4	0	+40	1.0	0.12	0.11	-0.11
40	Cylinder	4	0	-40	0.5	0.31	-0.15	-0.20
41	Cylinder	4	0	-40	1.0	0.77	-0.31	-0.54
42	Cylinder	4	45	0	0.5	0.11	0.13	-0.09
43	Cylinder	4	45	0	1.0	0.27	0.34	-0.30
44	Cylinder	4	45	+40	0.0	0.07	0.03	-0.03
45	Cylinder	4	45	+40	1.0	0.12	0.09	-0.10
46	Cylinder	4	45	-40	0.0	0.19	0.04	-0.21
47	Cylinder	4	45	-40	1.0	0.43	0.08	-0.58

## Appendix F: Burring Trials and Associated Force Results from Results Presented in Chapter 5

The following tables are the combinations of process parameters from the burring trials presented in Figure 5.4 and Figure 5.6. The burring trial # and the associated cutting force magnitudes in the X,Y, and Z direction are summarized in the following tables (Table F.1 and Table F.2).

Table F.1: Optimal combination set of process parameters

Burring Trial #	Tool Type	Tilt Angle (°)	Inclination Angle (°)	Depth of Cut (mm)	Overlap (%)	F <sub>x</sub> (N)	F <sub>y</sub> (N)	F <sub>z</sub> (N)
1	Sphere	0	0	0.5	0	1.88	0.45	-0.65
2	Sphere	0	0	0.5	50	1.36	0.66	-0.64
3	Sphere	0	0	1.0	0	2.09	0.68	-1.21
4	Sphere	0	0	1.0	50	2.22	1.43	-0.83
5	Sphere	0	+40	0.5	0	1.01	0.22	-0.39
6	Sphere	0	+40	0.5	50	0.65	0.29	-0.28
7	Sphere	0	+40	1.0	0	1.84	0.48	-0.94
8	Sphere	0	+40	1.0	50	1.19	0.69	-0.57
9	Sphere	0	-40	0.5	0	1.52	-0.61	-1.10
10	Sphere	0	-40	0.5	50	0.97	-0.25	-0.37
11	Sphere	0	-40	1.0	0	3.46	-0.56	-2.58
12	Sphere	0	-40	1.0	50	2.50	0.19	-0.93
13	Sphere	45	0	0.5	0	1.65	0.13	-1.16
14	Sphere	45	0	0.5	50	1.14	0.24	-0.87
15	Sphere	45	0	1.0	0	2.13	0.23	-2.13
16	Sphere	45	0	1.0	50	1.57	0.46	-1.32
17	Sphere	45	+40	0.5	0	1.07	0.22	-0.60
18	Sphere	45	+40	0.5	50	0.74	0.39	-0.37
19	Sphere	45	+40	1.0	0	1.74	0.48	-1.30
20	Sphere	45	+40	1.0	50	1.25	0.96	-0.88
21	Sphere	45	-40	0.5	0	1.40	-0.31	-0.83
22	Sphere	45	-40	0.5	50	1.13	0.08	-0.70
23	Sphere	45	-40	1.0	0	2.31	-0.69	-1.97
24	Sphere	45	-40	1.0	50	1.79	-0.14	-1.56
25	Cylinder	0	0	0.5	0	4.56	0.77	-0.62
26	Cylinder	0	0	0.5	50	2.27	0.87	-0.23

27	Cylinder	0	0	1.0	0	2.71	0.58	-0.84
28	Cylinder	0	0	1.0	50	2.58	1.30	-0.83
29	Cylinder	0	+40	0.5	0	0.28	0.17	-0.28
30	Cylinder	0	+40	0.5	50	0.09	0.09	-0.13
31	Cylinder	0	+40	1.0	0	0.31	0.25	-0.34
32	Cylinder	0	+40	1.0	50	0.45	0.53	-0.35
33	Cylinder	0	-40	0.5	0	1.16	-0.46	-0.78
34	Cylinder	0	-40	0.5	50	0.96	-0.30	-0.53
35	Cylinder	0	-40	1.0	0	3.05	-1.07	-2.18
36	Cylinder	0	-40	1.0	50	1.87	-0.45	-0.93
37	Cylinder	45	0	0.5	0	0.69	0.21	-0.52
38	Cylinder	45	0	0.5	50	0.49	0.34	-0.28
39	Cylinder	45	0	1.0	0	1.54	0.85	-1.04
40	Cylinder	45	0	1.0	50	0.91	0.78	-0.80
41	Cylinder	45	+40	0.5	0	0.34	0.08	-0.25
42	Cylinder	45	+40	0.5	50	0.18	0.10	-0.16
43	Cylinder	45	+40	1.0	0	0.71	0.13	-0.60
44	Cylinder	45	+40	1.0	50	0.28	0.21	-0.33
45	Cylinder	45	-40	0.5	0	0.78	0.09	-0.85
46	Cylinder	45	-40	0.5	50	0.49	0.12	-0.44
47	Cylinder	45	-40	1.0	0	1.71	0.41	-2.10
48	Cylinder	45	-40	1.0	50	0.92	0.23	-0.91

Table F.2: Suboptimal combination set of process parameters

Burring Trial #	Tool Type	Feed Rate (mm/s)	Depth of Cut (mm)	Overlap (%)	F <sub>x</sub> (N)	F <sub>y</sub> (N)	F <sub>z</sub> (N)
1	Sphere	2	0.5	0	1.08	0.10	-0.48
2	Sphere	2	0.5	10	0.91	0.30	-0.26
3	Sphere	2	1.0	0	0.88	0.17	-0.38
4	Sphere	2	1.0	10	1.02	0.43	-0.37
5	Sphere	6	0.5	0	1.10	0.27	-0.42
6	Sphere	6	0.5	10	2.29	1.57	-0.53
7	Sphere	6	1.0	0	1.30	0.32	-0.53
8	Sphere	6	1.0	10	0.71	0.37	-0.94
9	Cylinder	2	0.5	0	1.79	-0.05	-0.62
10	Cylinder	2	0.5	10	1.70	0.33	0.09
11	Cylinder	2	1.0	0	1.28	0.30	-0.06
12	Cylinder	2	1.0	10	1.06	0.31	-0.10
13	Cylinder	6	0.5	0	1.92	0.37	-0.18
14	Cylinder	6	0.5	10	2.02	0.49	-0.24
15	Cylinder	6	1.0	0	1.75	0.38	-0.24
16	Cylinder	6	1.0	10	2.05	0.82	-0.29

## **Appendix G: Characterization and Synthesis of the Acoustics Associated with Bone Burring**

In alignment with the future work of the current body of work, potential studies may include characterizing and synthesizing the acoustics associated with bone burring possibly for design of a surgical simulator. Previous work has been performed in capturing the acoustics of the machining process and detecting peak frequencies (due to the rotational speed of the tool, or self-excited chatter), albeit in milling a homogenous material [67]. A pilot study was conducted and presented within this appendix, in attempt to synthesize acoustics for use in a surgical simulator. The acoustics of the burring process was characterized at three separate rotational speeds of the tool (20,000, 45,000, and 75,000 rpm) and equations G.1-G.5 were generated accordingly. Additionally, a comparison between the synthesized sound and the authentic acoustics produced by the bone burring process at rotational speeds of the tool 15,000, 45,000 and 75,000 rpm are compared.

### *Characterization and Synthesis of the Acoustic Profile*

To generate a realistic synthesis of the acoustic profile, a method to develop synthesized sounds, dependent on the user's input for the tool's rotational speed, was developed and outlined in Figure G.1. The main goal of the developed synthesizer was to allow for the user to select a rotational speed of the tool; and to generate a synthesized sound according to the user's selection. The synthesized process is distinguished into two separate subsections: rotational speed of tool acoustic generation and noise profile generation. Figure G.1 outlines the process developed for sound synthesis; additional information for the characterization protocol follows.

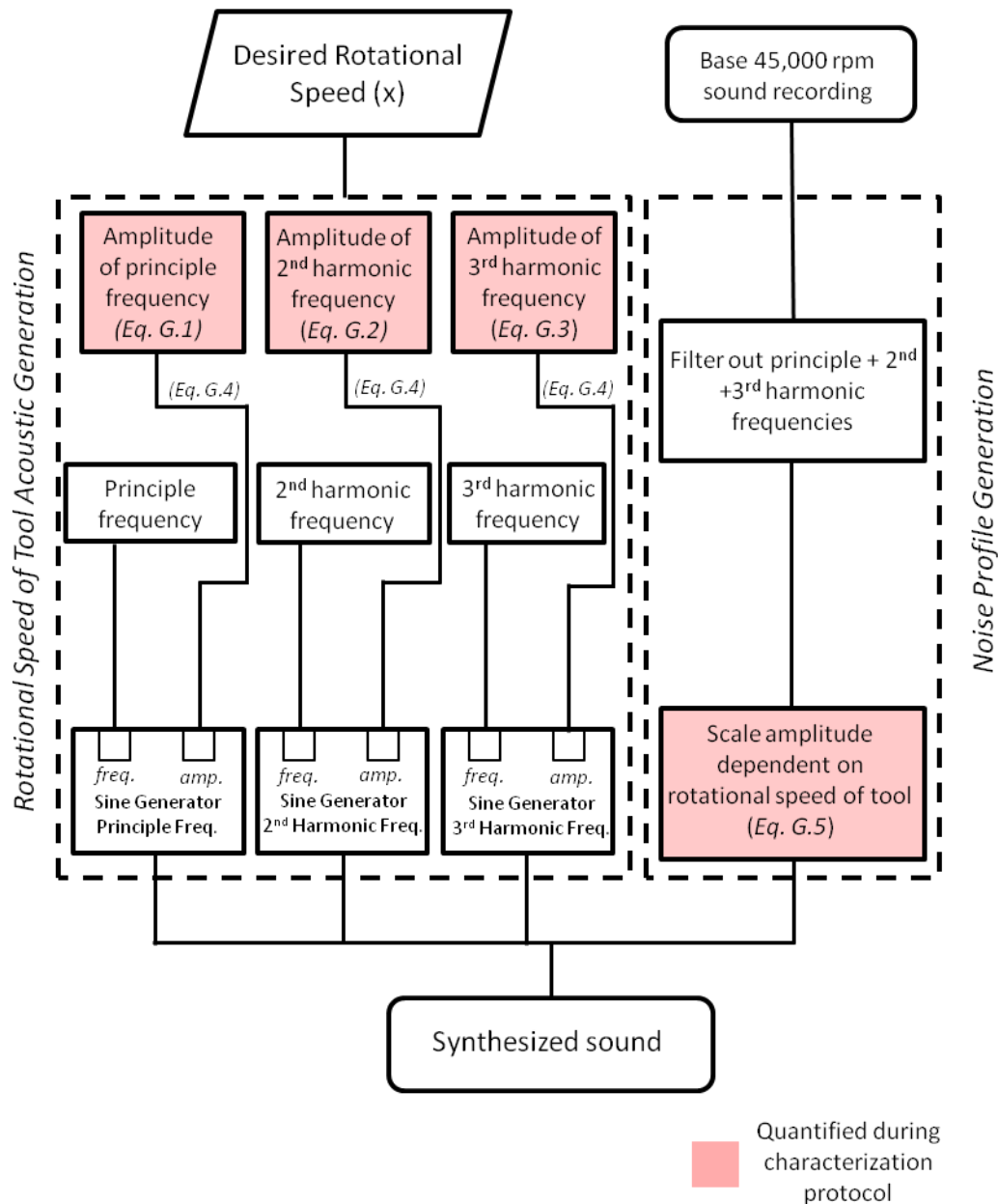


**Figure G.1: Developed process to synthesize sounds associated with bone burring**  
*The process taken to synthesize sound is outlined above. The synthesis process manipulates a 45,000 base sound recording to produce a noise profile of the tool, and through addition of principle and harmonic frequencies, dependent on the user's inputted rotational speed, synthesizes the associated acoustic profile. Equations associated with the synthesis process follow.*

### Characterization

Through the developmental work taken in characterizing the dynamic effects of bone burring in Chapter 2, it was found that the acoustic profile comprised of two separate distinct sounds: frequency due to the rotational speed of the tool, and the background frequencies associated with the noise due to the tool. It was also found that the magnitudes vary dependent on the rotational speed of the tool. Therefore, the main objective of the characterization process was to determine the trends of the acoustic profile and to generate linear scaling equations to allow for sound synthesis dependent on the user's selection of rotational speed.

An accelerometer was used to quantify the trends in the acoustics. The accelerometer was selected, over a microphone, as the accelerometer is less susceptible environmental noise. In characterizing the dynamic effects of the tool; the accelerometer produced a much cleaner signal for post processing and characterization purposes. Rotational speeds of 20,000, 45,000, and 75,000 rpm were used to characterize the acoustic profile.

### Rotational Frequencies (Principle, 2nd Harmonic, 3rd Harmonic)

The principle, second and third harmonic frequencies corresponding to the rotational speeds were examined in the frequency domain. The magnitudes associated with the peak frequencies were normalized to the 45,000 rpm and a linear scale was independently fitted to each of the measurements. The following equations were generated from fitting a linear line of best fit to the magnitudes of the three rotational speeds; and were subsequently used for determining the magnitude of an associated sinusoid wave. *Note:  $x$  = user input for rotational speed/1000*

$$\text{Amplitude}_{\text{principle}} = 0.2275x - 48.615 \quad (\text{G.1})$$

$$\text{Amplitude}_{\text{2nd Harmonic}} = 0.2011x - 20.385 \quad (\text{G.2})$$

$$\text{Amplitude}_{\text{3rd Harmonic}} = 0.2725x - 35.385 \quad (\text{G.3})$$

Subsequently, to generate a sinusoid in the time domain; a transformation equation was needed to determine the amplitude of the sine wave that corresponded to the previously calculated amplitudes. Therefore, a heuristic method was performed in generating various sine waves, and fitting an exponential line of best fit to their associated magnitudes in the frequency domain. The following equation was used to generate appropriate sinusoids that corresponded to the frequencies in equations G.1-G.3 ( $R^2=0.99$ ):

$$\text{Amplitude}_{\text{sinusoid}} = 1.35e^{0.11(\text{Amplitude}_{\text{frequency}})} \quad (\text{G.4})$$

Therefore, dependent on the user selection, the following equations were used to generate the amplitude of the principle (Eq. G.1), 2nd harmonic (Eq. G.2), and 3rd harmonic (Eq. G.3) frequencies. The specified amplitude was then substituted into Eq. G.4; to determine the appropriate amplitude for generation of three separate sinusoid signals.

### Noise Profile of Tool

A scaling factor was applied to the noise profile of the tool as it was found that the noise associated with the tool varied with rotational speed. Therefore, the principal and harmonic frequencies were filtered out of the initial measurements corresponding to the various rotational speeds (20,000, 45,000, and 75,000 rpm). Peak-to-peak measurements were then made on the filtered signal and a linear line of best fit was fitted to each of the

three measurements. The following scaling factor was produced and normalized to the base recording at 45,000 rpm:

$$\textit{Scaling Factor} = (0.0081x + 0.2231)/0.59 \quad (\text{G.5})$$

### *Synthesis of Sound*

The main goal in synthesizing sound was to have the ability to synthesize the acoustic profile at various increments within the range of the tool (15,000 to 75,000 rpm) dependent on the user's input. To produce the synthesized sound, a recording at 45,000 rpm was used as the base acoustic profile.

The recording was produced using a microphone, AKG (Acoustic and Cinema Equipment, Vienna, Austria) Perception 220 professional studio microphone, with a frequency bandwidth of 20 to 20,000 Hz, and a sampling frequency of 44100 Hz.

An overview of the synthesis process is found in Figure G.1.

### *Results of Synthesis vs. Authentic Acoustic Comparison*

To compare the synthesized sound to an authentic acoustic profile, rotational speeds of 15,000, 45,000, and 75,000 rpm were used. Although, the developed synthesized sound algorithm has the ability to produce an acoustic profile at continuous increments within the range of 15,000 to 75,000 rpm; the rotational speeds of 15,000, 45,000, and 75,000 rpm were selected to view the synthesizer's performance throughout the synthesizer's range.



The results of the comparison showed resemblance in the frequency domain; however, the synthesized sound contained fewer harmonic frequencies compared to the authentic sound (Figure G.2, Figure G.3, and Figure G.4). In the authentic sound, the fourth harmonic was present at 15,000, 45,000 and 75,000 rpm, illustrating a deficiency in the synthesizer's algorithm. The fourth harmonic was not reintroduced into the synthetic sound as the acoustic profile was characterized using the accelerometer; where only the principle, 2nd, and 3rd harmonic were present. The magnitudes of the principle and harmonic frequencies were similar in the authentic and synthesized sound at 15,000, 45,000 and 75,000 rpm.

In comparisons of the sound profiles; a suitable qualitative study should be taken to fully evaluate the synthesizer's output. Although viewing the results in the frequency domain is useful, it is difficult to truly judge and compare the synthesizer's ability to produce a realistic acoustic profile of the burring process. Therefore, moving forward qualitative studies, in terms of questioning a blinded user to distinguish between the authentic and synthesized sound should be taken to truly judge performance.

The developed process to synthesize sound outlined in the current appendix may serve as a building block in developing a sound synthesizer for a surgical simulator. The synthesizer discussed has the ability to produce acoustics that correspond to a variety rotational speeds associated with the bone burring process through use of a single base recording.

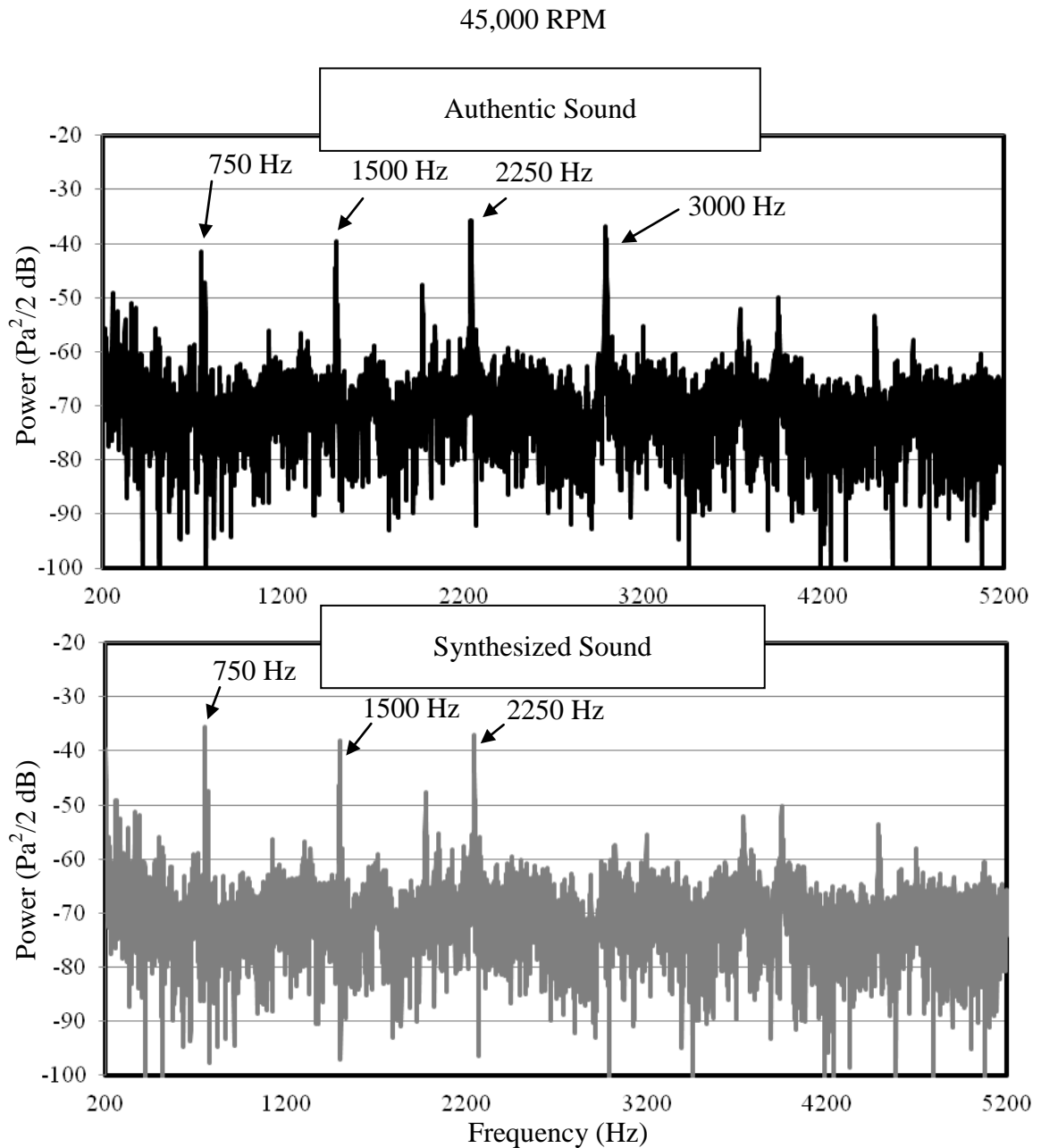


**Figure G.2: Authentic and synthesized sound at 45,000 rpm**

*A comparison between the authentic and synthesized sound at 45,000 rpm is shown above in the frequency domain. Although the authentic and synthesized sounds encompass data outside of the graphed regions (200-5200 Hz shown), it was largely comprised of noise beyond 5200 Hz; therefore only the range of 200-5200 Hz is shown for illustrative purposes.*

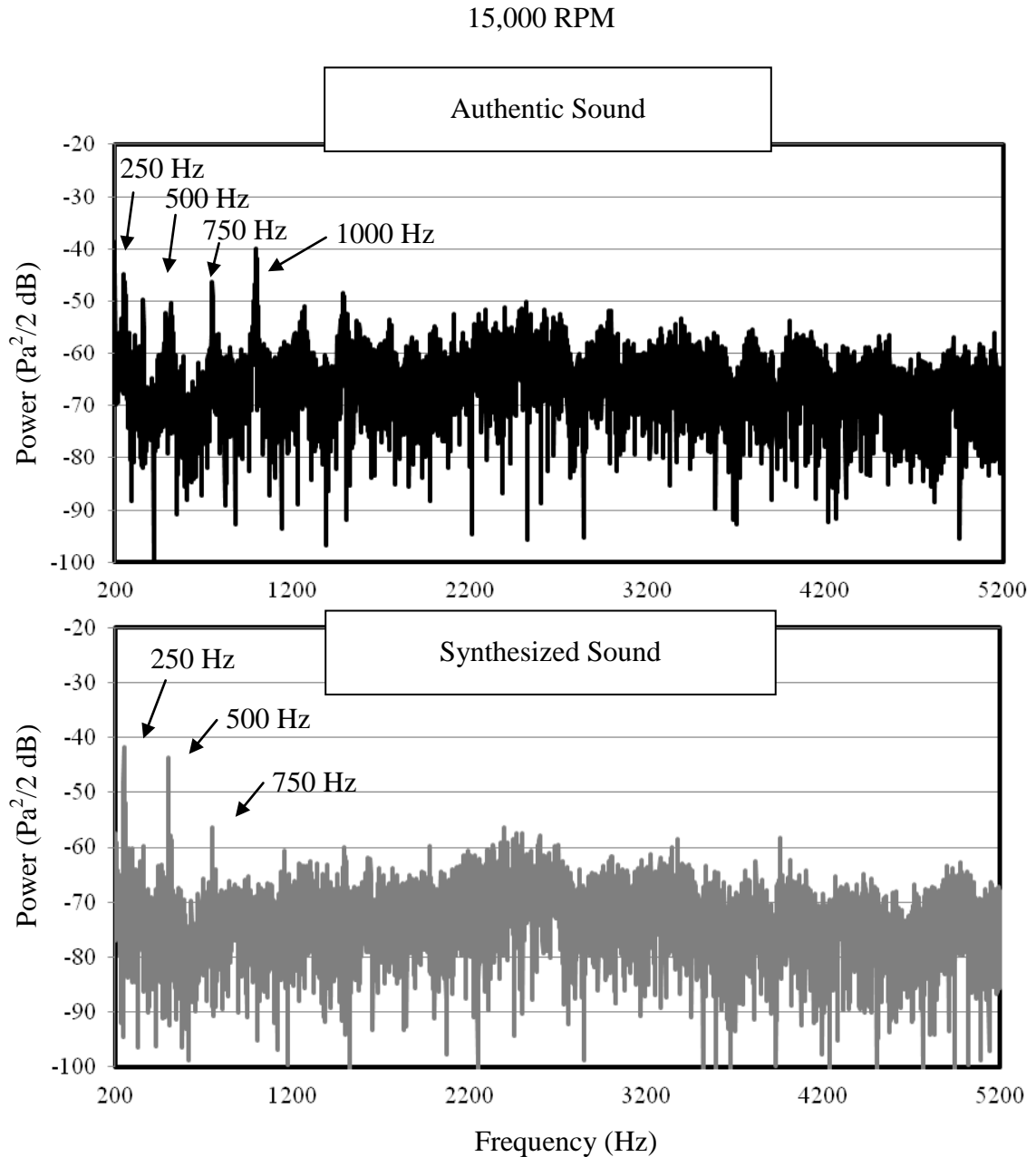


**Figure G.3: Authentic and synthesized sound at 15,000 rpm**

*A comparison between the authentic and synthesized sound at 15,000 rpm is shown above in the frequency domain. The fourth harmonic frequency (1000 Hz) is present in the authentic sound but not in the synthesized sound. The lack of the fourth harmonic present in the authentic sound illustrated a deficiency in the synthesizer's algorithm at reconstructing the authentic acoustics.*

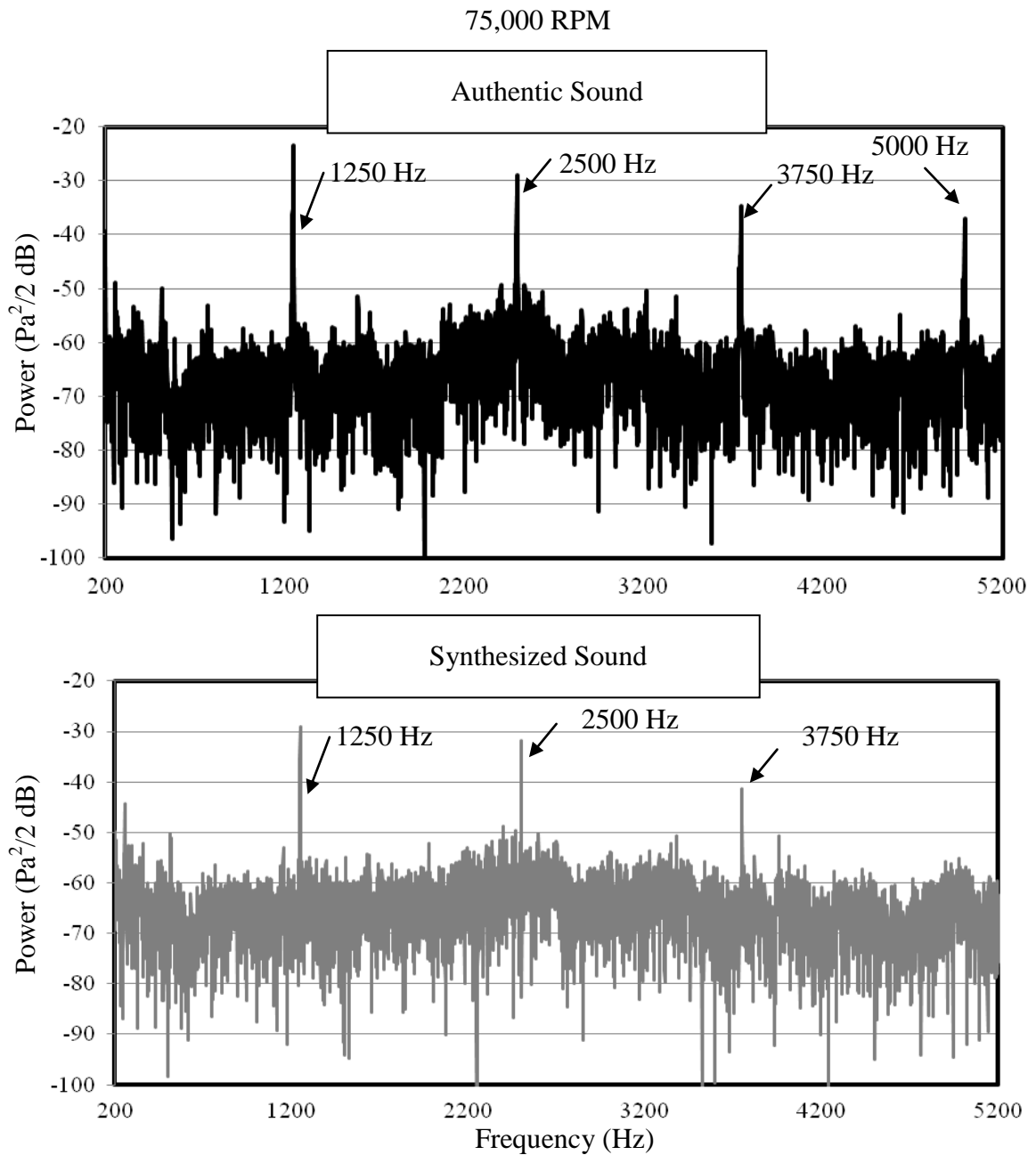


**Figure G.4: Authentic and synthesized sound at 75,000 rpm**

*A comparison between the authentic and synthesized sound at 75,000 rpm is shown above in the frequency domain. The magnitudes between the principle, 2nd, and 3rd harmonics are similar in the authentic and synthesized sound. The protocol taken in synthesizing sound, may prove useful as a building block in use in the design of a surgical simulator.*

**JONATHAN KUSINS**  
MEng Candidate

**Curriculum Vitae**

**EDUCATION**

- 2013 –** Candidate for MEng (Mechanical Engineering) in collaboration with Musculoskeletal Health Research, Expected: 2015  
*Supervisors: Dr. Louis Ferreira, Dr. Remus Tutunea-Fatan*  
**The University of Western Ontario, London Canada**
- 2009 – 2013** BEng (Mechanical Engineering)  
*Graduated with distinction, Deans list (2009-2013)*  
**The University of Western Ontario, London Canada**

**POSITIONS**

- 2013 –** **The University of Western Ontario**  
*Teaching Assistant (Fluid Dynamics II, Robotics & Manufacturing Automation, Dynamics and Kinematics of Machines)*  
Department of Mechanical and Materials Engineering
- 2012** **Indian Institute of Technology, Rajasthan, India**  
*Research Assistant to Dr. Anand Plappally*  
Summer Internship focused on water-related energy use
- 2010, 2011** **Lake Shore Gold, Timmins ON Canada**  
*Project Engineering Student*

**HONOURS and AWARDS**

- 2014** **Queen Elizabeth II Scholarship in Science and Technology (\$15,000)**  
The University of Western Ontario
- 2013-2015** **NSERC CREATE: Computer-Assisted Medical Intervention Scholarship (\$24,000)**  
The University of Western Ontario
- 2013** **JuMP Summer Research Student Scholarship (\$6,000)**  
The University of Western Ontario
- 2012** **Global Opportunities Award (\$2,000)**  
The University of Western Ontario
- 2009-2013** **Western Engineering Dean's Honour List**  
The University of Western Ontario
- 2009** **Entrance Scholarship (\$2,000)**  
The University of Western Ontario

## **PUBLICATIONS and PRESENTATIONS**

### **Papers Accepted to Refereed Journals**

1. A. Hasija, M. Jhaver, **J. Kusins**, N. K.Singh, N.Kumar, K. Singh, N.Kumar, N. Katiyar, Y. Kumar, C. Meena, P. Jawalkar, G. R. Goutham, V. K. Verma, A. K. Alwaria, A. Kumar, G. K.Joseph, R. Singhal, A.K. Plappally, Study of Water and Water-related Energy Use in the context of households in Western and Northern parts of India, Hydro. Current Res. 2013, 4:1

### **Proceedings of Refereed Conferences**

1. **J. Kusins**, O. Remus Tutunea-Fatan, L. Ferreira. Experimental Apparatus for Analysis of Bone Removal During Surgical Resurfacing Procedures. 25th Canadian Congress of Applied Mechanics. London, Ontario, Canada (2015, Podium).
2. **J. Kusins**, R. Willing, G. King, L. Ferreira. Development and Experimental Validation of a Computational Model of the Elbow Joint. Bone and Joint Injury and Repair. London, Ontario, Canada (2014, Poster).
3. **J. Kusins**, R. Willing, G. King, L. Ferreira. Development and Experimental Validation of a Computational Model of the Elbow Joint. 60th Annual Meeting of Orthopaedic Research Society. New Orleans, Louisiana, USA (2014, Poster).
4. **J. Kusins**, R. Willing, G. King, L. Ferreira. Development of a Computational Elbow Model. Canadian Orthopaedic Research Society Annual Meeting. Montreal, Quebec, Canada (2014, Podium).

## **COMMITTEES and OUTREACH ACTIVITIES**

1. **VP Social Committee – Western Mechanical Engineering Graduate Student Society (2014-2015)**  
Organized events and developed a social committee for mechanical engineering graduate students
2. **Discovery Camp – Western University (2014)**  
Taught and demonstrated concepts on *in-vitro* joint simulation to secondary school students
3. **Western Engineering International Student Buddy (2012-2014)**  
Aided first year international students in their transition to Canadian culture
4. **Western Preview Day Volunteer (2013-2015)**  
Demonstrated various labs to students interested in attending Western University

## **PROFESSIONAL MEMBERSHIPS**

**2015-** Professional Engineers of Ontario (PEO) - Engineer in Training (EIT)